An Arterial Spin Labelling Method for the Measurement of Myocardial Perfusion in Humans at 3 Tesla



Graeme A. Keith
St. Catherine's College
University of Oxford

A thesis submitted for the degree of
Doctor of Philosophy

Trinity 2017

An Arterial Spin Labelling Method for the Measurement of Myocardial Perfusion in Humans at 3 Tesla

Graeme A. Keith, St. Catherine's College, Trinity term 2017.
This thesis is submitted for the degree of Doctor of Philosophy.

Abstract

The assessment of Myocardial Blood Flow (MBF) is an important measure in clinical practice for evaluating the health of the heart. Multiple imaging methods have been employed to measure MBF, including applications of nuclear medicine, x-ray and contrast enhanced Magnetic Resonance Imaging (MRI). However, each of these modalities suffers from drawbacks, such as invasiveness due to radiation or intravenous contrast injection, difficulty in quantitation, and limited repeatability.

The aim of this thesis was to develop a non-invasive, quantitative and repeatable MRI method for the measurement of MBF, by applying the techniques of Arterial Spin Labelling (ASL). A novel cardiac ASL sequence was designed and thoroughly tested by simulation and phantom experiment. The method was applied in vivo in three slices of the human heart, to our knowledge the first cardiac ASL acquisition in multiple slices, in ten healthy volunteers. The resulting values of mid-ventricular MBF, averaged over multiple measurements, compared well with the literature values from multiple modalities. Repeat measures were then used in order to characterise the reproducibility and variation inherent in the method, showing that the expected change in MBF would be detectable with the ASL sequence. Segmental values of MBF, according to the AHA standard model, were also calculated and these compared well to previous PET literature. This work has been published in the journal Magnetic Resonance in Medicine.

Further to this work, the new cardiac ASL sequence was optimised with the ultimate goal of single breath hold acquisitions. The optimised sequence was shown to improve the results in terms of the balance between good signal-to-noise ratio and reducing spatial and temporal variation in MBF values. Though improvements were made, there remained a large variation in the measured values of MBF, meaning single breath hold acquisition in a clinical context is not yet practical. In addition to the optimisation, the online scanner reconstruction software was altered to produce parametric maps of both T_1 and MBF direct to the scanner operator. The sequence, along with online reconstruction is available for use in our laboratory for future clinical trials in the heart and liver.

Acknowledgements

A special thank you to Professor Matthew Robson, for first of all taking me on as a Postgraduate Research Assistant, then subsequently as a DPhil student. Our thanks to Professor Michael Chappell for our useful early discussions on arterial spin labelling methods and for welcoming me in to the ASL reading group. Thanks to Professor Christopher Rodgers for the early help in getting the sequence development off the ground, and to Professor Stefan Piechnik for the loan of his phantom. Special thanks also to Dr Betty Raman for her invaluable input on cardiology matters.

Thanks to everyone at OCMR, in particular Dr Aaron Hess for his constant reassurance and support and my other long suffering office mates Dr Yuehui Tao, Dr Elizabeth Tunnicliffe and Dr Sofia Dimoudi for putting up with numerous and frequent stupid questions and for politely ignoring the occasional use of industrial Glaswegian language when battling computer code. Thank you and more to Dr Ludovica Griffanti for her endless encouragement, inspiration and patience. Also, thanks to Dr Olivia Faull for picking up the pieces a couple of times.

Many thanks to everyone who volunteered to be scanned over the course of this project, especially the ones who didn't moan about it.

Finally, many special thanks to my family, Mum and Dad for your endless support, Sarah and Martin, my friends back home, in particular Alan and Andy for the many, mostly abusive, messages which kept me going.

Publications

Journal articles

1. **Keith GA**, Rodgers CT, Chappell MA, Robson MD. A Look-Locker acquisition scheme for quantitative myocardial perfusion imaging with FAIR Arterial Spin Labeling in humans at 3 tesla. *Magnet Reson Med* 2016.

2. Tao Y, Hess AT, **Keith GA**, Rodgers CT, Liu A, Francis JM, Neubauer S, Robson MD. Optimized saturation pulse train for human first-pass myocardial perfusion imaging at 7T. *Magnet Reson Med* 2015;73(4):1450-1456.

3. **Keith GA**, Rodgers CT, Hess AT, Snyder CJ, Vaughan JT, Robson MD. Automated tuning of an eight-channel cardiac transceive array at 7 tesla using piezoelectric actuators. *Magnet Reson Med* 2015;73(6):2390-2397.

Conference abstracts

1. **Keith GA**, Rodgers CT, Chappell, MA, Robson MD. Reproducibility and Variability of a Look-Locker FAIR ASL Sequence for Quantitative Measurement of Myocardial Blood Flow in Healthy Human Volunteers at 3T. *ISMRM 2016;* Singapore. p 1483.

2. **Keith GA**, Rodgers CT, Chappell, MA, Robson MD. A Look-Locker Acquisition Scheme for Quantitative Myocardial Perfusion Imaging by Arterial Spin Labelling in Humans at 3 T. *ISMRM 2015;* Toronto. p 2690.

3. **Keith GA**, Rodgers CT, Hess AT, Snyder C, Vaughan JT, Robson M. A Fully Integrated Automatic Tune and Match System for an 8-Channel Transmit/Receive Cardiac TEM Array at 7T: Initial Results in a Phantom and Volunteers. *ISMRM 2014;* Milan. p 1339.

4. Tao Y, Hess AT, **Keith GA**, Rodgers CT, Liu A, Francis JM, Neubauer S, Robson MD. HS8 Saturation Pulse Train for First-Pass Myocardial Perfusion Imaging At 7t. *ISMRM 2014;* Milan. p 0991.

5. **Keith GA**, Rodgers CT, Hess AT, Snyder C, Vaughan JT, Robson M. Computerised Tuning of an 8-channel Cardiac TEM Array at 7T: an Integrated System Using Piezoelectric Actuators and Power Monitors. *ISMRM 2013;* Salt Lake City. p 2743.

6. Tao Y, Hess AT, **Keith GA**, Rodgers CT, Robson MD. B0-Independent Quantitative Measurement of Low B1 Field for Human Cardiac MRI at 7T. *ISMRM 2013;* Salt Lake City. p 2596.

7. Hess AT, Snyder C, **Keith GA**, Rodgers CT, Neubauer S, Vaughan JT, Robson M. Coil Tuning with Piezoelectric Actuators Using the MRI Signal as the Optimization Parameter. *ISMRM 2013;* Salt Lake City. p 2745.

8. Rodgers CT, **Keith GA**, Hess AT, Snyder C, Vaughan JT, Robson M. An algorithm for automatic optimisation of transmit array coil tune and match applied in the heart at 7T. *ISMRM 2013;* Salt Lake City. p 4402.

Contents

Abstract i
Acknowledgements ii
Publications iii
List of Figures viii
List of Tables x

1 Introduction **1**
1.1 Motivation 2
1.2 Objectives 5
1.3 Outline of Chapters 6
References 10

2 Theory of Magnetic Resonance Imaging **16**
2.1 Nuclear Spin 16
2.2 The Quantum and Classical Models 18
2.3 Resonance and the Rotating Frame 22
2.4 Relaxation Times and Pulse Sequences 24
2.5 Magnetic Field Gradients and Image Formation 27
2.5.1 Frequency Encoding 29
2.5.2 Slice Selection 30
2.5.3 Phase Encoding 33
2.5.4 Spin Warp 34
2.5.5 k-space and the Fast Fourier Transform 34
2.6 Advanced Techniques 39
2.6.1 The bSSFP Sequence 39
2.6.2 Adiabatic Pulses 42
References 44

3 The Perfusion of the Heart **46**
3.1 The Heart . . . 46
3.1.1 The Coronary Arteries . . . 48
3.1.2 The Left Ventricle . . . 48
3.2 Myocardial Blood Flow . . . 49
3.2.1 Under Stress . . . 50
3.2.2 Ischaemia . . . 50
3.3 Imaging Methods for Measuring MBF . . . 51
3.3.1 PET . . . 51
3.3.2 SPECT . . . 52
3.3.3 CT . . . 52
3.3.4 CMR . . . 53
3.4 Summary . . . 54
References . . . 55

4 Arterial Spin Labelling **58**
4.1 The Spin Label Experiment . . . 58
4.2 Application of ASL to the Heart . . . 60
4.3 Flow-sensitive Alternating Inversion Recovery . . . 61
4.4 ASL in the Heart . . . 61
4.4.1 Single Inversion Time ASL . . . 62
4.4.2 Multiple Inversion Time ASL . . . 63
4.4.3 Steady-pulsed ASL . . . 64
4.5 Quantification of MBF . . . 64
4.5.1 Signal Difference Method . . . 66
4.5.2 Dual T_1 Method . . . 67
4.5.3 Arterial Transit Time . . . 67
4.6 Summary . . . 68
References . . . 69

5 Development of an ASL sequence for measurement of myocardial perfusion at 3T **74**
5.1 Methods . . . 75
5.1.1 Sequence Design . . . 75
5.1.2 On Scanner Implementation . . . 75
5.1.3 Simulations . . . 76
5.1.4 Phantom Studies . . . 78

5.1.5 In Vivo Studies . . . 79
5.1.6 Image Analysis . . . 80
5.1.7 Reproducibility and Variability Analysis . . . 83
5.1.8 Segmental Analysis . . . 83
5.2 Results . . . 84
5.2.1 Simulations . . . 84
5.2.2 Phantom Studies . . . 86
5.2.3 In Vivo Studies . . . 86
5.2.4 Reproducibility and Variability Analysis . . . 89
5.2.5 Segmental Analysis . . . 89
5.3 Discussion . . . 94
5.4 Conclusion . . . 99
References . . . 101

6 Optimisation of the LL-FAIR-ASL sequence for improved clinical viability 106
6.1 Methods . . . 106
6.1.1 Simulation . . . 106
6.1.2 Optimisation of the sequence In Vivo . . . 107
6.1.3 Online Image Reconstruction and Parametric Mapping . . . 110
6.2 Results . . . 111
6.2.1 Simulation . . . 111
6.2.2 Optimisation of the Sequence In Vivo . . . 111
6.2.3 Online Image Reconstruction and Parametric Mapping . . . 117
6.3 Discussion . . . 120
6.4 Conclusion . . . 126
References . . . 127

7 Conclusions 129
7.1 Future Directions . . . 131
7.2 Summary . . . 133
References . . . 135

Appendix: relevant publications 139

List of Figures

2.1 The hydrogen atom 18
2.2 The low and high energy states 19
2.3 Energy level diagram 20
2.4 Precession 21
2.5 The behaviour of the magnetisation in the laboratory frame 23
2.6 Free Induction Decay (FID) 25
2.7 A simple Inversion Recovery NMR pulse sequence 27
2.8 Inversion Recovery and longitudinal relaxation of the magnetisation . 28
2.9 A magnetic field gradient 29
2.10 A simple Gradient Echo NMR pulse sequence 31
2.11 Slice selection gradient 31
2.12 Slice selection in a cylindrical sample 32
2.13 The effect of phase encoding 33
2.14 The phase encoding gradient 34
2.15 The Spin Warp imaging pulse sequence 35
2.16 The k-space domain 36
2.17 Magnitude and phase 38
2.18 A single TR of a balanced SSFP sequence 39
2.19 Evolution of the magnetisation during one TR of a bSSFP sequence . 40
2.20 Amplitude and frequency profiles of the Hyperbolic Secant (HS) pulse 42
2.21 The amplitude modulation function of the HS8 pulse envelope 43

3.1 The human heart 47
3.2 The coronary arteries 49

4.1 Flow-sensitive Alternating Inversion Recovery (FAIR) in the heart . . 59
4.2 The single inversion time FAIR-bSSFP sequence 62
4.3 The steady-pulsed ASL sequence (spASL) 65

5.1 Schematic of the LL-FAIR-ASL pulse sequence 77
5.2 Slice positioning in the heart 80
5.3 Analysis pipeline 81
5.4 Correlation of simulated slice selective and globally selective T_1*s . . 84
5.5 Simulation of inversion/readout pulse profile interactions 85
5.6 Simulation of heart rate effects on T_1 and T_1* 87
5.7 A typical slice-selective/globally-selective Inversion Recovery pair . . 88
5.8 MBF/HR results from in vivo scans in three slices 90
5.9 Bland-Altman reproducibility plots 91
5.10 Segmental MBF results 92

6.1 Simulation of the effect of SNR on T_1, T_1* and MBF calculations . . 112
6.2 Effects of varying receive bandwidth/TR on SNR 113
6.3 Effects of varying receive bandwidth/TR on temporal SNR 114
6.4 Effects of varying receive bandwidth/TR on spatial CoV 114
6.5 SNR as a function of flip angle 115
6.6 Temporal SNR as a function of flip angle 116
6.7 Spatial coefficient of variation as a function of flip angle 117
6.8 Bland-Altman plots: T_1 values with varying bandwidth/TR 118
6.9 Bland-Altman plots: T_1 values with varying flip angle 119
6.10 Output of parameter maps to the scanner console 121
6.11 Enlarged MBF colourmap masked for myocardial value of T_1 122

List of Tables

5.1 MBF results from in vivo scans in three slices 89
5.2 Segmental MBF results 93
5.3 Comparison of MBF results with literature values 95

Chapter 1

Introduction

Myocardial perfusion is an important marker of the health of the heart. Perfusion is the process by which blood passes through the circulatory system to the capillary bed of the muscle of the heart. This blood flow to the myocardial muscle delivers a nutrient rich, oxygenated supply of blood to the myocardium via the coronary arteries. This feeds the arterioles and on into the capillary bed, depositing the energy producing oxygen before draining away back to the heart via the venous system. If the supply of blood to the myocardium is in anyway impaired, for instance due to an occlusion in one of the coronary arteries, then the target tissue can become ischaemic, whereby the tissue does not receive the required level of oxygen and nutrients and the function of the heart can become impaired. If this is left untreated, the myocardium can undergo tissue death, known as infarction. This is particularly relevant in the myocardium of the left ventricle (LV), the muscle which pumps the oxygenated blood around the tissues of the body, and which is supplied by the left circumflex artery (LCX) and the left anterior descending artery (LAD), the coronary artery most likely to become occluded.

It is therefore important that the perfusion of the left ventricular myocardium can be measured in vivo in order to assess the health of the tissue. To date, measurement

of myocardial perfusion has been achieved by a variety of imaging methods in the fields of nuclear medicine, x-ray and Magnetic Resonance Imaging (MRI). However, these techniques are often invasive, difficult to quantify and are not easily repeatable.

1.1 Motivation

The motivation behind this work was the need for a truly non-invasive, quantitative and repeatable method of measuring myocardial perfusion in vivo. Cardiovascular Magnetic Resonance (CMR) is an inherently non-invasive imaging platform and as such, is an attractive modality for this application. The aim of this thesis is to develop such a method by application of the technique of Arterial Spin Labelling (ASL)[1, 2] to CMR imaging methods.

Currently, many applications of both clinical and research measurement of in vivo human myocardial perfusion are carried out by the application of invasive imaging modalities. These most often involve the use of ionising radiation which, though doses may be low, can cause damage to tissue. These methods include the nuclear medicine based applications of Positron Emission Tomography (PET), whereby a myocardial perfusion agent is labelled with a radionuclide tracer[3, 4, 5, 6, 7], and Single Photon Emission Computed Tomography (SPECT)[8, 9], the most common imaging methodology applied in the clinic[8] to the problem of in vivo measurement of myocardial perfusion. Also involving ionising radiation is the x-ray Computed Tomography (CT) method[10, 11]. As well as a high radiation dose from the x-rays, due to the dynamic nature of the technique, the CT method also involves the intravenous injection of a contrast agent bolus, which serves to highlight the contrast between areas of myocardium with low blood-flow, to those with normal blood flow or increased blood flow under conditions of pharmacological stress.

As well as being invasive, these methods pose difficulties in the absolute quan-

tification of Myocardial Blood Flow (MBF). In PET, the MBF is calculated from a series of dynamic images and involves corrections for various parameters[6]. PET is also impractical as a routine methodology due to its high cost, inflated still by the need for an on-site cyclotron to produce the necessary radioisotopes, such as ^{15}O[3] and ^{13}N[4]. Though in common use, SPECT is generally used as a purely qualitative measure of myocardial perfusion, as the possibility of quantitation is not viable due to its inherently low sensitivity, and low spatial and temporal resolutions[9]. Quantification of MBF from CT data involves offline deconvolution to fit time-attenuation curves[11], however the values of MBF can be influenced by the effects of the presence of the iodinated contrast agent.

CMR techniques are already widely used for the investigation of myocardial blood flow, particularly in a research setting[12, 13]. Though, of course, the use of an MRI scanner does not involve any harmful radiation, in a first-pass perfusion experiment the injection of a paramagnetic contrast agent, usually gadolinium based, is required. The use of the contrast agent in this context brings its own problems, as it adds the cost of purchasing the agent, it can be dangerous to renal patients[14] and the use of a contrast agent restricts the ability to perform too many repeated scans. First-pass perfusion CMR, like the ionising radiation based methods described above also suffers from difficulties with absolute quantification[15]. This is due to the assumption that the agent is in fast-exchange with the myocardial tissue, such that all the myocardium has received equal exposure to the agent, and also the relationship between the concentration of the agent and the resultant MR signal is both non-linear and is dependant upon the particular imaging parameters employed. Finally, first-pass perfusion images remain subject to artefact, such as the characteristic "dark rim" artefact[16], which could potentially be mistaken for a region of low blood flow.

As outlined above, the problems associated with the existing imaging methods of measuring myocardial perfusion are three-fold. The inherently invasive nature of the

techniques, the difficulties posed in achieving absolute quantification and the inability to perform repeated measurements, whether due to concerns about the radiation dose or the lingering effect of contrast agents.

The application of arterial spin labelling techniques[1, 2] is an attractive alternative to the above outlined imaging modalities. As an MRI method which employs the water content of blood as an endogenous tracer, ASL is a truly non-invasive technique. ASL uses Magnetic Resonance (MR) techniques to change the spin state of the hydrogen nuclei in the water, such that the blood is "magnetically labelled". It should not suffer from the same troubles with quantification as other methods as the ASL signal difference is directly proportional to the blood flow[17], due to the tracer employed being the blood itself, albeit there are competing models of quantification[18, 19]. Finally, due again to the absence of either ionising radiation or an exogenous contrast agent, it is an entirely repeatable measure of perfusion, with the caveat that any planned pharmacological stress test could, of course, not be endlessly repeated. ASL techniques can be implemented on standard clinical MRI scanners, which are widely available and in routine use.

To date, a handful of ASL methods have previously been applied to the heart, largely employing the Flow-sensitive Alternating Inversion Recovery (FAIR) labelling scheme[20, 21].These include two similar inversion recovery methods employing a single imaging readout per inversion, the first of which was carried out in both pigs and humans at 1.5 T[22] but which suffered from high physiological noise and the magnetic relaxation properties (T_1) of blood at lower field strength.The second study employed a different imaging sequence at 3 T[23] to combat these issues, but was susceptible to variations in heart rate due to the quantification model employed and required both spatial and temporal averaging. This sequence was later employed in a clinical study to detect increases in MBF under pharmacological stress in patients with coronary artery disease (CAD). Other methods include a saturation recovery

method[24, 25] that used multiple saturation times, but which was shown to overestimate values of MBF[17], and a different approach termed steady-pulsed ASL[26]. This employed free breathing and a pseudo-continuous style spin labelling scheme[27], such as is commonly used in the brain, but which suffered from respiratory motion and poor labelling efficiency. Many of these methods have shown some promise in the measurement of MBF, however none has, as yet, stood out as a gold standard non-invasive, quantitative and repeatable method of measuring myocardial perfusion.

1.2 Objectives

The purpose of this thesis was to develop a new method of measuring blood flow with ASL suited to the particular challenges of cardiac MR imaging. As such, the particular objectives of this work were:

- To apply the robust and widely used methods of cardiac T_1 mapping to the problem of measuring myocardial perfusion non-invasively and quantitatively by combining it with arterial spin labelling, beginning with a technique in which spatial and temporal averaging are employed to reduce the effects of both thermal and physiological noise.

- To thoroughly test the sequence against a variety of varying parameters, such as T_1 and heart rate, in order to characterise its behaviour.

- To apply the technique in the heart on normal volunteers to measure myocardial blood flow, both globally and segmentally, for comparison with literature values. In addition, to test the variation and reproducibility of MBF results both within- and between-sessions, evaluating the inherently repeatable nature of the technique.

- To optimise the sequence, with the goal that measurement of MBF is achievable

within a single breath hold, negating the need for spatial and temporal averaging of MBF. In addition, given the T_1 mapping origins of the proposed technique, to validate the ASL T_1 maps against existing and widely used techniques[28, 29, 30].

- Finally, to implement the online scanner reconstruction of pixel-wise maps of MBF. The motivation being two-fold, to provide the scanner operator with a near instant qualitative indication of MBF across the whole myocardium, and to simplify quantification, such that simply drawing a region of interest, either online or offline, gives a direct measure of MBF within the specified area.

1.3 Outline of Chapters

Chapter 2 introduces the basic concepts of magnetic resonance physics and imaging techniques which underlie this thesis, from the early discoveries by the pioneers of Nuclear Magnetic Resonance (NMR), via inherent magnetic properties such as relaxation times, to the formation of images with combinations of radiofrequency pulses and magnetic field gradients, and Fast Fourier Transforms (FFT). Further, more advanced imaging techniques, with direct relevance to this work, such as the balanced Steady-State Free Precession (bSSFP) sequence and adiabatic pulses, are also introduced.

Chapter 3 gives a simple overview of the heart. The anatomy and function of the heart are described, with particular emphasis on the areas of most relevance to this thesis, the left ventricle and the coronary arteries. The concept of Myocardial Blood Flow (MBF), which the work presented in this thesis endeavours to measure, is introduced and the effects of pharmacological stress and inadequate blood flow (ischaemia) are described. Finally, the various existing methods of measuring MBF in vivo are described in greater depth, including Positron Emission Tomography (PET), Single

Photon Emission Computed Tomography (SPECT), x-ray Computed Tomography (CT) and contrast enhanced, first-pass perfusion methods of CMR. The principles behind each method are introduced and the respective merits and drawbacks are discussed.

In chapter 4, the theory behind the Arterial Spin Labelling (ASL) family of techniques is presented. The basic principles behind ASL are described, whereby spins are "magnetically labelled" using bespoke MR pulse sequences, such that two discrete states are created and taking the difference removes the influence of the unchanging static tissue, leaving only the contribution from the inflowing blood. Particular emphasis is given in this chapter to the Flow-sensitive Alternating Inversion Recovery (FAIR) labelling scheme[20, 21], which employs two inversion recovery pulses with differing slice-selection gradients to create the two states, and which forms the basis of this work. Following this, the existing literature on application of ASL techniques to the heart is discussed in greater detail, including the difficulties inherent in myocardial applications of ASL and the particular benefits and drawbacks of the existing methods. This chapter then includes a comparison of the two methods of quantifying MBF, the signal difference method and the dual T_1 method, before briefly introducing the concept of Arterial Transit Time (ATT).

Chapter 5 describes the development of a new application of ASL techniques to the quantitative measurement of perfusion in the heart. A newly developed sequence, based on the Flow-sensitive Alternating Inversion Recovery (FAIR) labelling scheme and with a Look-Locker readout[31] is introduced. Validation of the sequence is described, first with Bloch equation simulations, to investigate the response of the sequence to a range of input T_1s, and also to investigate interactions between the slice profiles of the inversion pulse and readout pulses. Second, phantom experiments are described to test the robustness of the sequence to subject heart rate, and to investigate the difference in response in the calculations of T_1 and T_1*. An in vivo

study is then described in which ten healthy volunteers were each scanned twice, with the ASL protocol run on each in three slices with six measurements averaged in each slice, and with repeat scans run in the mid-ventricular slice. The quantitative MBF results of this study were compared with the literature values for various modalities, including MRI using ASL, MRI first-pass perfusion using an intravenous contrast agent, and PET perfusion, using ^{82}Rb and ^{15}O labelled tracers. The within-session and between-session repeat data were then used to perform a reproducibility study on the technique, where statistical measures for the inherent reproducibility and variability of the technique are described. Finally, results for the calculation of MBF values at a segmental level are presented, and compared with what little quantitative segmental MBF results exist in myocardial PET perfusion literature[3]. This work was published in the scientific journal Magnetic Resonance in Medicine[32].

Chapter 6 describes efforts to make measurement of MBF with cardiac ASL more practical and viable in a clinical setting. The approach to this was twofold. First, the sequence parameters were varied in order to optimise for SNR and minimise variation in the MBF calculation as far as possible in order to move towards a single breath hold, non-averaged implementation of the technique. This was first investigated in Bloch simulations, in order to determine the dominant source of variation in the MBF calculation, low SNR or artefact due to physiological motion. Following this, a three part in vivo study was carried out to first find the optimal value of the receive bandwidth and corresponding minimum achievable repetition time (TR), and secondly to find the optimal value of the readout flip angle. The third part of the study was to validate the myocardial T_1 maps produced from the ASL sequence against traditional Look-Locker T_1 mapping methods[30]. Finally, the online scanner reconstruction of the ASL data was expanded to facilitate the reconstruction of both T_1 maps and maps of MBF on the scanner console.

In conclusion, Chapter 7 summarises and discusses the work that has been pre-

sented in this thesis and describes possible future directions for development of the method.

References

[1] John A. Detre, John S. Leigh, Donald S. Williams, and Alan P. Koretsky. Perfusion imaging. *Magn. Reson. Med.*, 23(1):37–45, January 1992.

[2] John A. Detre, Weiguo Zhang, David A. Roberts, Afonso C. Silva, Donald S. Williams, Donald J. Grandis, Alan P. Koretsky, and John S. Leigh. Tissue specific perfusion imaging using arterial spin labeling. *NMR Biomed.*, 7(1-2):75–82, March 1994.

[3] P. Chareonthaitawee, P. A. Kaufmann, O. Rimoldi, and P. G. Camici. Heterogeneity of resting and hyperemic myocardial blood flow in healthy humans. *Cardiovascular research*, 50(1):151–161, April 2001.

[4] Y. Choi, S. C. Huang, R. A. Hawkins, W. G. Kuhle, M. Dahlbom, C. K. Hoh, J. Czernin, M. E. Phelps, and H. R. Schelbert. A simplified method for quantification of myocardial blood flow using nitrogen-13-ammonia and dynamic PET. *Journal of nuclear medicine : official publication, Society of Nuclear Medicine*, 34(3):488–497, March 1993.

[5] Osamu Manabe, Keiichiro Yoshinaga, Chietsugu Katoh, Masanao Naya, Robert A. deKemp, and Nagara Tamaki. Repeatability of rest and hyperemic myocardial blood flow measurements with 82Rb dynamic PET. *Journal of nuclear medicine : official publication, Society of Nuclear Medicine*, 50(1):68–71, January 2009.

[6] W. G. Kuhle, G. Porenta, S. C. Huang, D. Buxton, S. S. Gambhir, H. Hansen, M. E. Phelps, and H. R. Schelbert. Quantification of regional myocardial blood flow using 13N-ammonia and reoriented dynamic positron emission tomographic imaging. *Circulation*, 86(3):1004–1017, September 1992.

[7] J. Cal-Gonzalez, J. L. Herraiz, S. Espana, M. Desco, J. J. Vaquero, and J. M. Udias. Positron range effects in high resolution 3D PET imaging. In *2009 IEEE Nuclear Science Symposium Conference Record (NSS/MIC)*, pages 2788–2791. IEEE, October 2009.

[8] Michael Salerno and George A. Beller. Noninvasive assessment of myocardial perfusion. *Circulation. Cardiovascular imaging*, 2(5):412–424, September 2009.

[9] Grant T. Gullberg, Bryan W. Reutter, Arkadiusz Sitek, Jonathan S. Maltz, and Thomas F. Budinger. Dynamic single photon emission computed tomography–basic principles and cardiac applications. *Physics in medicine and biology*, 55(20), October 2010.

[10] Richard T. George, Michael Jerosch-Herold, Caterina Silva, Kakuya Kitagawa, David A. Bluemke, Joao A. Lima, and Albert C. Lardo. Quantification of myocardial perfusion using dynamic 64-detector computed tomography. *Investigative radiology*, 42(12):815–822, December 2007.

[11] SungMok Kim, YooNa Kim, and YeonHyeon Choe. Adenosine-stress dynamic myocardial perfusion imaging using 128-slice dual-source CT: optimization of the CT protocol to reduce the radiation dose. *The International Journal of Cardiovascular Imaging (formerly Cardiac Imaging)*, 29(4):875–884, October 2013.

[12] N. M. Wilke, M. Jerosch-Herold, A. Zenovich, and A. E. Stillman. Magnetic resonance first-pass myocardial perfusion imaging: clinical validation and future applications. *Journal of magnetic resonance imaging : JMRI*, 10(5):676–685, November 1999.

[13] S. D. Wolff, J. Schwitter, R. Coulden, M. G. Friedrich, D. A. Bluemke, R. W. Biederman, E. T. Martin, A. J. Lansky, F. Kashanian, T. K. Foo, P. E. Licato,

and C. R. Comeau. Myocardial first-pass perfusion magnetic resonance imaging: a multicenter dose-ranging study. *Circulation*, 110(6):732–737, August 2004.

[14] Martin A. Sieber, Philipp Lengsfeld, Jakob Walter, Heiko Schirmer, Thomas Frenzel, Fred Siegmund, Hanns-Joachim J. Weinmann, and Hubertus Pietsch. Gadolinium-based contrast agents and their potential role in the pathogenesis of nephrogenic systemic fibrosis: the role of excess ligand. *Journal of magnetic resonance imaging : JMRI*, 27(5):955–962, May 2008.

[15] Bernhard L. Gerber, Subha V. Raman, Krishna Nayak, Frederick H. Epstein, Pedro Ferreira, Leon Axel, and Dara L. Kraitchman. Myocardial first-pass perfusion cardiovascular magnetic resonance: history, theory, and current state of the art. *Journal of cardiovascular magnetic resonance*, 10(1):18+, April 2008.

[16] E. V. Di Bella, D. L. Parker, and A. J. Sinusas. On the dark rim artifact in dynamic contrast-enhanced MRI myocardial perfusion studies. *Magnetic resonance in medicine*, 54(5):1295–1299, November 2005.

[17] Frank Kober, Terrence Jao, Thomas Troalen, and Krishna S. Nayak. Myocardial arterial spin labeling. *Journal of cardiovascular magnetic resonance*, 18, April 2016.

[18] V. Belle, E. Kahler, C. Waller, E. Rommel, S. Voll, K. H. Hiller, W. R. Bauer, and A. Haase. In vivo quantitative mapping of cardiac perfusion in rats using a noninvasive MR spin-labeling method. *Journal of magnetic resonance imaging : JMRI*, 8(6):1240–1245, 1998.

[19] R. B. Buxton, L. R. Frank, E. C. Wong, B. Siewert, S. Warach, and R. R. Edelman. A general kinetic model for quantitative perfusion imaging with arterial spin labeling. *Magnetic resonance in medicine*, 40(3):383–396, September 1998.

[20] Seong-Gi Kim. Quantification of relative cerebral blood flow change by flow-sensitive alternating inversion recovery (FAIR) technique: Application to functional mapping. *Magn. Reson. Med.*, 34(3):293–301, September 1995.

[21] Seong-Gi Kim and Nikolaos V. Tsekos. Perfusion imaging by a flow-sensitive alternating inversion recovery (fair) technique: Application to functional brain imaging. *Magn. Reson. Med.*, 37(3):425–435, March 1997.

[22] B. P. Poncelet, T. M. Koelling, C. J. Schmidt, K. K. Kwong, T. G. Reese, P. Ledden, H. L. Kantor, T. J. Brady, and R. M. Weisskoff. Measurement of human myocardial perfusion by double-gated flow alternating inversion recovery EPI. *Magnetic resonance in medicine*, 41(3):510–519, March 1999.

[23] Zungho Zun, Eric C. Wong, and Krishna S. Nayak. Assessment of myocardial blood flow (MBF) in humans using arterial spin labeling (ASL): feasibility and noise analysis. *Magnetic resonance in medicine*, 62(4):975–983, October 2009.

[24] C. M. Wacker, M. Bock, A. W. Hartlep, G. Beck, G. van Kaick, G. Ertl, W. R. Bauer, and L. R. Schad. Changes in myocardial oxygenation and perfusion under pharmacological stress with dipyridamole: assessment using t*2 and t1 measurements. *Magnetic resonance in medicine*, 41(4):686–695, April 1999.

[25] Christian M. Wacker, Florian Fidler, Christian Dueren, Stefan Hirn, Peter M. Jakob, Georg Ertl, Axel Haase, and Wolfgang R. Bauer. Quantitative assessment of myocardial perfusion with a spin-labeling technique: preliminary results in patients with coronary artery disease. *Journal of magnetic resonance imaging : JMRI*, 18(5):555–560, November 2003.

[26] Thibaut Capron, Thomas Troalen, Benjamin Robert, Alexis Jacquier, Monique Bernard, and Frank Kober. Myocardial perfusion assessment in humans using

steady-pulsed arterial spin labeling. *Magnetic resonance in medicine*, 74(4):990–998, October 2015.

[27] David C. Alsop, John A. Detre, Xavier Golay, Matthias Günther, Jeroen Hendrikse, Luis Hernandez-Garcia, Hanzhang Lu, Bradley J. MacIntosh, Laura M. Parkes, Marion Smits, Matthias J. van Osch, Danny J. Wang, Eric C. Wong, and Greg Zaharchuk. Recommended implementation of arterial spin-labeled perfusion MRI for clinical applications: A consensus of the ISMRM perfusion study group and the european consortium for ASL in dementia. *Magnetic resonance in medicine*, 73(1):102–116, January 2015.

[28] Daniel R. Messroghli, Aleksandra Radjenovic, Sebastian Kozerke, David M. Higgins, Mohan U. Sivananthan, and John P. Ridgway. Modified Look-Locker inversion recovery (MOLLI) for high-resolution t1 mapping of the heart. *Magnetic resonance in medicine*, 52(1):141–146, July 2004.

[29] Daniel R. Messroghli, Andreas Greiser, Mirko Fröhlich, Rainer Dietz, and Jeanette Schulz-Menger. Optimization and validation of a fully-integrated pulse sequence for modified look-locker inversion-recovery (MOLLI) t1 mapping of the heart. *Journal of magnetic resonance imaging : JMRI*, 26(4):1081–1086, October 2007.

[30] Stefan K. Piechnik, Vanessa M. Ferreira, Erica Dall'Armellina, Lowri E. Cochlin, Andreas Greiser, Stefan Neubauer, and Matthew D. Robson. Shortened modified Look-Locker inversion recovery (ShMOLLI) for clinical myocardial t1-mapping at 1.5 and 3 t within a 9 heartbeat breathhold. *Journal of cardiovascular magnetic resonance*, 12, November 2010.

[31] D. C. Look and D. R. Locker. Time saving in measurement of NMR and EPR relaxation times. *Review of Scientific Instruments*, 41(2):250–251, February 1970.

[32] Graeme A. Keith, Christopher T. Rodgers, Michael A. Chappell, and Matthew D. Robson. A look-locker acquisition scheme for quantitative myocardial perfusion imaging with FAIR arterial spin labeling in humans at 3 tesla. *Magnetic Resonance in Medicine*, September 2016.

Chapter 2

Theory of Magnetic Resonance Imaging

The phenomenon of Nuclear Magnetic Resonance in solids and liquids was first described in 1946, separately, by Felix Bloch[1] working at Stanford University and Edward Purcell[2], working at MIT. Their work followed on from that of Isidor Rabi[3] who had described and measured NMR in molecular beams. In 1952, Bloch and Purcell were jointly awarded the Nobel prize in physics for their work.

2.1 Nuclear Spin

In the nucleus of an atom, where there are an even number of protons and neutrons present, the nucleons will pair up, just as is observed with orbital electrons. Where the number of protons and/or neutrons is odd and therefore pairing is impossible, there arises the phenomenon of nuclear spin, whereby a nucleus will behave as though it is revolving about its own axis. Spin is quantified in terms of the spin quantum number, I, which can take a value of integer or half-integer form[4], where each unpaired nucleon is said to contribute a spin of 1/2. The first case, of an integer value of I, occurs where the mass number of the atom in question is even. An example of this

would be atomic Nitrogen, ^{14}N, which has both an unpaired proton and neutron, thus giving it a spin of I = 1. An example of the latter, more common case half-integer would be hydrogen, ^{1}H, the nucleus of which consists of a single proton, giving it a spin of I = 1/2.

The presence of this intrinsic nuclear spin means that the nucleus possesses the property of angular momentum along its spin axis. This is described by the equation,

$$\mathbf{p} = \hbar\mathbf{I} \tag{2.1}$$

where $\mathbf{p}$ is the angular momentum and $\hbar$ is Planck's constant divided by 2π, representing the relationship between the nucleon's energy and its angular frequency. As the nucleus of any atom has a positive total charge due to the protons and the neutrons, which have no net charge, the system amounts to a spinning positive charge. This rotation of charge creates a magnetic field around the nucleus with an associated direction, the magnetic moment, $\boldsymbol{\mu}$. This is related to the angular momentum of the spinning nucleus by,

$$\boldsymbol{\mu} = \gamma\mathbf{p} \tag{2.2}$$

where γ is a constant, for a given nucleus, known as the gyromagnetic ratio (in rad s^{-1} T^{-1}).

As this nuclear magnetic field has direction, with all the associated vector properties, the nucleus essentially acts as a small bar magnet with the magnetic moment representing the north/south axis, as depicted in Figure 2.1. In magnetic resonance applications, it is how this nuclear magnetic moment behaves when placed in an external magnetic field that is of interest. In the absence of a strong magnetic field (on Earth the nucleus will always be subject to the planet's magnetic field of the order of tens of μT) the magnetic moments of the nuclei will take on random orientation.

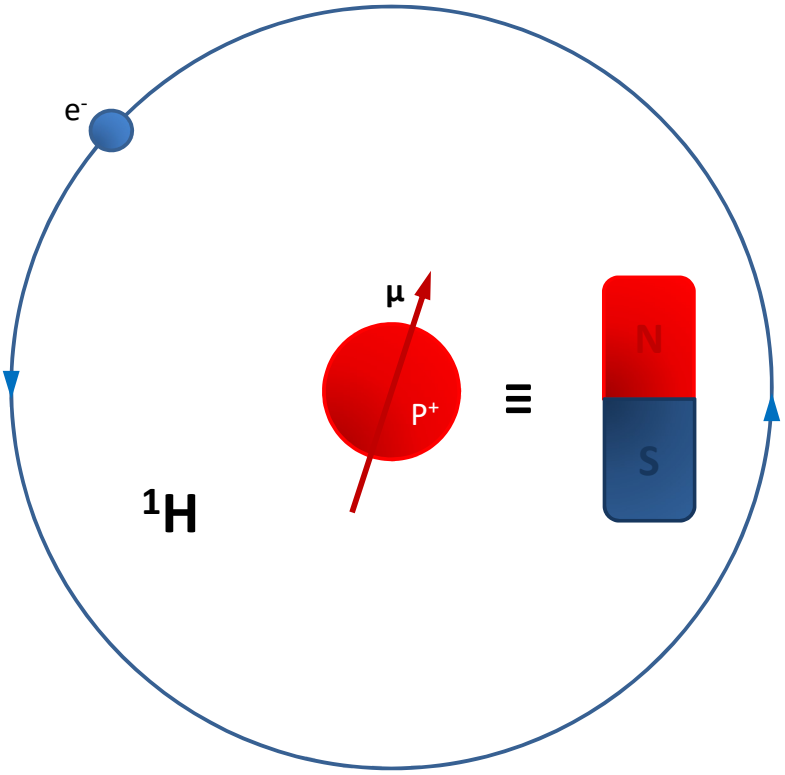


Figure 2.1: The hydrogen atom. The nucleus obtains magnetic moment with the property of spin, becoming equivalent to a bar magnet.

When an external magnetic field, $\mathbf{B}_0$, is applied however, the moments will tend to align with the direction of $\mathbf{B}_0$[5]. In order to understand the behaviour of the magnetic moment in an external field it is necessary to describe two models, based on quantum and classical mechanics.

2.2 The Quantum and Classical Models

Where imaging applications are concerned, the nucleus of most interest is that of ^{1}H which has a spin of I = 1/2. According to the quantum model, the ^{1}H nucleus has two possible energy states in the external field (equal to 2I+1). Some of the nuclei will align parallel with the direction of $\mathbf{B}_0$. These "spin-up" nuclei occupy the lower

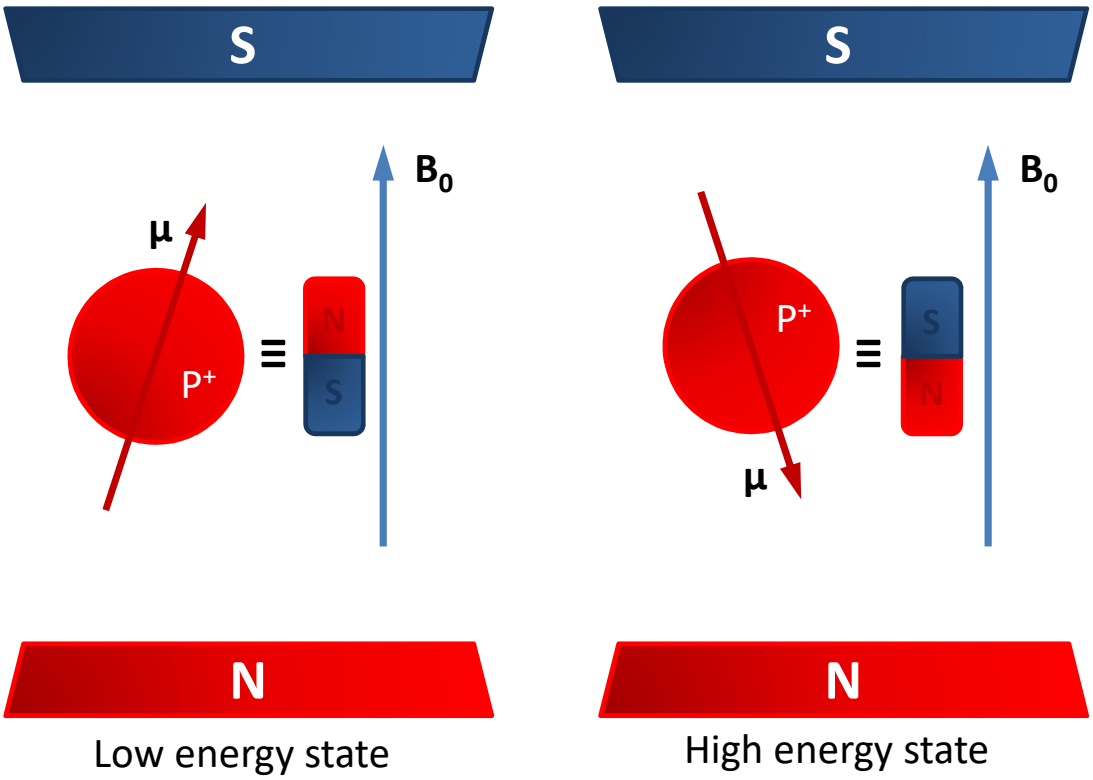


Figure 2.2: The low and high energy states. Those nuclei with low energy will align with the $\mathbf{B}_0$ field. Those with high energy will be able to oppose it.

energy state. Some of the nuclei will align anti-parallel to the direction of $\mathbf{B}_0$. These are known as "spin-down" nuclei and occupy the higher energy state (Figure 2.2).

How the nuclei align is dependent on the strength of the external field and on the thermal energy of the nucleus in question. Those nuclei with low thermal energy will not be able to oppose the $\mathbf{B}_0$ field, whereas those with greater thermal energy will. As the strength of the field is increased, the energy required for the nuclei to oppose the field also increases. When the system is at equilibrium there will always be a greater population of spins in the lower energy state. This gives rise to a net magnetisation parallel to the $\mathbf{B}_0$ direction.

The number of nuclei occupying each level is easily predicted for the I = 1/2 system with just two discrete energy levels. If N_l is the number of particles in the lower energy population and N_u the number in the higher energy population then,

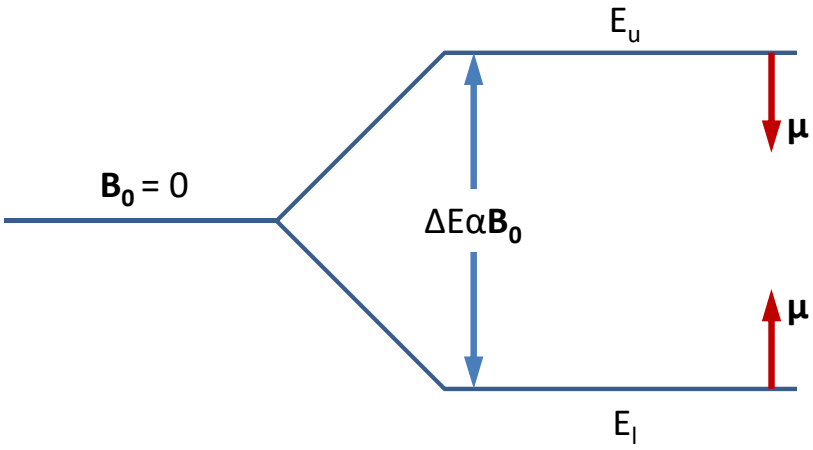


Figure 2.3: The energy level diagram for I = 1/2 system

$$\frac{N_l}{N_u} = exp\left(\frac{\Delta E}{kT}\right) \tag{2.3}$$

where ΔE is the difference in energy between the two levels (as shown in Figure 2.3), k is Boltzmann's constant ($k = 1.381 \times 10^{-23} JK^{-1}$) and T is the absolute temperature in Kelvin.

It is the difference in the size of the two populations which is important however, as the NMR signal (discussed later) is proportional to this fractional difference as described by,

$$\frac{(N_l - N_u)}{N_u} \approx \frac{\hbar \boldsymbol{\omega_L}}{kT} = \frac{\hbar \gamma \mathbf{B_0}}{kT} \tag{2.4}$$

At this point it becomes useful to introduce the model based on classical mechanics. Under the influence of the external magnetic field, each spinning nucleus experiences an additional rotational motion known as precession, as its magnetic moment follows a circular path about the $\boldsymbol{B_0}$ direction[5]. This precession is represented in Figure 2.4. The precession of the nucleus takes place at a frequency known as the Larmor frequency, $\boldsymbol{\omega_L}$, which can be related to $\boldsymbol{B_0}$ by,

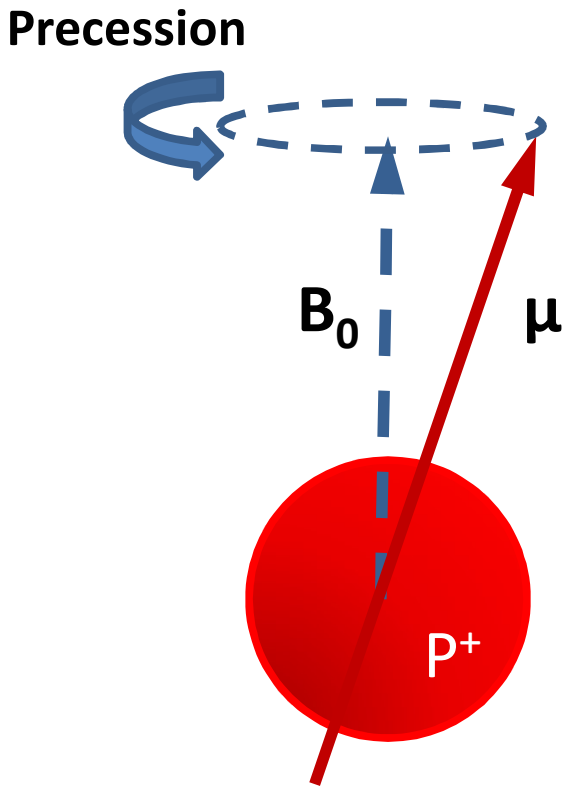


Figure 2.4: The precession of the magnetic moment μ of the hydrogen nucleus around the external $\boldsymbol{B_0}$ field.

$$\boldsymbol{\omega_L} = -\gamma \mathbf{B_0} \tag{2.5}$$

where γ is the gyromagnetic ratio. However it is not the behaviour of individual spins which is of interest but the combined effect of all the nuclei of interest in the sample. This is known as the bulk magnetisation, $\mathbf{M}$, where,

$$\mathbf{M} = \sum \boldsymbol{\mu} \tag{2.6}$$

which represents the sum of the effects of the fractional excess of spins as predicted in Equation 2.4.

2.3 Resonance and the Rotating Frame

The magnetic moments of the individual nuclei all precess about the direction of $\boldsymbol{B_0}$ as described, however they are not in phase. This means that the transverse components of the magnetisation cancel at thermal equilibrium and there is only the longitudinal component in the direction of $\boldsymbol{B_0}$, known as the equilibrium magnetisation, M_0. However, before this can be used to acquire an NMR signal, the magnetisation, $\mathbf{M}$, must be perturbed from its equilibrium state, so that it precesses about the direction of $\boldsymbol{B_0}$ at the Larmor frequency, as shown in Figure 2.5. This perturbation is achieved by making use of the phenomenon of resonance.

When a nucleus is exposed to energy which oscillates at a frequency at, or close to, its Larmor frequency, resonance occurs. In this regime, the nucleus is able to gain energy from the external source. In the quantum model, this means that nuclei in the lower energy state can gain enough energy to move to the higher energy state. Energy oscillating at $\boldsymbol{\omega_L}$ for the ^{1}H nucleus at all clinical MRI field strengths corresponds to electromagnetic energy in the radiofrequency (RF) range.

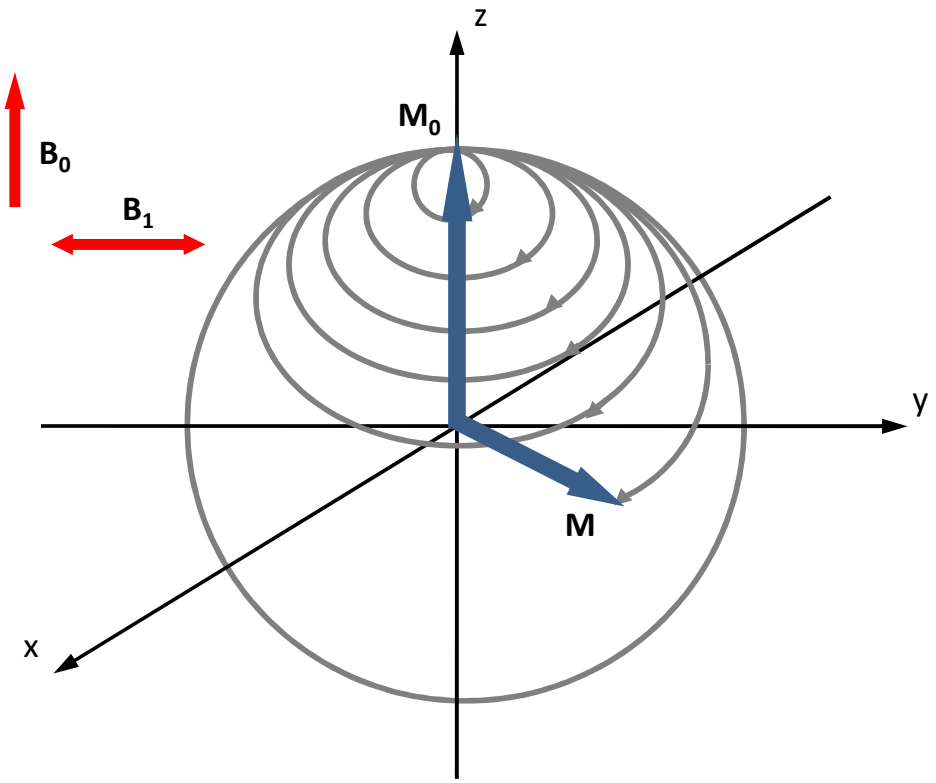


Figure 2.5: The behaviour of the magnetisation in the laboratory frame.

To observe what occurs in the classical model when RF energy is applied, we must introduce the idea of the rotating frame of reference. When the stationary, laboratory frame is used it is difficult to assess what the effect of applying a radiofrequency pulse is. Instead we use axes which are said to rotate around the z-axis (the direction of $\mathbf{B}_0$) at the Larmor frequency of the nucleus in question. In the rotating frame the axes in the rotating, transverse plane are known as x′ and y′ (where z′ would be the same as z).

When a resonant RF pulse (also known as a $\boldsymbol{B_1}$ field) is applied, the magnetisation is perturbed such that it moves out of alignment with the external magnetic field, $\boldsymbol{B_0}$. The angle that is achieved from the $\boldsymbol{B_0}$ direction is known as the flip angle. If an RF pulse is applied along the x′-axis, of amplitude and duration such that the net magnetisation, $\mathbf{M}$, is flipped through an angle of 90° then in the rotating frame the vector will now lie along the y′-axis. This means that in the laboratory frame the magnetisation is now precessing about the direction of $\boldsymbol{B_0}$ in the x-y plane. According to Faraday's laws of induction, if a receiver coil is placed in an area of magnetic flux, a voltage will be induced in the coil. As the magnetisation, $\mathbf{M}$, is precessing at the Larmor frequency in the transverse plane, an induced voltage will be produced in the coil. This voltage is the NMR signal. When the $\boldsymbol{B_1}$ field is removed the induced voltage begins to decrease, thus giving rise to the characteristic Free Induction Decay (FID) signal, as shown in Figure 2.6.

2.4 Relaxation Times and Pulse Sequences

In the absence of the $\mathbf{B}_1$ field, the magnetisation begins to lose the energy absorbed from the RF pulse and return to its equilibrium state. The longitudinal component of the magnetisation, M_z, recovers towards its equilibrium value, M_0. This is known as spin-lattice relaxation. It is caused by the nuclei exchanging energy with their

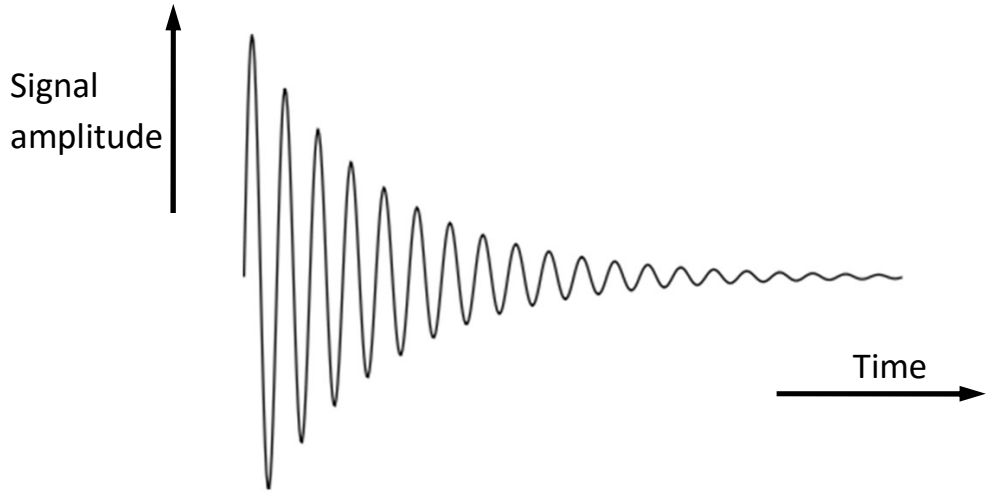


Figure 2.6: The Free Induction Decay (FID) signal.

surroundings (or lattice). It is described by the time constant T_1, which is defined as the time it takes for the longitudinal magnetisation to recover 63% (from [1-1/e]) of its equilibrium value. Typical values of the T_1 relaxation time in the heart are 966 ± 48 ms at 1.5 T and 1166 ± 60 ms at 3T for healthy myocardium[6] and 1800 ± 250 ms at 1.5 T[7] and 2074 ± 139 ms at 3 T[8]. It can be inferred from these values that the value of T_1 is dependent on the applied external field $\boldsymbol{B_0}$. The efficiency of the T_1 relaxation process is related to the correlation time, τ_c, of the molecule in question, which describes its molecular tumbling rate as the time it takes for the molecule to rotate by one radian. Molecular motion is one of the major drivers of magnetic field fluctuations local to a spin. The longitudinal relaxation is most efficient, and therefore has a lower value of T_1, when τ_c is closest to the larmor frequency. As $\boldsymbol{B_0}$ increases the larmor frequency also increases, such that the value of $\boldsymbol{\omega_L}$ is further from τ_c, meaning that the relaxtion process is less efficient and therefore the value of the relaxation constant, T_1, also increases.

In the transverse plane the magnetisation begins to decay due to the effects of dephasing. This occurs as the magnetic field of each nucleus interacts with the fields of its neighbours, causing the nuclei begin to precess at slightly different rates which

means that the magnetic moments of the nuclei begin to dephase leading the transverse magnetisation, M_{xy}, to decay to zero. This is known as spin-spin relaxation and is described by the time constant T_2, the time it takes for 63% (from [1/e])of the transverse magnetisation to be lost. If the longitudinal magnetisation fully recovers then all transverse magnetisation will be lost so $T_2 \leq T_1$.

In reality, inhomogeneities in the magnetic field, $\boldsymbol{B_0}$, mean that different parts of the sample experience a slightly different value of magnetic field strength. This means that nuclei which experience a different $\boldsymbol{B_0}$ field will also have a slightly different precessional frequency. This also contributes to the dephasing of the transverse magnetisation and is known as pseudo-relaxation. The combined effects of the two components of dephasing lead to the decay of the FID. This is described by the time constant T_2^*, defined as,

$$\frac{1}{T_2^*} = \frac{1}{T_2} + \gamma \Delta \mathbf{B_0} \tag{2.7}$$

where γ is the gyromagnetic ratio and $\Delta \mathbf{B}_0$ is the variation of the external magnetic field across the sample region.

By applying particular sequences of radiofrequency pulses to a sample the values of T_1 and T_2 can be measured. In order to calculate the value of T_1, a sequence known as Inversion Recovery can be used (Figure 2.7). This sequence employs a 180° pulse followed, after an inversion time, TI, by a 90° pulse.

At the 180° pulse the longitudinal magnetisation, M_z, is flipped to align with the negative z-axis. After the pulse is applied, M_z begins to recover towards its equilibrium value (shrinking up the z-axis), as shown in Figure 2.8. Following an inversion time, TI, the 90° pulse is applied, which causes the magnetisation to precess in the transverse plane, where it begins to dephase, producing the FID signal. By repeating the sequence, altering the value of TI to allow varying amounts of relaxation, a curve can be drawn to show a value proportional to the longitudinal magnetisation,

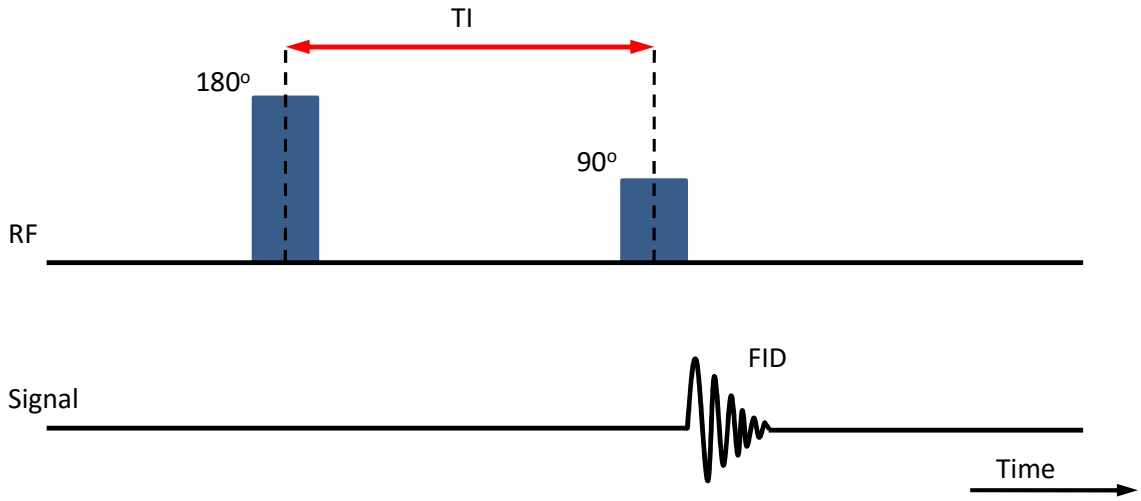


Figure 2.7: A simple Inversion Recovery NMR pulse sequence, with a 180° pulse followed by a 90° pulse after time TI, producing an FID.

M_z, against time, thus tracing its recovery. By fitting the curve to the equation,

$$M_z(TI) = M_0 \left[1 - 2exp\left(-\frac{TI}{T_1}\right)\right] \tag{2.8}$$

where M_z (TI) is the longitudinal magnetisation at time TI (equivalent to the signal at that time) and M_0 is the equilibrium value of the magnetisation, a value for the spin-lattice relaxation time, T_1, can be calculated.

2.5 Magnetic Field Gradients and Image Formation

Magnetic Resonance Imaging (MRI) is a powerful imaging technique based on the above outlined principles of NMR. It has the advantage over other imaging techniques, such as Positron Emission Tomography (PET), Single Photon Emission Computed Tomography (SPECT) and x-ray Computed Tomography (CT), of not carrying with it a dose of ionising radiation for the patient. In order to make use of the phenomenon of NMR to form an image, we must be able to localise and selectively excite those

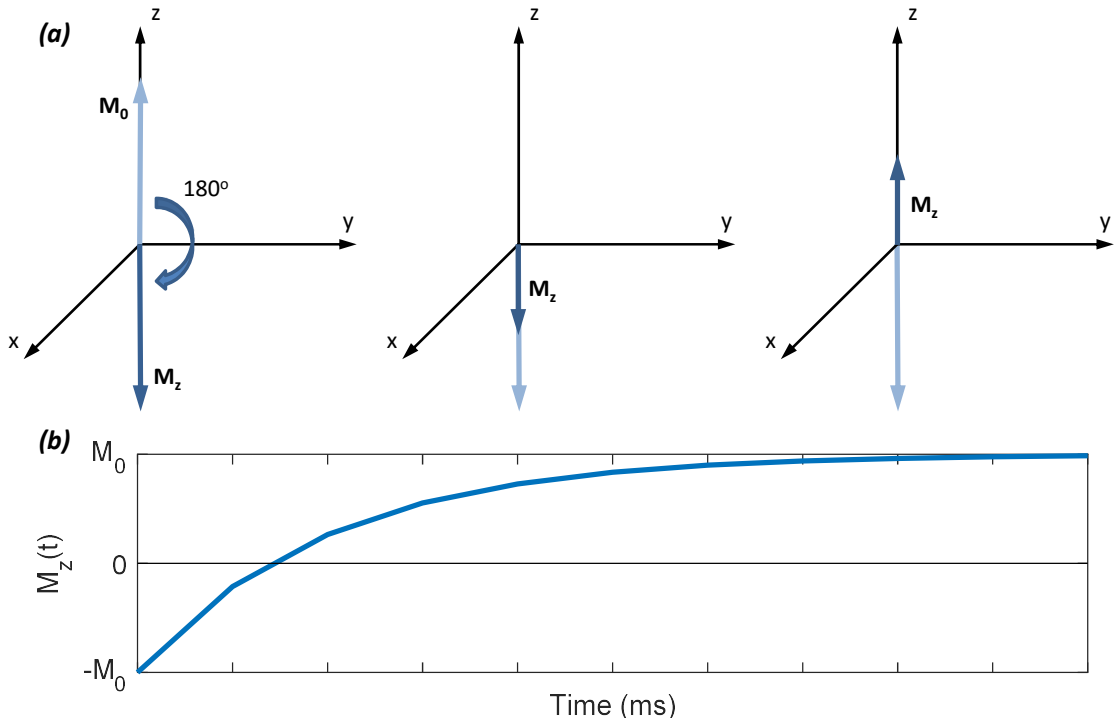


Figure 2.8: Inversion Recovery and longitudinal relaxation of the magnetisation showing, (a) the behaviour of the magnetisation vector, and (b) the value of M_z over time.

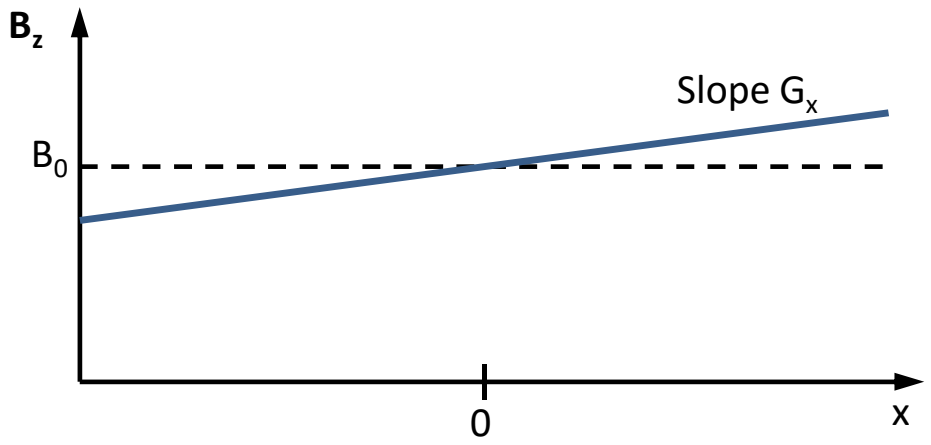


Figure 2.9: A magnetic field gradient of strength G_x applied in the x-direction.

spins within the region of interest, preferentially detect the signal of those spins, and reconstruct that information into an image. To achieve this we must introduce the concept of magnetic field gradients.

2.5.1 Frequency Encoding

An MRI scanner has three additional coils fitted within the bore of the main magnet for the purpose of producing magnetic field gradients. They do this along the three orthogonal axes x, y and z (the direction of $\boldsymbol{B_0}$ in the majority of modern clinical systems). When a current is passed through one of these coils it produces a field which varies linearly with position, as shown in Figure 2.9. The total field is always defined along the z-axis. If a gradient, G_x, is applied in the x-direction, where $G_x = dB_z/dx$, the field experienced is therefore calculated as,

$$B_z(x) = \mathbf{B_0} + xG_x \tag{2.9}$$

where x is the position in the x-direction and G_x is the strength of the gradient in T m^{-1}. The gradient is applied, such that, at the centre of the magnet (x=0, or

isocentre), the contribution of the gradient is zero and the field experienced is simply $\boldsymbol{B_0}$. As the x-position is varied, however, the strength of the field experienced will also vary. This means that the frequency of the precession of the nuclear spins will also vary with position. The resonant frequency of a nucleus under the influence of a gradient in the x-direction is therefore a function of its position in x (but not y or z). The NMR signal which is received from nuclei at different positions in x will be of different frequency, thus providing spatial information in the x-direction. This is known as Frequency Encoding or the readout gradient.

In order to acquire all the necessary information, the signal must be observed in the presence of the frequency encoding gradient, as shown in Figure 2.10. When current is passed to the gradient coil it takes time to achieve the required strength. This is known as the ramp time, and gives rise to the characteristic trapezoid shape of gradients in MR pulse sequence diagrams. If the signal is collected straight after the 90° pulse then the beginning of the FID, which contains important information about lower spatial frequencies, may be lost. Instead, immediately after the radiofrequency pulse, a strong, negative gradient is applied. As this gradient is causing the spins to precess at slightly different frequencies, dephasing begins to occur. This is then quickly followed by a weaker, positive gradient which begins to rephase the magnetisation vectors. As this rephasing occurs the MR signal is produced, with the maximum signal occurring at the point where the area under the rephase gradient is equal to the area under the dephase gradient. This refocussed signal is known as the gradient echo and contains the frequency encoding information defined above. The echo can then be sampled at n discrete points for an image of n x n pixels.

2.5.2 Slice Selection

In order to form an MR image we want to be able to excite only those spins within a thin slice in the sample. This is done by selective excitation. A gradient is

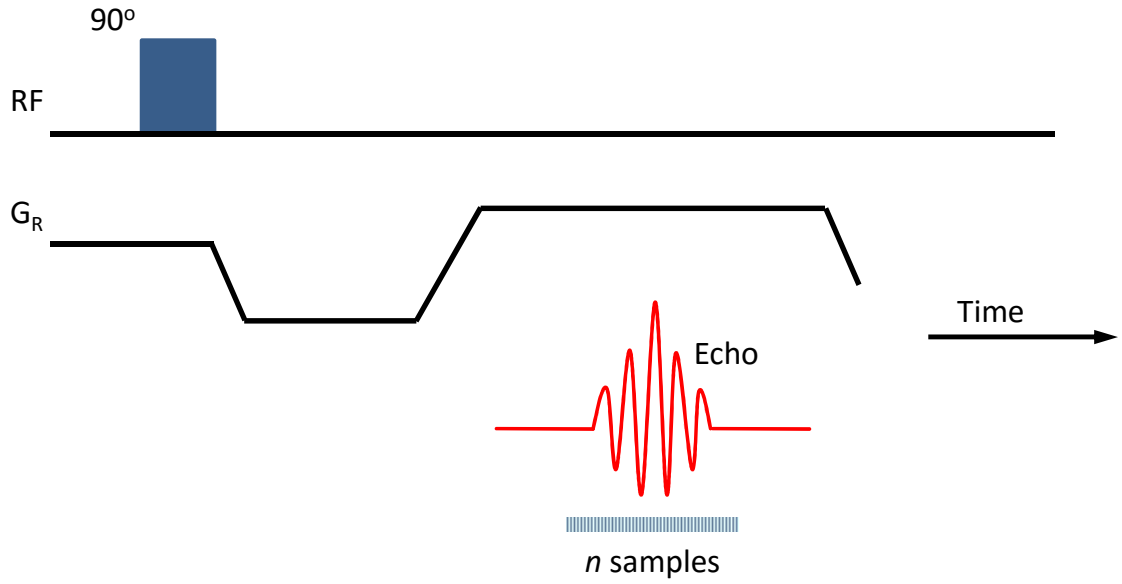


Figure 2.10: A simple Gradient Echo NMR pulse sequence. Following a 90° pulse, the readout gradient, G_R is applied to first dephase, then rephase the NMR signal to form an echo at time TE.

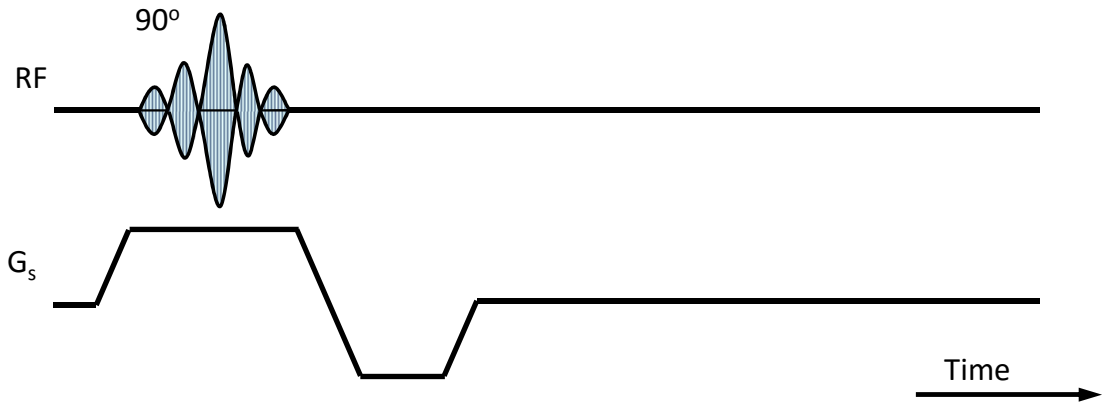


Figure 2.11: A sinc-shaped RF pulse and slice-selection gradient.

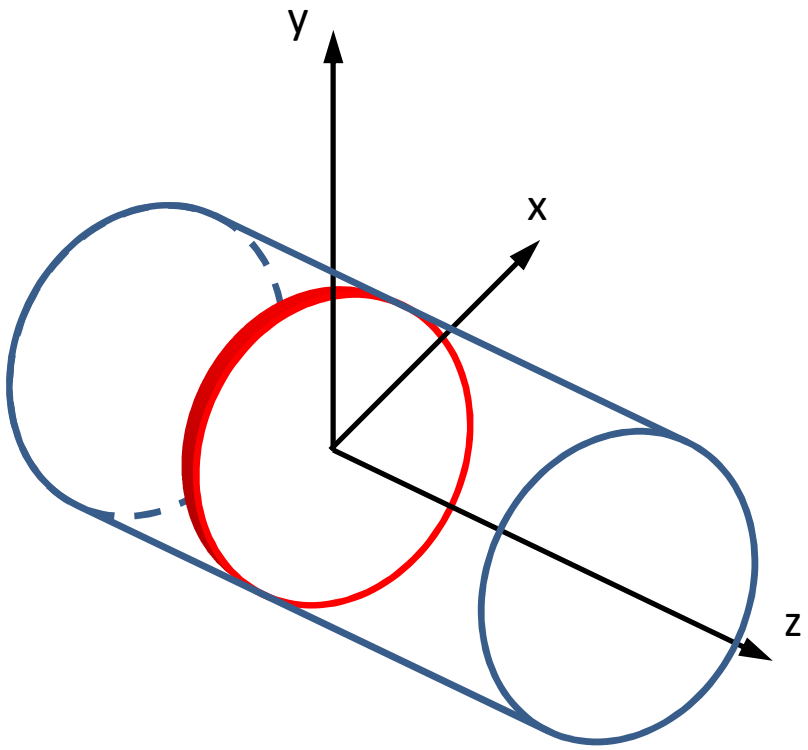


Figure 2.12: A thin slice in a cylindrical sample is excited by the application of slice selection and a shaped RF pulse.

applied in the z-direction during the time for which the RF pulse is on. This means that the precessional frequency of spins will vary along the length of a sample in the z-direction. The slice selection gradient is used in conjunction with a radiofrequency pulse with a shaped envelope, for instance a Gaussian or sinc shaped pulse (Figure 2.11). This shaped pulse contains a small range of frequencies which centre on the Larmor frequency, $\boldsymbol{\omega_L}$. Only those spins whose precessional frequencies are contained within the bandwidth of the pulse will produce an MR signal, so a thin slice in the sample which centres on the point z = 0, where the spins precess at $\boldsymbol{\omega_L}$ will be excited, as seen in Figure 2.12. The selection gradient is then immediately followed by a negative gradient lobe, the area under which is half the size of the preceding positive gradient lobe. This brings the spins back into phase across the slice.

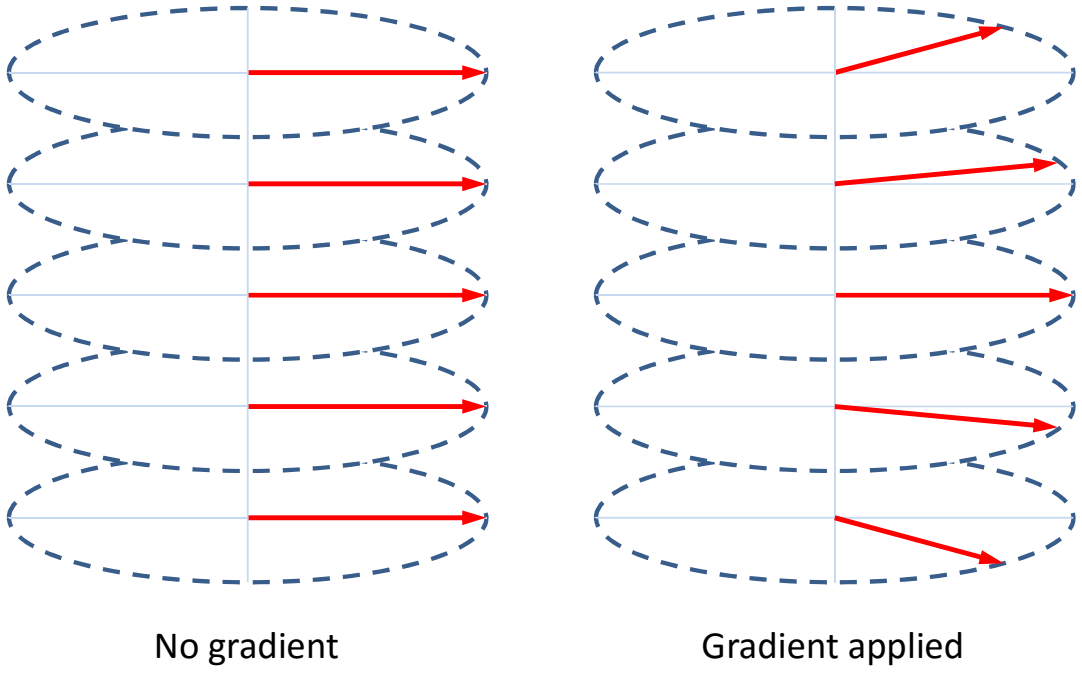


Figure 2.13: The effect of phase encoding. When a gradient is applied the spins begin to precess at different frequencies. When the gradient is removed the spins return to the Larmor frequency while retaining their different phase angles.

2.5.3 Phase Encoding

The third gradient, in the y-direction, is used for phase-encoding. Following the application of the excitation RF, a gradient pulse is applied in order to dephase the spins along the y-direction as shown in Figure 2.13. When the gradient is turned off, the spins return to precessing at the Larmor frequency, but in the dephased state introduced by the gradient. Thus, the spins are said to be "phase encoded" in the y-direction, as different spin locations along this axis will have different phase angles, which increase with the strength of the gradient. The spins remain phase encoded until another gradient is applied, or the signal decays with T_2 relaxation. The phase encoding gradient is incremented in steps for each repetition of the sequence as shown in Figure 2.14. For an image of n x n pixels, there will be n phase-encoding steps. This requirement can be reduced by the use of parallel imaging techniques, where data

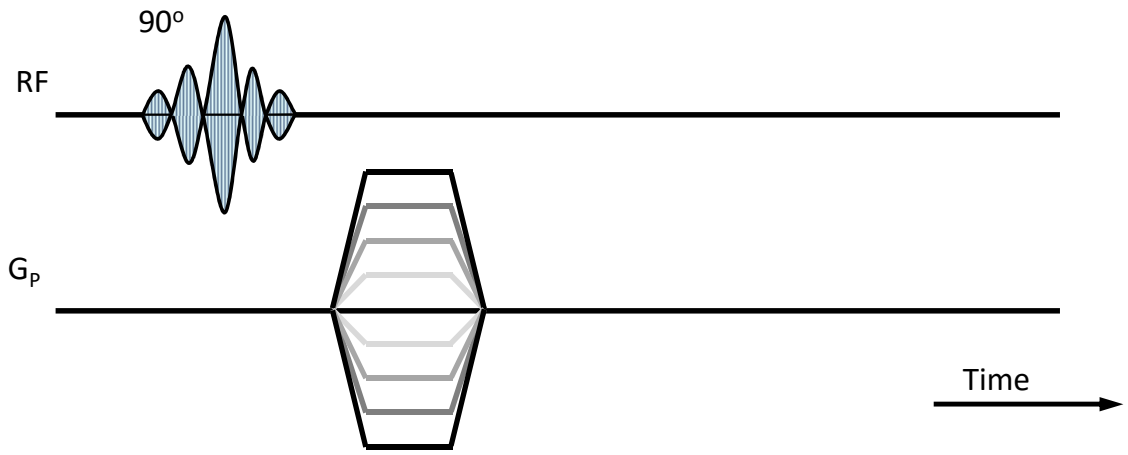


Figure 2.14: The phase encoding gradient. Each repetition of the sequence employs a different strength of gradient following the application of the RF excitation pulse.

acquired with a phased array coil is undersampled in the phase encoding direction and reconstructed by exploiting the sensitivity profiles of individual receive elements.

2.5.4 Spin Warp

The three orthogonal gradients, employing the above described principles of frequency encoding, selective excitation and phase encoding, can be applied together to form the basic spin warp imaging sequence, which was developed in Aberdeen in the late 1970s[9]. The sequence is repeated n times for an image of n x n pixels. From this a matrix of n rows of raw data is collected from the sequence. The process of two-dimensional Fourier transformation (described below) can then be performed on the data to provide the pixel intensity information necessary to form an image. Figure 2.15 shows the basic gradient echo spin warp sequence with readout, slice selection and phase-encoding gradients.

2.5.5 k-space and the Fast Fourier Transform

The basic Spin Warp experiment described above provides an n x n matrix. However, these raw data represent a 2D map in the spatial frequency domain[10], not the

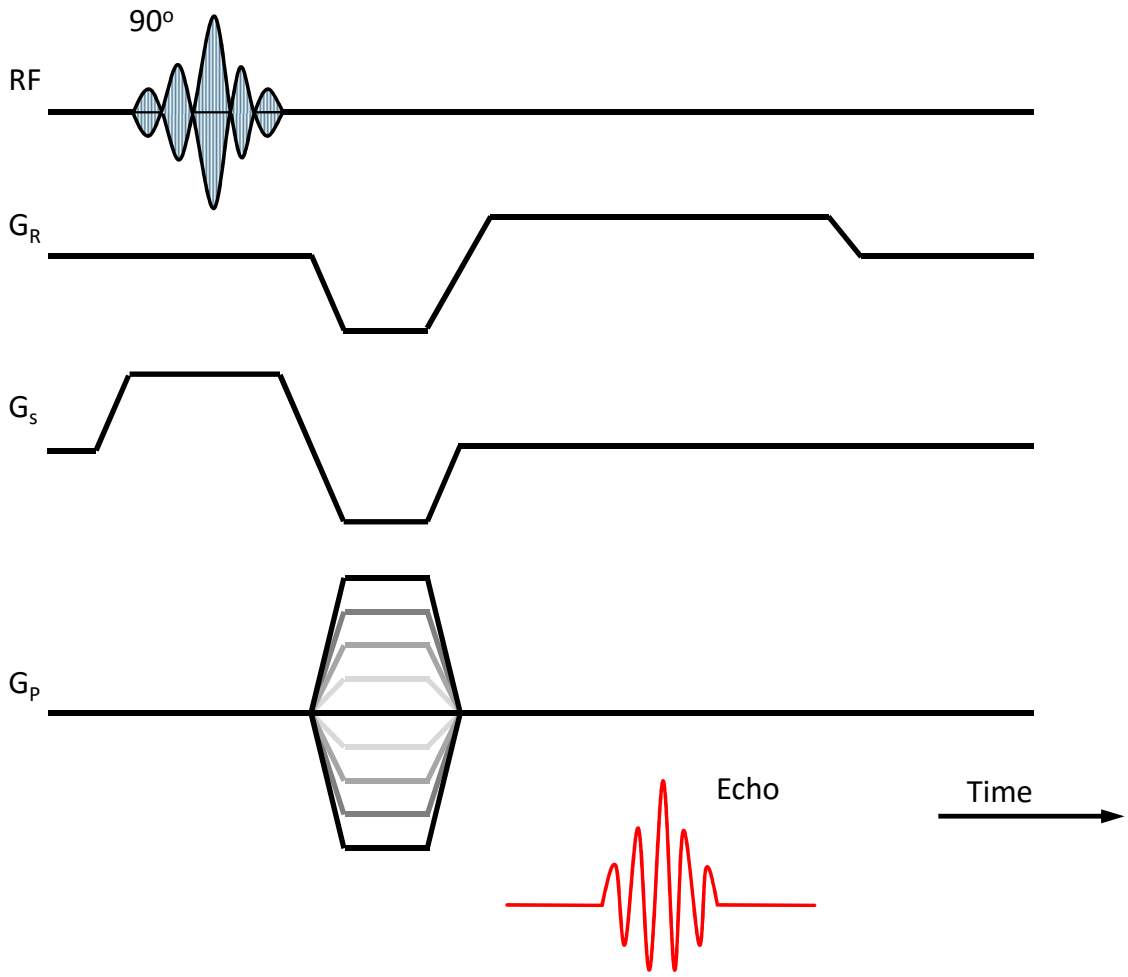


Figure 2.15: The Spin Warp imaging pulse sequence[9], incorporating a selective RF excitation pulse, a readout gradient, G_R, a slice selection gradient, G_S, and a phase encoding gradient, G_P.

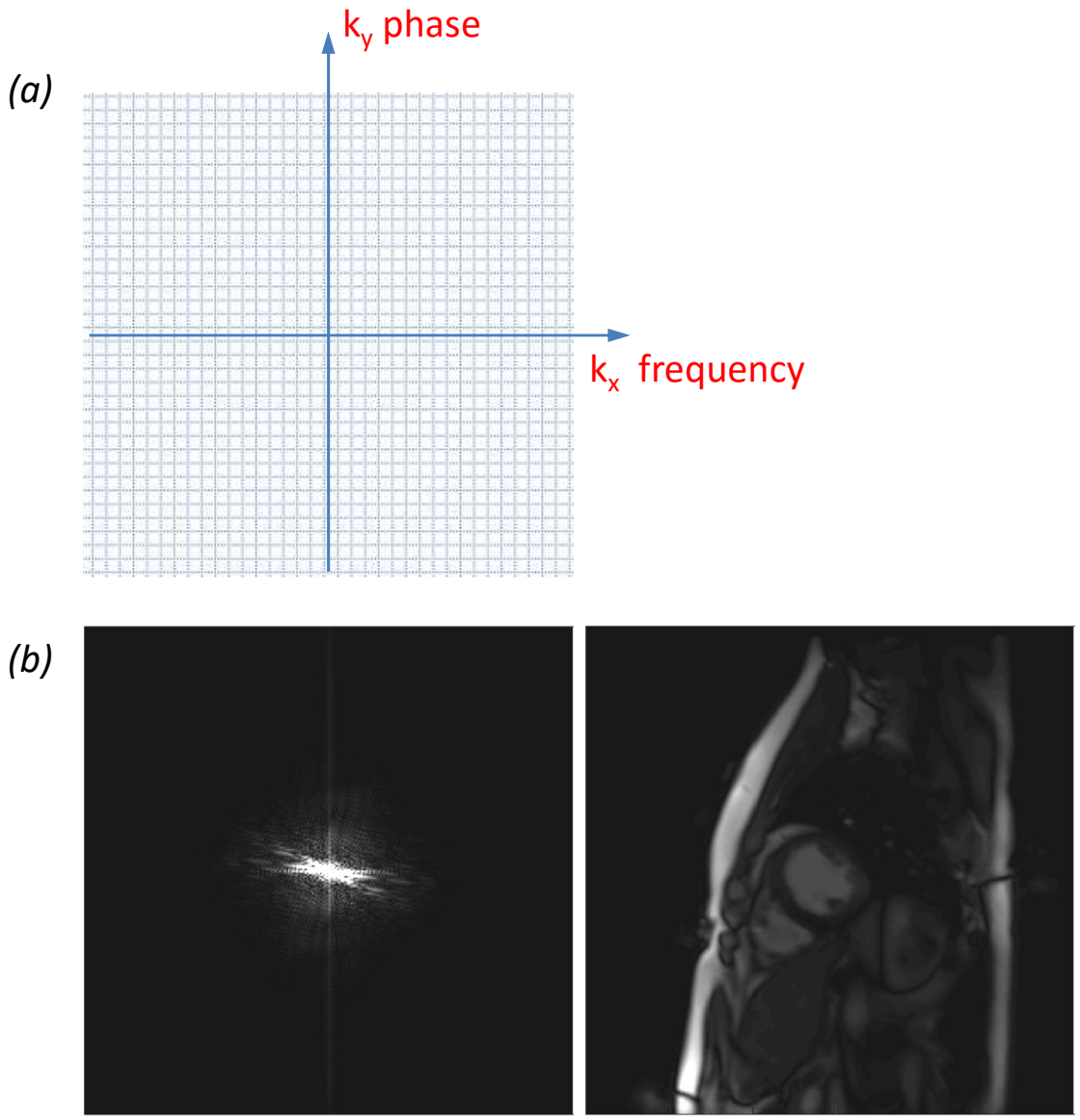


Figure 2.16: The k-space domain. (a) The k-space axes representing frequency encoding in the x-direction and phase encoding in the y-direction, and (b) some k-space data and it's corresponding magnitude image from 2D fast Fourier transform.

final MR image. This domain is known in MR as k-space. The digitised MR signal collected during a readout fills a single line of the k-space domain. Upon the next acquisition, the step change in the phase encode gradient causes a different line to be filled. Thus a discrete point in k-space has coordinates of (k_x,k_y) where, in the frequency encoding direction,

$$k_x = \bar{\gamma} G_{FE} m \Delta t \tag{2.10}$$

and in the phase encoding direction,

$$k_y = \bar{\gamma} n \Delta G_{PE} \tau \tag{2.11}$$

where $\bar{\gamma}$ is the gyromagnetic ratio divided by 2π, G_{FE} and ΔG_{PE} are the frequency encoding gradient and change in the phase encoding gradient respectively, m and n are the sample numbers in the FE and PE directions, Δt is the sampling time and τ is the duration of ΔG_{PE}[11]. A representation of the k-space axes is shown in Figure 2.16(a), and an example of acquired k-space data is shown in Figure 2.16(b) along with the corresponding MR image.

It can be observed in 2.16(b) that much of the spatial frequency information in the k-space data lies in the centre, in the low frequency region. This is where the gross information concerning contrast and signal is located. The higher frequency information, around the edges of the k-space domain, represent the sharpness and boundaries in the image. The position in image space (x,y) and the spatial frequency (k_x,k_y) comprise a Fourier transform pair. This means that the encoded frequency and phase information constituting k-space can be used to produce an MR image by the process of two-dimensional Fourier transform (2DFT).

The basis of the Fourier transform is that the MR signal can be represented as a series of sine and cosine functions of different amplitude and frequency. The k-space

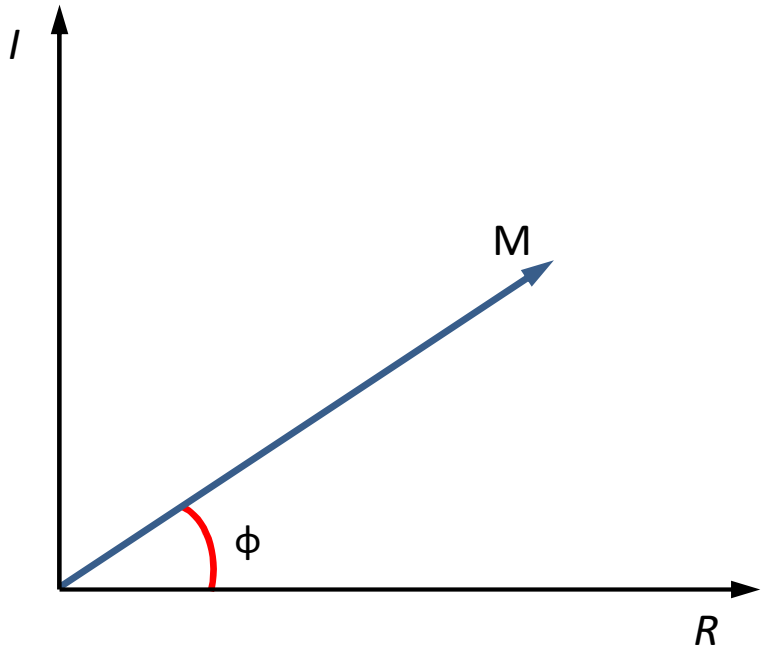


Figure 2.17: Magnitude and phase values are calculated form real and imaginary parts following 2D Fourier transform of raw k-space data.

data are the coefficients of the sine/cosine waves which give the signal depicted in the MR image and are the Fourier transform pair of the spin density in the image object. Image reconstruction in Fourier-based MR imaging involves performing a 2DFT (Fourier transforming in both the frequency and phase directions) to give a complex matrix which is used to determine the magnitude (M) and phase (ϕ) of the resulting images(s) from,

$$M = \sqrt[2]{R^2 + I^2} \tag{2.12}$$

and,

$$\phi = tan^{-1}\frac{I}{R} \tag{2.13}$$

where R and I are the real and imaginary parts of the complex matrix. This is further described in Figure 2.17.

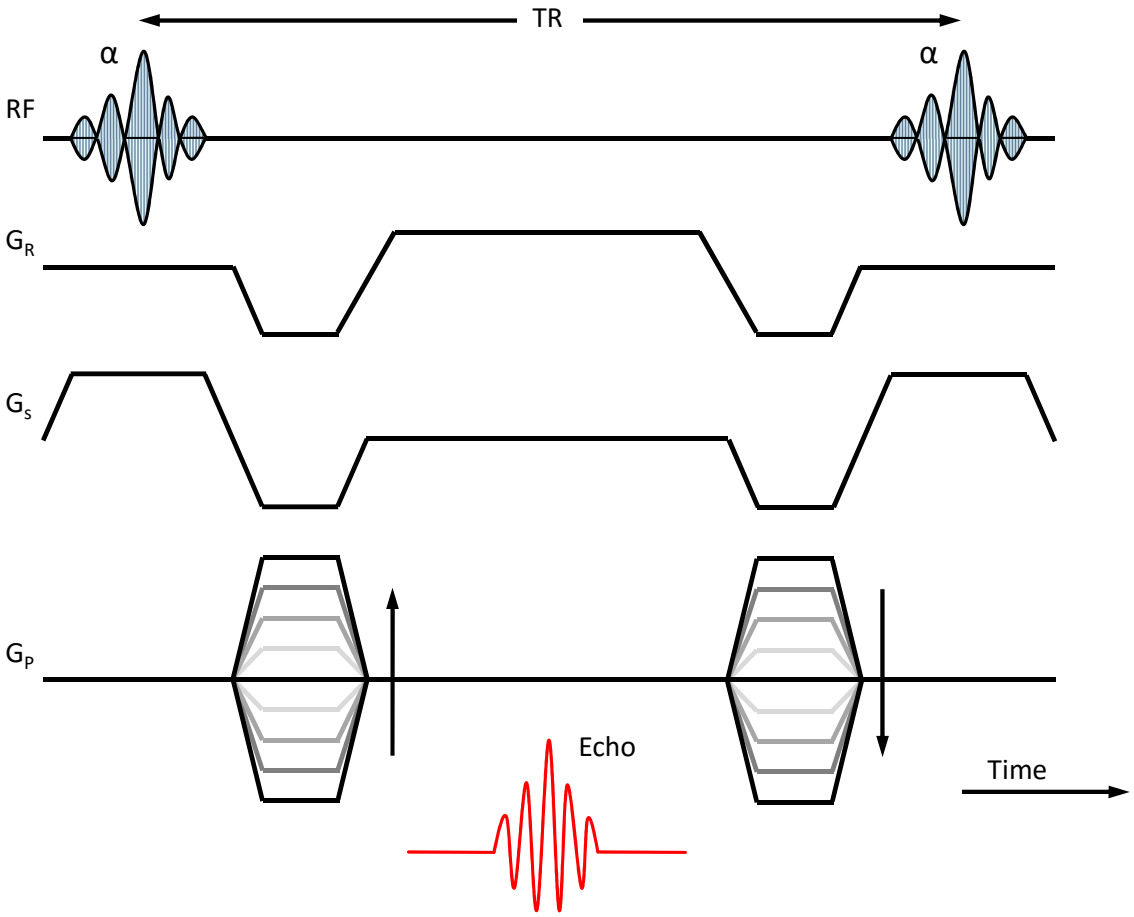


Figure 2.18: A single repetition time of a balanced SSFP sequence, with a net gradient moment of zero.

2.6 Advanced Techniques

2.6.1 The bSSFP Sequence

Rapid imaging of the heart can be a challenge, particularly at high field strengths (3.0 T and upwards) as shorter T_2* values and $\boldsymbol{B_0}$ inhomogeneities caused by susceptibility differences between the heart tissue and the lung add to the usual issues of cardiac and respiratory motion. With these challenges in mind, balanced Steady-State Free Precession (bSSFP) has emerged as one of the most useful sequences in the CMR arsenal, offering high signal-to-noise ratio (SNR) per unit time and excellent contrast between myocardial tissue and the blood pool[12].

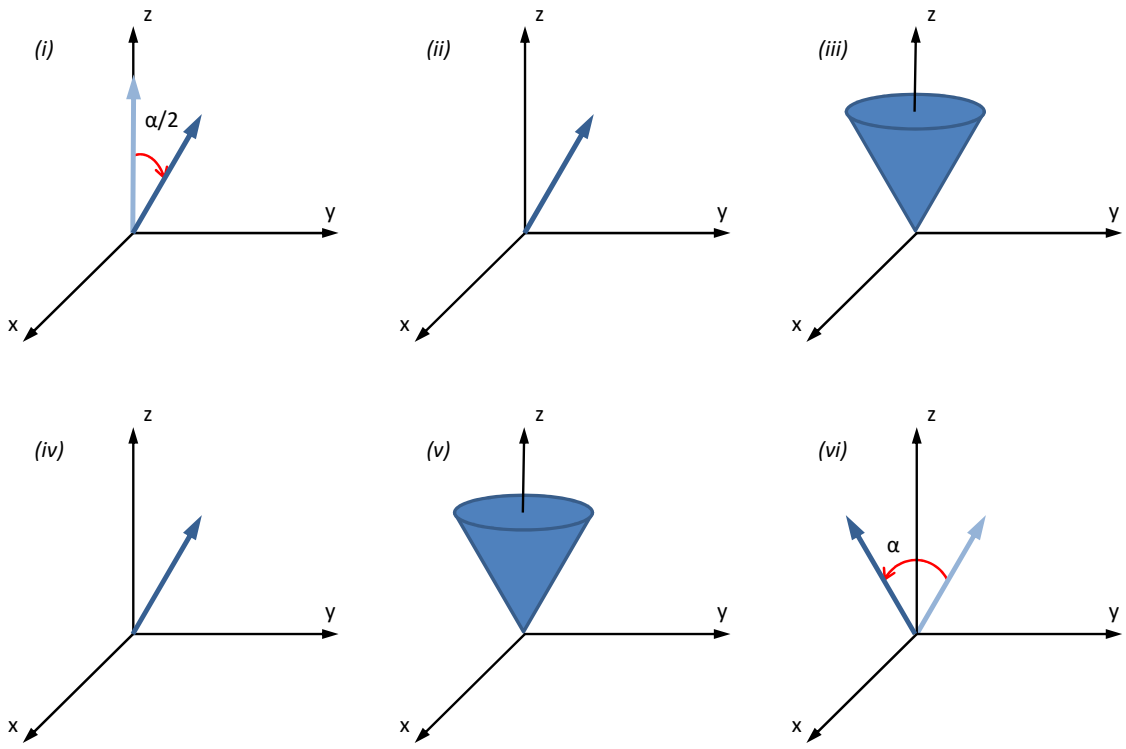


Figure 2.19: The evolution of the magnetisation throughout one repetition time (TR) of a bSSFP sequence. (i) The initial preparation pulse or train of pulses flips the magnetisation into the transverse plane. (ii) After the pulse, the magnetisation remains in the x-y plane. (iii) the spins dephase due to the negative readout gradient lobe. (iv) the polarity of the gradient is switched and the spins rephase at the echo time (TE) to produce an echo. (v) The spins continue to dephase. (vi) The gradient polarity is switched again to balance the gradient moment and rephase the spins to a single magnetisation vector in time for the next $\pm\alpha$ pulse.

SSFP sequences are a group of rapid gradient echo based sequences, where a train of excitation pulses are applied with constant, short repetition time (TR). Each pulse tips the magnetisation from equilibrium into the transverse plane by a flip angle of α, where it begins to dephase under the influence of a readout gradient lobe. The gradient polarity is then switched in order to rephase the magnetisation into an echo. After the end of the TR period the next excitation pulse, of flip angle -α, acts upon the leftover magnetisation. When constant values of $\pm\alpha$ and TR are used throughout the sequence the magnetisation will eventually reach a coherent steady state, where the spins reach an equilibrium in both longitudinal and transverse magnetisation, such that the magnetisation state is the same at each RF pulse.

The balanced SSFP (bSSFP) sequence is a special case where the net gradient moment across each TR is zero, typically in a regime where the TR is of the order of 3 ms or less. This means that dephasing due to gradients across each TR is also zero, such that each excitation pulse acts upon a single, in phase magnetisation vector. This is achieved by every gradient pulse being compensated, or *balanced*, by one of opposite polarity within each TR. A single TR of a bSSFP pulse sequence is shown in Figure 2.18. The steady-state signal of the bSSFP sequence is described by the equation,

$$M_{SS} = \frac{1}{2} M_0 \sqrt{\frac{T_2}{T_1}} \tag{2.14}$$

where M_{SS} is the steady-state magnetisation, M_0 is the equilibrium magnetisation and T_1 and T_2 are the longitudinal and transverse relaxation times.

If the bSSFP employed is simply a train of $\pm\alpha$ pulses however, the approach to steady state will have a long duration and a volatile, fluctuating signal response[13, 14] and it can anywhere between 50 and 500 excitation pulses before the magnetisation reaches the steady state[15]. This is known as the transient response, and can be alleviated by the use of smaller flip angle preparation pulses, in the simplest case

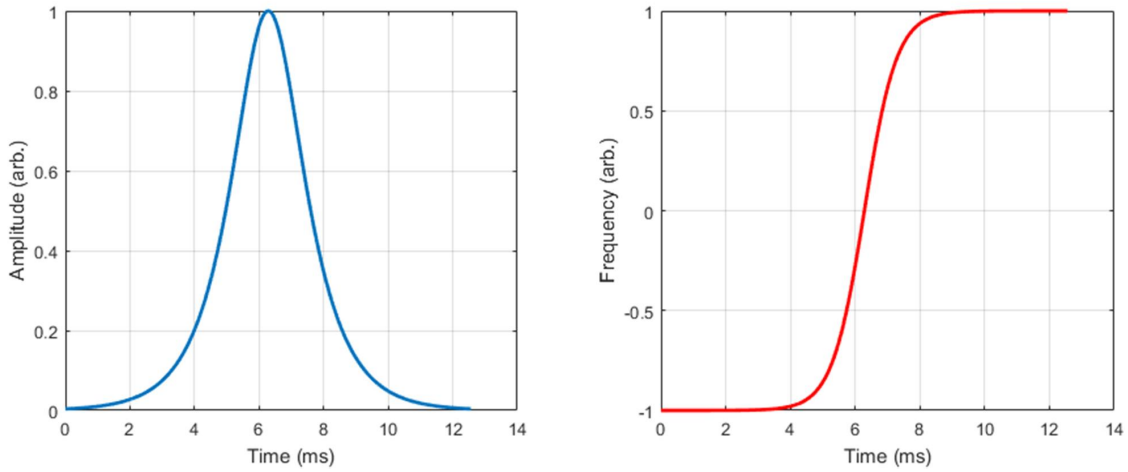


Figure 2.20: The amplitude and frequency profiles of the Hyperbolic Secant (HS) pulse.

employing a single $\alpha/2$ pulse at a time-point $TR/2$, prior to the first $\pm\alpha$ pulse of the excitation pulse train. The effect on the magnetisation of a bSSFP sequence during one TR, including an initial $\alpha/2$ pulse, is described in Figure 2.19. In practice, preparation is more commonly achieved with a linear ramp of around 5-10 RF pulses of increasing flip angle preceding the main excitation pulse train.

2.6.2 Adiabatic Pulses

Adiabatic pulses are a group of RF pulses which are both amplitude- and frequency-modulated[16]. During their application, the pulse's carrier frequency is swept through a range centred on the resonance frequency, in a time short compared to the relaxation times of the sample. By covering a range of frequencies, use of an adiabatic pulse gives a consistent flip angle even in the presence of $\boldsymbol{B_1}$ inhomogeneities.

One of the most popular forms of adiabatic pulse is the hyperbolic secant (HS) inversion pulse, a form of adiabatic fast passage (AFP) with amplitude which varies as a hyperbolic secant function and frequency which varies as a hyperbolic tangent function. These functions were derived from an analytical solution of the Bloch Equations and are plotted in Figure 2.20. The HS pulse is extremely attractive due

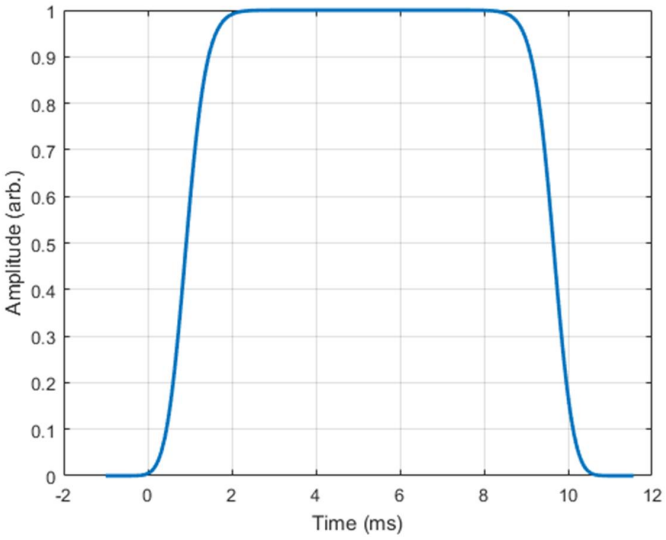


Figure 2.21: The amplitude modulation function of the HS8 pulse envelope.

to its particular insensitivity to inhomogeneity of the $\boldsymbol{B_1}$ field and the flat inversion profile of the pulse. However, in order to more efficiently perform rotations using less $\boldsymbol{B_1}$ power, a pulse with a flatter amplitude modulation function is desirable, such that the pulse's energy is better distributed in time. This is achieved by employing the HSn variant, whereby the factor n is used to flatten the peak of the pulse and to smooth the transition to zero, such that the amplitude modulation function is equal to $\text{sech}(\beta\tau^n)$, where β is a scaling factor which determines the length of the pulse. The amplitude modulation function of the HS8 pulse is shown in Figure 2.21.

References

[1] F. Bloch. Nuclear induction. *Phys. Rev.*, 70(7-8):460–474, October 1946.

[2] E. M. Purcell, H. C. Torrey, and R. V. Pound. Resonance absorption by nuclear magnetic moments in a solid. *Phys. Rev.*, 69(1-2):37–38, January 1946.

[3] I. I. Rabi, J. R. Zacharias, S. Millman, and P. Kusch. A new method of measuring nuclear magnetic moment. *Phys. Rev.*, 53:318, February 1938.

[4] R. A. Jones, J. Kværness, P. A. Rinck, and T. E. Southon. *The magnetic resonance phenomenon*, pages 5–18. Blackwell Wissenschafts-Verlag, 4 sub edition, May 2001.

[5] Catherine Westbrook, Carolyn K. Roth, and John Talbot. *MRI in practice*, pages 1–16. Wiley-Blackwell, 2011.

[6] Stefan K. Piechnik, Vanessa M. Ferreira, Erica Dall'Armellina, Lowri E. Cochlin, Andreas Greiser, Stefan Neubauer, and Matthew D. Robson. Shortened modified Look-Locker inversion recovery (ShMOLLI) for clinical myocardial t1-mapping at 1.5 and 3 t within a 9 heartbeat breathhold. *Journal of cardiovascular magnetic resonance*, 12, November 2010.

[7] J. E. Wagenseil, L. O. Johansson, and C. H. Lorenz. Characterization of t1 relaxation and blood-myocardial contrast enhancement of NC100150 injection in cardiac MRI. *Journal of magnetic resonance imaging : JMRI*, 10(5):784–789, November 1999.

[8] Nadine Kawel, Evrim B. Turkbey, Jeffrey J. Carr, John Eng, Antoinette S. Gomes, W. Gregory Hundley, Craig Johnson, Sofia C. Masri, Martin R. Prince, Rob J. van der Geest, João A. C. Lima, and David A. Bluemke. Normal left

ventricular myocardial thickness for Middle-Aged and older subjects with Steady-State free precession cardiac magnetic ResonanceClinical perspective. *Circulation: Cardiovascular Imaging*, 5(4):500–508, July 2012.

[9] W. A. Edelstein, J. M. Hutchison, G. Johnson, and T. Redpath. Spin warp NMR imaging and applications to human whole-body imaging. *Physics in medicine and biology*, 25(4):751–756, July 1980.

[10] D. B. Twieg. The k-trajectory formulation of the NMR imaging process with applications in analysis and synthesis of imaging methods. *Medical physics*, 10(5):610–621, 1983.

[11] Donald W. McRobbie, Elizabeth A. Moore, Martin J. Graves, and Martin R. Prince. *Spaced out: spatial encoding*. Cambridge University Press, 2006.

[12] Michael Schär, Sebastian Kozerke, Stefan E. Fischer, and Peter Boesiger. Cardiac SSFP imaging at 3 tesla. *Magnetic resonance in medicine*, 51(4):799–806, April 2004.

[13] Brian A. Hargreaves, Shreyas S. Vasanawala, John M. Pauly, and Dwight G. Nishimura. Characterization and reduction of the transient response in steady-state MR imaging. *Magn. Reson. Med.*, 46(1):149–158, July 2001.

[14] Patrick Le Roux. Simplified model and stabilization of SSFP sequences. *Journal of Magnetic Resonance*, 163(1):23–37, July 2003.

[15] Klaus Scheffler and Stefan Lehnhardt. Principles and applications of balanced SSFP techniques. *European radiology*, 13(11):2409–2418, November 2003.

[16] A. Tannús and M. Garwood. Adiabatic pulses. *NMR in biomedicine*, 10(8):423–434, December 1997.

Chapter 3

The Perfusion of the Heart

The heart is a muscular pump, responsible for the collection of oxygenated blood from the lungs and its circulation to all the tissues of the body. It is also responsible for the collection of the blood returning from the tissues, pumping it to the lungs for reoxygenation and collecting it once more before the cycle begins over again. Its proper function is vital to leading a normal and healthy life.

3.1 The Heart

The heart is composed of four chambers, the left and right atria and the left and right ventricles. The main function of the upper chambers, the atria, is to collect returning blood. In the case of the left atrium, oxygenated blood which has returned from the lungs, and in the case of the right atrium, deoxygenated blood which has returned from the rest of the body. The blood collected in the atria is then pumped to the left and right ventricles, via the mitral and tricuspid valves respectively. The valves serve to ensure a single direction of flow between the upper and lower chambers of the heart.

From the larger and more powerful ventricles, the blood is then pumped into the pulmonary artery (from the right ventricle) and the aorta (from the left ventricle),

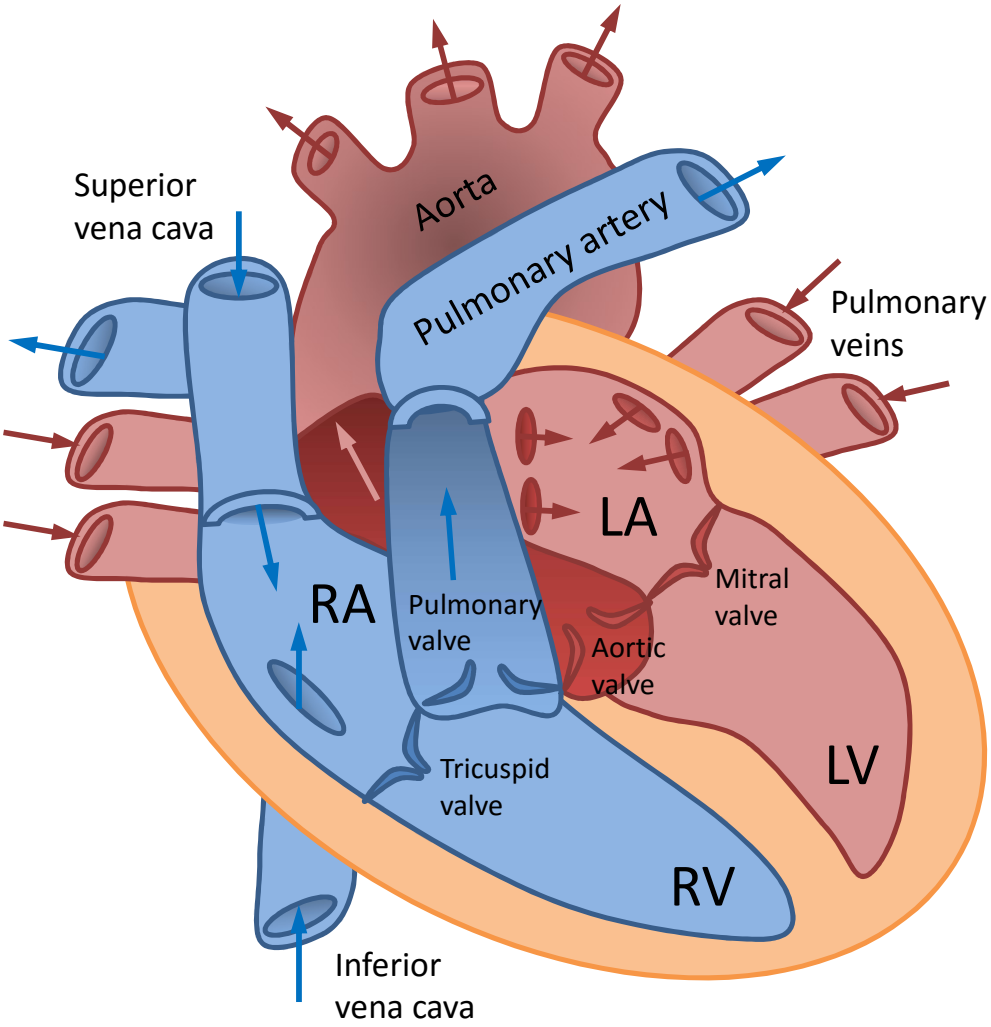


Figure 3.1: The human heart, including left and right atria (LA and RA), left and right ventricles (LV and RV) and major blood vessels.

passing the pulmonary and aortic valves. The pulmonary artery carries the deoxygenated blood to the lungs, while the aorta distributes blood to the rest of the tissues of the body, carrying oxygen for exchange, along with other nutrients. The basic anatomy of the heart is depicted in Figure 3.1.

The wall of the heart is made up of three layers. The outer epicardium, consisting of serous membrane, the middle myocardium, which is the the cardiac muscle tissue and the inner endocardium, or endothelial lining. It is the inner two of these layers which is of interest in perfusion studies, where the subendocardium, between the myocardium and endocardium, is most vulnerable to ischaemia.

3.1.1 The Coronary Arteries

Oxygenated blood is delivered to the myocardium by the coronary arteries, which branch off from the aorta just above the aortic valve. The arteries then circle the heart within the epicardium. The right coronary artery (RCA) supplies the muscle of the right atrium and right ventricle and also provides a collateral supply to the left ventricle and the interventricular septum. A short distance from its branch with the aorta, the left coronary artery splits into the left anterior descending artery (LAD) and the left circumflex artery (LCX). The LAD supplies most of the blood flow to the septum and the anterior, lateral and apical walls of the left ventricle, as well as collateral flow to the anterior right ventricle. The LCX supplies most of the blood flow to the left atrium, along with the posterior and lateral free walls of the LV and, in tandem with the LAD, the anterior papillary muscle of the bileaflet valve. The most common site of coronary artery occlusion is in the LAD.

3.1.2 The Left Ventricle

The cardiac chamber of greatest interest in this work is the left ventricle (LV). As a muscular pump required to deliver oxygen rich blood to tissues around the body,

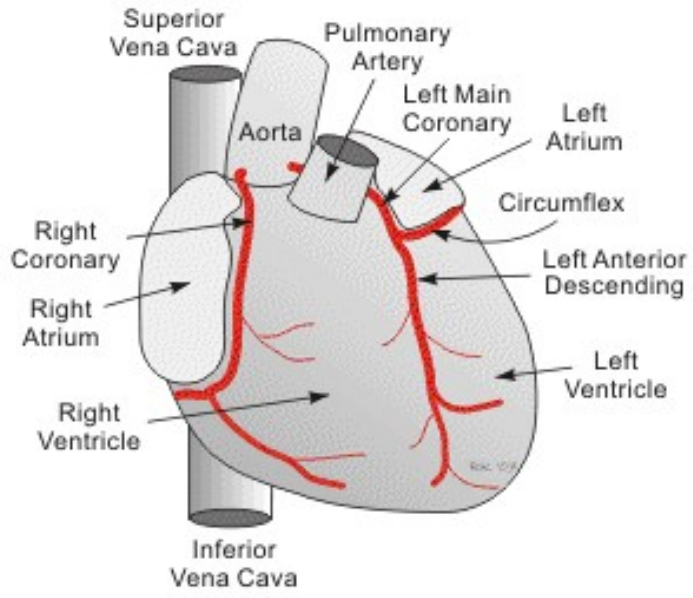


Figure 3.2: The coronary arteries, including the right coronary artery (RCA), the left anterior descending artery (LAD) and the left circumflex artery (LCX). SOURCE: www.heartupdate.com

the left ventricle requires a layer of myocardium thicker than the right ventricle. The mean LV myocardial thickness has been reported as 6.3 $\pm$ 1.1 mm in end-diastole[1], compared to 4 $\pm$ 0.35 mm in the right ventricle[2]. It is therefore vital, with such an important role to play in the body, that the myocardium of the LV is well perfused and not subject to low blood flow caused by occlusion of the LAD or LCX.

3.2 Myocardial Blood Flow

When the arteries reach the target tissue of the myocardium, they begin to branch into smaller blood vessels called arterioles, and further into capillaries which supply oxygenated blood to all the cells of the myocardium. This oxygen is used in the production of adenosine triphosphate (ATP), an important component of cellular energy, by the process of oxidative phosphorylation. This perfusion of the blood into the tissue via the capillary beds is known as Myocardial Blood Flow (MBF) and

can be measured quantitatively in units of millilitres of blood per gram (or hundred grams) of tissue per minute (ml/g/min). MBF is of a smaller order than arterial blood flow as it is dependant on the mass of tissue under perfusion. MBF can vary from 0.5 to 5.0 ml/g/min[3] depending on whether the measurement is made at rest or under stress, whereas the arterial blood flow is a tubular flow on the order of 250 ml/min at rest[4]. With such comparatively small values, the absolute quantification of MBF is a considerable technical challenge.

3.2.1 Under Stress

Oxygen extraction from the arterial blood in the myocardium is maximum at rest and to meet the increased demands during exercise coronary blood flow increases as the resistance is auto-regulated. The increase in MBF from the resting baseline due to stress can be on the order of 3-5 times that of resting conditions. In clinical practice, when investigating the myocardium for perfusion defects, a comparison of rest vs stress states of MBF is often required. This is because perfusion defects do not always manifest at rest. The stressing of the heart is achieved by administering a pharmacological vasodilator, such as adenosine. The vasodilator causes the widening of the blood vessels by the relaxation of the smooth muscle cells of the vessel wall, leading to a decrease in vascular resistance.

3.2.2 Ischaemia

With a build up of fat and cholesterol upon the endoluminal surface of a coronary artery, the walls become thickened and the vessel narrows. This build up is known as atherosclerotic plaque and can become calcified, leading to stenosis, where the resistance to blood flow in the vessel is increased. The causes the tissue being supplied by the vessel to be deprived of its full quota of oxygen and nutrients. The effect may be small at rest, but when the muscle is under stress, such as during exercise, the

demand for nutrients is greater than the available supply and the muscle's metabolic needs are unfulfilled. This inadequate supply can lead to ischaemia, where the tissue switches from aerobic to anaerobic metabolism, and causes the impairment of both the electrical and mechanical function of the heart.

A chronic lack of oxygen supply can lead to conditions where the contractile motion of the heart becomes abnormal, such as myocardial hibernation or myocardial stunning[5]. It is possible to reverse this contractile abnormality. Alternatively, the partial or complete blockage of one of the coronary arteries can lead to acute myocardial infarction, also known as a heart attack[6]. This is most often caused by atherosclerotic plaque breaking off and flowing downstream where it becomes lodged in a narrower vessel. This causes the blood flow to part of the myocardial tissue to decrease or stop, leading to infarction, the death of the tissue.

3.3 Imaging Methods for Measuring MBF

A number of imaging modalities can be employed in the in vivo measurement of MBF. A brief review of some of these methods is below.

3.3.1 PET

Perhaps the most common research tool in the literature for quantitative measures of MBF is Positron Emission Tomography (PET). PET works by the injection of an radionuclide tracer such as ^{15}O-water[7], ^{13}N-ammonia[8] or ^{82}Rb[9]. Compartmental models, based on the specific tracer kinetics of the chosen radionuclide tracer are employed to fit a tissue time-activity curve (TAC). The arterial input function (AIF) is acquired from a dynamic image series during the first pass of the contrast agent and this information is used to calculate a measure of MBF. Absolute quantification requires correction for partial volume effects, spillover and heterogeneities in spatial

resolution [10].

Routine clinical use of PET for measurement of MBF, however, isn't practical. PET is a high cost method and, due to the short half-life of the radionuclides involved, requires the on-site presence of a cyclotron. Though ^{82}Rb is a positron emitter which does not require a cyclotron for production, it has a longer positron range than ^{15}O and ^{13}N (a mean of 4.24 mm in water compared with 2.00 and 1.31 mm respectively[11]) and thus gives a higher dose and lower spatial resolution[12].

3.3.2 SPECT

A lower cost and more readily available alternative to PET is Single Photon Emission Computed Tomography (SPECT). SPECT is the most commonly employed imaging method of assessing perfusion in the clinic[12]. SPECT scanners are far more widely available than PET scanners and the radionuclides employed for tracing, such as ^{99m}Tc and ^{201}Tl have longer half-lives and, as such, do not require the presence of an on-site cyclotron. However, SPECT suffers from low sensitivity and low spatial and temporal resolution when compared with PET, which makes the absolute quantification of MBF with SPECT impractical[13]. SPECT methods also suffer from long acquisition times and significant issues with motion artefacts, while the radionuclides employed deliver a higher dose of ionising radiation than those used in PET.

3.3.3 CT

Research into measuring perfusion with x-ray computed tomography (CT) has benefited from recent hardware advances in detector technology. An iodinated contrast agent, which increases the absorption of x-rays, is injected intravenously. Areas of myocardium which suffer from low blood flow, and therefore low levels of the contrast agent, cause less attenuation of the x-rays. Myocardial perfusion images by CT are quick to acquire and benefit from high spatial resolution. Absolute quantification

of MBF from CT data has been demonstrated[14], however during the first-pass of the contrast agent, there is significant diffusion of the contrast into the extravascular space, the effects of which require careful modelling. Also significantly, the iodinated contrast agent is not haemodynamically inert, and thus can itself have an effect on the coronary blood flow. Further disadvantages of using CT to assess myocardial perfusion are that, with high heart rates, such as under pharmacological stress, image quality is impaired, while the dose of radiation involved can be high, in the range of 9.2 to 12.5 mSv[15] for a 128-slice dual-source CT scanner, due to the dynamic nature of the technique.

3.3.4 CMR

Using MRI to measure myocardial perfusion provides a method that does not rely on exposing the patient to ionising radiation. Cardiovascular Magnetic Resonance (CMR) studies do however involve the use of a clinically approved contrast agent, usually gadolinium-DTPA. The gadolinium is a paramagnetic substance, which typically means it has an unpaired orbital electron and thus has a magnetic moment, which will interact with its immediate surroundings. The paramagnetic effect is quite small, but the substance does exhibit some small magnetic susceptibility. The effect of this susceptibility, from the interaction of the unpaired electrons and the water protons of the tissue, is to cause an increase in the relaxation rate of the protons, in particular manifesting as a shortened T_1. Thus, tissues with a large concentration of the contrast agent, such as well perfused myocardium, show as bright regions on a T_1 weighted image, while areas of ischaemia, which the contrast agent has not reached will have low signal intensity. The gadolinium ion is bonded with the chelating agent, such as diethylenetriamine penta-acetic acid (DTPA), which acts as a carrier molecule and counters the toxity of the gadolinium.

In a CMR study of perfusion, the first pass of the contrast bolus through the

circulatory system is observed. The contrast agent is injected intravenously, and saturation recovery preparation is combined with a rapid readout, such as FLASH or bSSFP, throughout the cardiac cycle. Absolute quantification of MBF from first-pass CMR data can be achieved by measuring the arterial input function (AIF) for the myocardium, and deconvolving it from the tissue response curve. However, there are a number of issues which make absolute quantification of MBF with CMR difficult[16]. Firstly the relationship between the concentration of contrast in the tissue and the MR signal is non-linear, especially with higher concentrations and longer saturation times. It is also uncertain whether the fast exchange condition, such that all the target tissue is expected to have received the contrast, can be assumed. In addition to these difficulties in quantification, CMR first-pass perfusion techniques continue to suffer from artefacts, such as the characteristic "dark rim" artefact[17] which can be confused with perfusion defect. The method also suffers from the high cost of the agent, currently £101.26 for a single 15 ml vial (Gadovist, Bayer), the risk of the contrast agent causing nephrogenic systemic fibrosis (NSF) in patients with severely impaired renal function[18], and concerns over performing multiple serial evaluations owing to the lingering presence of the contrast agent, leading to long delays between repeat measurements[19].

3.4 Summary

In the arsenal of imaging techniques which can be applied to the problem of measuring MBF, there is a gap for a truly non-invasive method, with the potential for absolute quantification.

References

[1] Nadine Kawel, Evrim B. Turkbey, Jeffrey J. Carr, John Eng, Antoinette S. Gomes, W. Gregory Hundley, Craig Johnson, Sofia C. Masri, Martin R. Prince, Rob J. van der Geest, João A. C. Lima, and David A. Bluemke. Normal left ventricular myocardial thickness for Middle-Aged and older subjects with Steady-State free precession cardiac magnetic ResonanceClinical perspective. *Circulation: Cardiovascular Imaging*, 5(4):500–508, July 2012.

[2] S. Y. Ho and P. Nihoyannopoulos. Anatomy, echocardiography, and normal right ventricular dimensions. *Heart*, 92(suppl 1):i2–i13, April 2006.

[3] Frank Kober, Terrence Jao, Thomas Troalen, and Krishna S. Nayak. Myocardial arterial spin labeling. *Journal of cardiovascular magnetic resonance*, 18, April 2016.

[4] Uttam Shrestha and Youngho Seo. Myocardial blood flow as a biomarker. In Vinood B. Patel and Victor R. Preedy, editors, *Biomarkers in Cardiovascular Disease*, Biomarkers in Disease: Methods, Discoveries and Applications, pages 1057–1076. Springer Netherlands, 2016.

[5] C. R. Conti. The stunned and hibernating myocardium: a brief review. *Clinical cardiology*, 14(9):708–712, September 1991.

[6] Grant W. Reed, Jeffrey E. Rossi, and Christopher P. Cannon. Acute myocardial infarction. *The Lancet*, 389(10065):197–210, January 2017.

[7] P. Chareonthaitawee, P. A. Kaufmann, O. Rimoldi, and P. G. Camici. Heterogeneity of resting and hyperemic myocardial blood flow in healthy humans. *Cardiovascular research*, 50(1):151–161, April 2001.

[8] Y. Choi, S. C. Huang, R. A. Hawkins, W. G. Kuhle, M. Dahlbom, C. K. Hoh, J. Czernin, M. E. Phelps, and H. R. Schelbert. A simplified method for quantification of myocardial blood flow using nitrogen-13-ammonia and dynamic PET. *Journal of nuclear medicine : official publication, Society of Nuclear Medicine*, 34(3):488–497, March 1993.

[9] Osamu Manabe, Keiichiro Yoshinaga, Chietsugu Katoh, Masanao Naya, Robert A. deKemp, and Nagara Tamaki. Repeatability of rest and hyperemic myocardial blood flow measurements with 82Rb dynamic PET. *Journal of nuclear medicine : official publication, Society of Nuclear Medicine*, 50(1):68–71, January 2009.

[10] W. G. Kuhle, G. Porenta, S. C. Huang, D. Buxton, S. S. Gambhir, H. Hansen, M. E. Phelps, and H. R. Schelbert. Quantification of regional myocardial blood flow using 13N-ammonia and reoriented dynamic positron emission tomographic imaging. *Circulation*, 86(3):1004–1017, September 1992.

[11] J. Cal-Gonzalez, J. L. Herraiz, S. Espana, M. Desco, J. J. Vaquero, and J. M. Udias. Positron range effects in high resolution 3D PET imaging. In *2009 IEEE Nuclear Science Symposium Conference Record (NSS/MIC)*, pages 2788–2791. IEEE, October 2009.

[12] Michael Salerno and George A. Beller. Noninvasive assessment of myocardial perfusion. *Circulation. Cardiovascular imaging*, 2(5):412–424, September 2009.

[13] Grant T. Gullberg, Bryan W. Reutter, Arkadiusz Sitek, Jonathan S. Maltz, and Thomas F. Budinger. Dynamic single photon emission computed tomography–basic principles and cardiac applications. *Physics in medicine and biology*, 55(20), October 2010.

[14] Richard T. George, Michael Jerosch-Herold, Caterina Silva, Kakuya Kitagawa,

David A. Bluemke, Joao A. Lima, and Albert C. Lardo. Quantification of myocardial perfusion using dynamic 64-detector computed tomography. *Investigative radiology*, 42(12):815–822, December 2007.

[15] SungMok Kim, YooNa Kim, and YeonHyeon Choe. Adenosine-stress dynamic myocardial perfusion imaging using 128-slice dual-source CT: optimization of the CT protocol to reduce the radiation dose. *The International Journal of Cardiovascular Imaging (formerly Cardiac Imaging)*, 29(4):875–884, October 2013.

[16] Bernhard L. Gerber, Subha V. Raman, Krishna Nayak, Frederick H. Epstein, Pedro Ferreira, Leon Axel, and Dara L. Kraitchman. Myocardial first-pass perfusion cardiovascular magnetic resonance: history, theory, and current state of the art. *Journal of cardiovascular magnetic resonance*, 10(1):18+, April 2008.

[17] E. V. Di Bella, D. L. Parker, and A. J. Sinusas. On the dark rim artifact in dynamic contrast-enhanced MRI myocardial perfusion studies. *Magnetic resonance in medicine*, 54(5):1295–1299, November 2005.

[18] Martin A. Sieber, Philipp Lengsfeld, Jakob Walter, Heiko Schirmer, Thomas Frenzel, Fred Siegmund, Hanns-Joachim J. Weinmann, and Hubertus Pietsch. Gadolinium-based contrast agents and their potential role in the pathogenesis of nephrogenic systemic fibrosis: the role of excess ligand. *Journal of magnetic resonance imaging : JMRI*, 27(5):955–962, May 2008.

[19] Adrian S. Cheng, Tammy J. Pegg, Theodoros D. Karamitsos, Nick Searle, Michael Jerosch-Herold, Robin P. Choudhury, Adrian P. Banning, Stefan Neubauer, Matthew D. Robson, and Joseph B. Selvanayagam. Cardiovascular magnetic resonance perfusion imaging at 3-tesla for the detection of coronary artery disease: a comparison with 1.5-tesla. *Journal of the American College of Cardiology*, 49(25):2440–2449, June 2007.

Chapter 4

Arterial Spin Labelling

Cardiovascular Magnetic Resonance (CMR) imaging is a powerful tool for the investigation of common pathologies of the heart such as congenital heart disease, coronary artery disease and cardiomyopathies[1]. One of the most useful processes that CMR allows us to investigate is the perfusion of blood in the myocardial tissue. In clinical practice this is achieved with the use of first-pass perfusion techniques, as described in Chapter 3.3.4. An attractive alternative to first-pass perfusion CMR techniques and other, nuclear based modalities, such as Single-Photon Emission Computed Tomography (SPECT)[2, 3] or Positron Emission Tomography (PET)[4, 5], would be to use Arterial Spin Labelling (ASL). ASL is a non-invasive technique which uses magnetic labelling strategies to allow the proton spins present in the blood water to act as an endogenous contrast agent[6, 7].

4.1 The Spin Label Experiment

Though relatively unexplored in the investigation of myocardial perfusion, ASL is a very mature technique when employed in the brain. By magnetically labelling the arterial blood, with inversion or saturation pulses, and performing two measurements of the tissue signal, one where the inflowing blood has been labelled and one where it

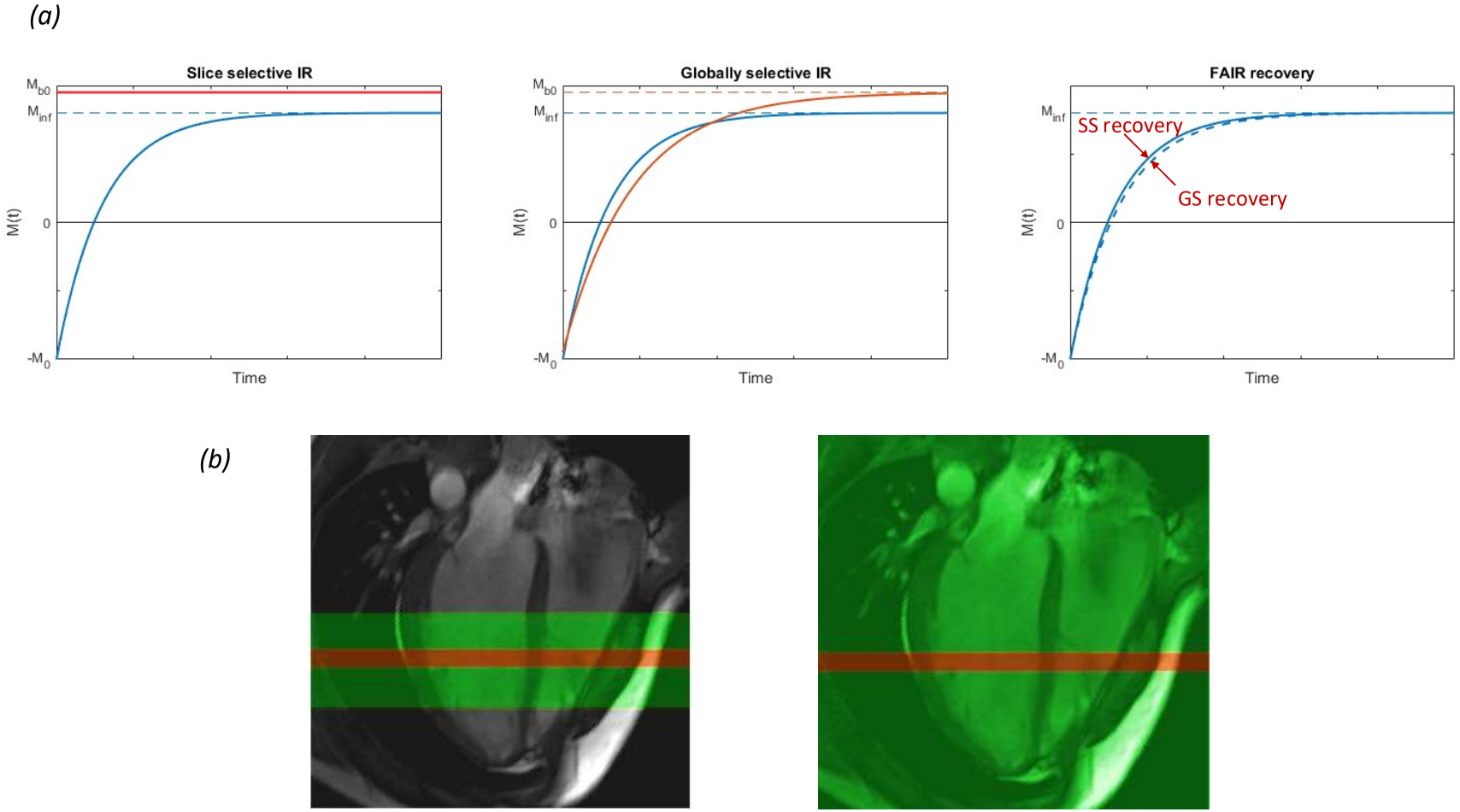


Figure 4.1: (a) Slice-selective and globally-selective inversion recoveries with the left ventricular blood pool response plotted in red and the myocardial response in blue, and the ASL signal difference in the FAIR experiment. In the SS case, the blood pool is assumed to be non-inverted. In reality the blood will consist of a mixture of inverted and non-inverted spins, dependent on the extent of the inversion pulse. (b) Slice placements. The shaded green areas represent the extent of the SS and GS inversion respectively, with the shaded read areas representing the image slice.

has not, two discrete states are created, the label and control. While the blood flowing into the slice of interest experiences these two states, the static tissue of interest has the same state in each case, dependent on the labelling scheme. This is explained further for the FAIR labelling case in section 4.3. Thus, by performing a subtraction of the two images the contribution of the static tissue is removed, leaving only the difference in the blood magnetisation between the label and control.

4.2 Application of ASL to the Heart

Though the implementation of a non-contrast method of measuring MBF is very attractive, there are a number of drawbacks in applying ASL to the heart as compared with spin labelling in the brain. As with all cardiac imaging, the motion of the chest and of the heart itself beating present a considerable challenge. These are traditionally overcome with the use of breath holds to limit bulk motion of the chest and with electrocardiogram (ECG) triggering to target acquisitions to quiescent periods of the cardiac cycle, such as mid-diastole. Though these techniques are well used and relatively robust, they inevitably limit the amount of time available for data collection. In addition to this, the depth of the heart within the chest cavity means that there is some distance between the tissue and the RF receive array coil elements. This, along with the greater RF coil volume required in the chest, and the acquisition time limit due to the motion of the cardiac cycle, means that the achievable signal-to-noise ratio (SNR) is limited, and has been estimated to be around a third of the achievable SNR in the brain[8]. However, there is some compensation in the stronger ASL signal in the heart, due to the higher blood flow in the myocardium compared with brain tissue[8].

4.3 Flow-sensitive Alternating Inversion Recovery

In one common and robust ASL labelling scheme, known as Flow-sensitive Alternating Inversion Recovery (FAIR)[9, 10], two images or sets of images are collected, one in which a globally-selective (GS) inversion pulse is applied prior to the readout (the control image) such that the spins of the myocardial tissue of interest and those of the inflowing blood are both inverted. The second image set is preceded by a slice-selective (SS) inversion through a slice of the myocardium (the tag or label image) such that the myocardial tissue in the imaging slice is again inverted but the blood water spins flowing into the image slice remain in thermomagnetic equilibrium. The effect of the presence of these inflowing spins in the slice-selective experiment is to cause an apparent shortening of the longitudinal relaxation time (T_1) of the tissue. It is the difference in the observed T_1 values between the two measurements that allows us to quantitatively evaluate the blood flow to this slice of the myocardium. A representation of this is shown in Figure 4.1.

4.4 ASL in the Heart

A small number of studies have previously applied ASL to the problem of measuring MBF in humans non-invasively[11, 12, 13, 14]. A majority of these have employed a version of FAIR for the purpose of labelling, but have differed in the imaging method and in quantification. These FAIR implementations have been split between methods employing a single inversion time (TI) and those with multiple TIs. The earliest cardiac ASL experiments carried out in humans were published in 1999 by Poncelet et al.[15] and Wacker et al[12].

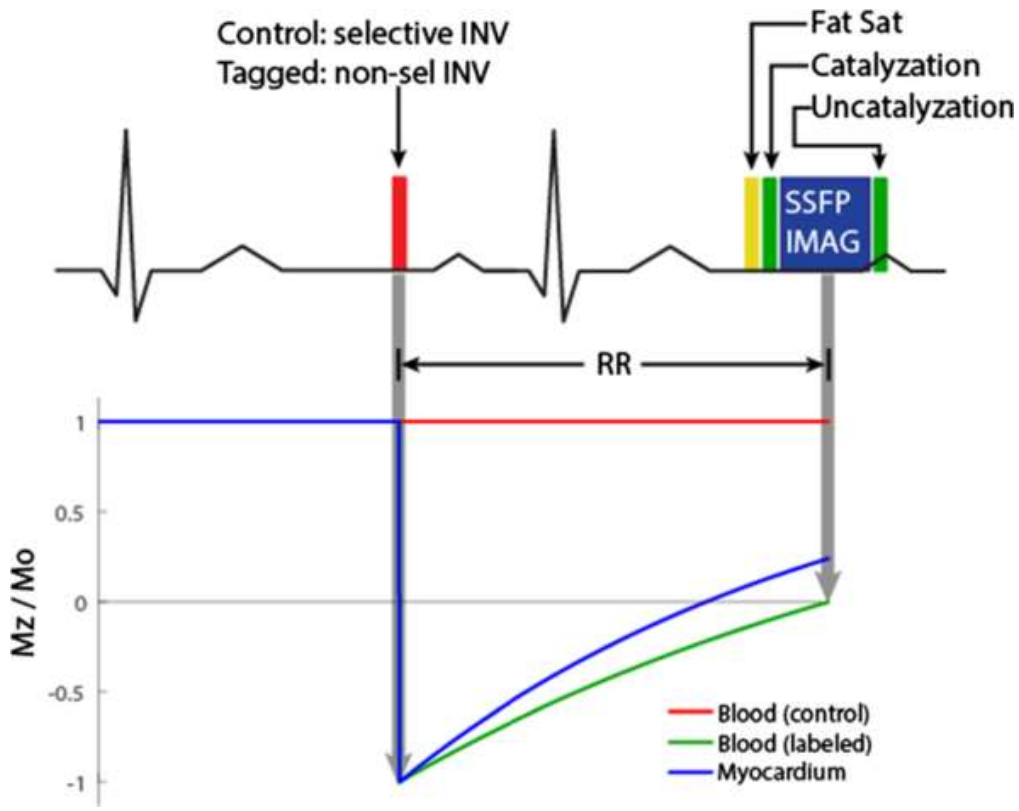


Figure 4.2: The single inversion time FAIR-bSSFP sequence, with TI = RR. SOURCE: Zun et al.[11].

4.4.1 Single Inversion Time ASL

Poncelet et al. employed a FAIR labelling scheme with a single-shot EPI readout at 1.5 T. The label and readout were separately gated to the same period of the cardiac cycle, either end-systole or mid-diastole, such that the TI would vary throughout with the heart rate of the subject. The authors termed this approach "double-gating". Forty-six pairs of control and label images were collected with synchronised breathing, along with further images with short TI, and with no inversion, in order to plot a pair of inversion recovery curves. The method suffered from poor temporal SNR of approximately 30 due to physiological noise, largely due to respiratory motion, and a small ASL signal difference, a mean of 1.6 $\pm$ 0.61%, due to the short T_1 of blood at 1.5 T.

Zun et al.[11] employed a similar single TI strategy, with a bSSFP readout following FAIR labelling at 3 T. Six breath held acquisitions were performed with the TI for both the control and label images equal to the RR-interval measured on the ECG trace, as shown in Figure 4.2. The control and label acquisitions were separated by a delay of 6 seconds in order to allow for some recovery of the magnetisation. The same sequence was later employed in a study of 29 patients suspected of having coronary artery disease (CAD)[16]. The authors showed a statistically significant increase in MBF under adenosine stress in the normal subjects ($p < 0.0001$.) and between normal segments and the most ischaemic segments ($p = 0.0011$) in the the patient group. The study was carried out in a single mid-ventricular short-axis slice of myocardium and suffered from high levels of physiological noise and required signal averaging both spatially across the myocardium and temporally across several repeated acquisitions.

4.4.2 Multiple Inversion Time ASL

Wacker et al.[12] employed a saturation recovery (SR) equivalent of a FAIR labelled sequence at 1.5 T, using alternating slice-selective and globally-selective 90° preparation pulses in place of inversion. Snapshot FLASH images were then collected at multiple saturation times of TS = 100, 200, 300, 400, 600, 800, 1000, 1200 and 1400 ms, with the trigger delay altered for each value of TS, such that imaging always occurred during mid-diastole. However, this meant that the saturation labelling occurred in different phases of the cardiac cycle, which has been postulated as a possible reason for the overestimation of MBF values in this study[8].

Wang et al.[13] implemented a FAIR-bSSFP sequence similar to that of Zun, but employing multiple inversion times of TI = 200, 500, 900, 1300 and 1700 ms at 1.5 T. Navigator gating was used to allow free breathing acquisitions, with the readout occurring in the end-expiration respiratory phase. A non-rigid motion correction algorithm was then applied to try to remove the influence of residual motion. The

application of motion correction increased the intraclass correlation coefficient from 0.61 to 0.89 and decreased the coefficient of variation from 26.2% to 21.8% for the MBF results, leading the authors to suggest it's use increased the reliability of the method.

4.4.3 Steady-pulsed ASL

Capron et al. employed a different approach to myocardial spin labelling, which the authors termed steady-pulsed ASL (spASL)[14]. The sequence aimed to achieve higher SNR than the pulsed ASL techniques described above, by driving the magnetisation into a steady-state in manner similar to pseudo-continuous ASL (pcASL) techniques commonly used in neuroimaging applications of ASL[17]. For this purpose, the labelling slab was placed outside the imaging slice, at the aortic root. For the control images, the inversion slab was placed symmetrically about the imaging slice from the location of the labelling slab, in order to compensate for magnetisation transfer effects. Both the slice placement and pulse sequence are described further in Figure 4.3. 128 bSSFP images each were acquired for the label and control states, in a free breathing acquisition that took approximately 4 minutes. However, the authors noted issues with respiratory motion, due to the free breathing approach, and with the labelling efficiency due to the large labelling slab of 60 mm thickness, which was required to provide robustness to respiratory motion.

4.5 Quantification of MBF

The quantification of MBF from in vivo myocardial ASL data can be achieved by the application of two different models. The first is based on the difference in the MR signal measured in the myocardium in the control and label states, the other on the ratio of the apparent T_1s in the two states.

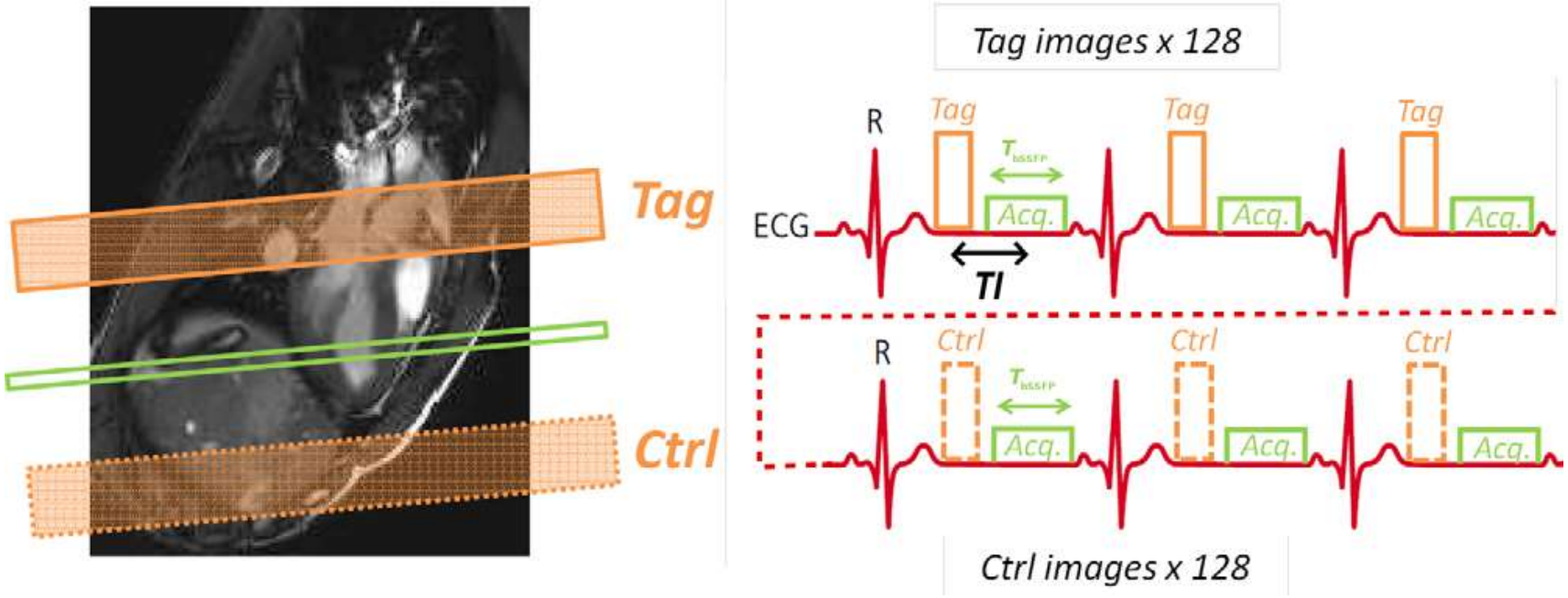


Figure 4.3: The steady-pulsed ASL sequence (spASL). The location of the label (tag) and control inversion slabs, and pulse sequence diagram. SOURCE: Capron et al.[14].

4.5.1 Signal Difference Method

The signal difference method employs a simplified derivation of the general kinetic model. The model was derived by Buxton et al.[18], and takes the form,

$$MBF = \frac{\Delta S}{2M_0.TI.exp\left(\frac{TI}{T_1}\right)} \tag{4.1}$$

where ΔS is the signal difference between the globally-selective inversion and slice-selective inversion images, such that a subtraction of the two images gives a signal difference map, M_0 is measured from a baseline image (with no inversion preparation), TI is the inversion time and T_1 is the T_1 of blood at the relevant field strength.

If the TI is set to be constant for each pair of images, control and label, for instance with TI = RR, where RR is the time between subsequent R-waves on the ECG trace, this allows for the direct subtraction of the images to give a perfusion weighted image. However, any change in heart rate will lead to errors in the quantification, as this could lead to a different slice of myocardium being excited due to the motion of the heart throughout the cardiac cycle. This was the approach employed by Zun et al.[11, 16]. To counter this issue, the labelling pulses and readout trains can each be separately gated to the same phase of the cardiac cycle, thus ensuring the same slice is excited each time. However, as this means that the TI varies, direct subtraction between control and label image pairs cannot be carried out. Instead, additional image data must be collected at short and long TIs in order to fit a pair of inversion recovery curves, and the signal difference at a chosen average TI inferred from the difference in the curves. This was the model employed by Poncelet et al.[15], and was later further validated by Do et al.[19]. The simple kinetic model described does not, however, take account of the difference between the T_1 of blood and that of myocardium.

4.5.2 Dual T_1 Method

The alternative quantification method is based on a ratio of the T_1s of the myocardium in the control and label images. It takes the form,

$$MBF = \frac{\lambda}{T_1^{blood}} \left(\frac{T_1^{GS}}{T_1^{SS}} - 1 \right) \tag{4.2}$$

where $\lambda = 0.92$ ml/g[20] is the blood-tissue partition coefficient of water, T_1^{blood} is the relaxation time of the blood pool of the left ventricle and T_1^{GS} and T_1^{SS} are the values for the longitudinal relaxation time measured for the myocardium, from the global and slice-selective experiments respectively. This formulation was verified in rat hearts by Belle et al.[21] based on earlier theoretical work by Detre et al.[6] and Bauer et al.[22]. In humans this was the approach used by Wacker et al.[23] and Northrup et al.[24] and is the most common quantification model employed in cardiac ASL in animals[25, 26]. This method of quantification has been validated against microsphere measurements of MBF in rat hearts[27], and T_1 calculation has been shown to be robust at a range of normal heart rates and for a range of T_1s[28], though the model has shown greater sensitivity to transit delays, as discussed in the next section[29].

4.5.3 Arterial Transit Time

Both of the quantification methods described above can lead to errors from the effect of varying values of Arterial Transit Time (ATT). This is the time taken for the labelled blood to reach the image slice from the labelling slab. Wang et al.[13] used a development of the signal difference kinetic model to fit simultaneously for both MBF and ATT and published the only literature value for myocardial ATT in humans thus far, a mean of 363 $\pm$ 111 ms from a set of eleven healthy volunteers, employing a labelling slab of 30-40 mm thickness and an imaging slice of 8 mm,

with the same position in the mid-ventricle. However, it is known from ASL work in the brain that transit time varies between regions in the target tissue, between people, and when there is pathology present[17]. This means that, without knowing the ATT in quantitative terms, its effect on the quantification of the blood flow is unknown. This could be accounted for by introducing a long delay between labelling and imaging, however this would mean that the label is subject to T_1 decay, such that the measurable ASL signal is decreased.

In an investigation of the effect of ATT on quantification of Cerebral Blood Flow (CBF) using FAIR, it was found that the effect of a finite transit time is to decrease the ASL signal difference[29] and thus lead to an underestimation of CBF. By contrast, the dual T_1 quantification method can lead to an under or overestimation of the value of CBF, as it is dependent on the value of the transit time itself. This occurs as, following either the globally-selective (GS) or slice-selective-selective inversion what follows is in fact a period of GS recovery followed by a period of SS recovery, with only the switching time between the two depending on the inversion[29, 26]. Thus the quantification depends on how well this biexponential response for each inversion is fitted as a monoexponential T_1 recovery.

4.6 Summary

Though some work has been done on the application of ASL techniques to the measurement of myocardial perfusion, there remains no single technique which is simple, robust to motion and heart rate variation, and short enough to be employed during a clinical cardiac MR exam.

References

[1] Dudley J. Pennell, Udo P. Sechtem, Charles B. Higgins, Warren J. Manning, Gerald M. Pohost, Frank E. Rademakers, Albert C. van Rossum, Leslee J. Shaw, E. Kent Yucel, European Society of cardiology, and Soceity for Cardiovascular Magnetic Resonance. Clinical indications for cardiovascular magnetic resonance (CMR): Consensus panel report. *Journal of cardiovascular magnetic resonance*, 6(4):727–765, 2004.

[2] Simona Ben-Haim, Venkatesh L. Murthy, Christopher Breault, Rayjanah Allie, Arkadiusz Sitek, Nathaniel Roth, Jolene Fantony, Stephen C. Moore, Mi-Ae A. Park, Marie Kijewski, Athar Haroon, Piotr Slomka, Kjell Erlandsson, Rafael Baavour, Yoel Zilberstien, Jamshed Bomanji, and Marcelo F. Di Carli. Quantification of myocardial perfusion reserve using dynamic SPECT imaging in humans: A feasibility study. *Journal of nuclear medicine : official publication, Society of Nuclear Medicine*, 54(6):873–879, June 2013.

[3] Ernest V. Garcia. Are SPECT measurements of myocardial blood flow and flow reserve ready for clinical use? *European journal of nuclear medicine and molecular imaging*, 41(12):2291–2293, December 2014.

[4] S. R. Bergmann, P. Herrero, J. Markham, C. J. Weinheimer, and M. N. Walsh. Noninvasive quantitation of myocardial blood flow in human subjects with oxygen-15-labeled water and positron emission tomography. *Journal of the American College of Cardiology*, 14(3):639–652, September 1989.

[5] Mireille Lortie, Rob S. Beanlands, Keiichiro Yoshinaga, Ran Klein, Jean N. Dasilva, and Robert A. DeKemp. Quantification of myocardial blood flow with 82Rb dynamic PET imaging. *European journal of nuclear medicine and molecular imaging*, 34(11):1765–1774, November 2007.

[6] John A. Detre, John S. Leigh, Donald S. Williams, and Alan P. Koretsky. Perfusion imaging. *Magn. Reson. Med.*, 23(1):37–45, January 1992.

[7] John A. Detre, Weiguo Zhang, David A. Roberts, Afonso C. Silva, Donald S. Williams, Donald J. Grandis, Alan P. Koretsky, and John S. Leigh. Tissue specific perfusion imaging using arterial spin labeling. *NMR Biomed.*, 7(1-2):75–82, March 1994.

[8] Frank Kober, Terrence Jao, Thomas Troalen, and Krishna S. Nayak. Myocardial arterial spin labeling. *Journal of cardiovascular magnetic resonance*, 18, April 2016.

[9] Seong-Gi Kim. Quantification of relative cerebral blood flow change by flow-sensitive alternating inversion recovery (FAIR) technique: Application to functional mapping. *Magn. Reson. Med.*, 34(3):293–301, September 1995.

[10] Seong-Gi Kim and Nikolaos V. Tsekos. Perfusion imaging by a flow-sensitive alternating inversion recovery (fair) technique: Application to functional brain imaging. *Magn. Reson. Med.*, 37(3):425–435, March 1997.

[11] Zungho Zun, Eric C. Wong, and Krishna S. Nayak. Assessment of myocardial blood flow (MBF) in humans using arterial spin labeling (ASL): feasibility and noise analysis. *Magnetic resonance in medicine*, 62(4):975–983, October 2009.

[12] C. M. Wacker, M. Bock, A. W. Hartlep, G. Beck, G. van Kaick, G. Ertl, W. R. Bauer, and L. R. Schad. Changes in myocardial oxygenation and perfusion under pharmacological stress with dipyridamole: assessment using t*2 and t1 measurements. *Magnetic resonance in medicine*, 41(4):686–695, April 1999.

[13] Danny J. Wang, Xiaoming Bi, Brian B. Avants, Tongbai Meng, Sven Zuehlsdorff, and John A. Detre. Estimation of perfusion and arterial transit time in my-

ocardium using free-breathing myocardial arterial spin labeling with navigator-echo. *Magnetic resonance in medicine*, 64(5):1289–1295, November 2010.

[14] Thibaut Capron, Thomas Troalen, Benjamin Robert, Alexis Jacquier, Monique Bernard, and Frank Kober. Myocardial perfusion assessment in humans using steady-pulsed arterial spin labeling. *Magnetic resonance in medicine*, 74(4):990–998, October 2015.

[15] B. P. Poncelet, T. M. Koelling, C. J. Schmidt, K. K. Kwong, T. G. Reese, P. Ledden, H. L. Kantor, T. J. Brady, and R. M. Weisskoff. Measurement of human myocardial perfusion by double-gated flow alternating inversion recovery EPI. *Magnetic resonance in medicine*, 41(3):510–519, March 1999.

[16] Zungho Zun, Padmini Varadarajan, Ramdas G. Pai, Eric C. Wong, and Krishna S. Nayak. Arterial spin labeled CMR detects clinically relevant increase in myocardial blood flow with vasodilation. *JACC. Cardiovascular imaging*, 4(12):1253–1261, December 2011.

[17] David C. Alsop, John A. Detre, Xavier Golay, Matthias Günther, Jeroen Hendrikse, Luis Hernandez-Garcia, Hanzhang Lu, Bradley J. MacIntosh, Laura M. Parkes, Marion Smits, Matthias J. van Osch, Danny J. Wang, Eric C. Wong, and Greg Zaharchuk. Recommended implementation of arterial spin-labeled perfusion MRI for clinical applications: A consensus of the ISMRM perfusion study group and the european consortium for ASL in dementia. *Magnetic resonance in medicine*, 73(1):102–116, January 2015.

[18] R. B. Buxton, L. R. Frank, E. C. Wong, B. Siewert, S. Warach, and R. R. Edelman. A general kinetic model for quantitative perfusion imaging with arterial spin labeling. *Magnetic resonance in medicine*, 40(3):383–396, September 1998.

[19] Hung Phi P. Do, Andrew J. Yoon, Michael W. Fong, Farhood Saremi, Mark L.

Barr, and Krishna S. Nayak. Double-gated myocardial ASL perfusion imaging is robust to heart rate variation. *Magnetic resonance in medicine*, 77(5):1975–1980, May 2017.

[20] S. R. Bergmann, K. A. Fox, A. L. Rand, K. D. McElvany, M. J. Welch, J. Markham, and B. E. Sobel. Quantification of regional myocardial blood flow in vivo with H215O. *Circulation*, 70(4):724–733, October 1984.

[21] V. Belle, E. Kahler, C. Waller, E. Rommel, S. Voll, K. H. Hiller, W. R. Bauer, and A. Haase. In vivo quantitative mapping of cardiac perfusion in rats using a noninvasive MR spin-labeling method. *Journal of magnetic resonance imaging : JMRI*, 8(6):1240–1245, 1998.

[22] W. R. Bauer, F. Roder, K. H. Hiller, H. Han, S. Fröhlich, E. Rommel, A. Haase, and G. Ertl. The effect of perfusion on t1 after slice-selective spin inversion in the isolated cardioplegic rat heart: measurement of a lower bound of intracapillary-extravascular water proton exchange rate. *Magnetic resonance in medicine*, 38(6):917–923, December 1997.

[23] Christian M. Wacker, Florian Fidler, Christian Dueren, Stefan Hirn, Peter M. Jakob, Georg Ertl, Axel Haase, and Wolfgang R. Bauer. Quantitative assessment of myocardial perfusion with a spin-labeling technique: preliminary results in patients with coronary artery disease. *Journal of magnetic resonance imaging : JMRI*, 18(5):555–560, November 2003.

[24] Benjamin E. Northrup, Kyle S. McCommis, Haosen Zhang, Shuddhadeb Ray, Pamela K. Woodard, Robert J. Gropler, and Jie Zheng. Resting myocardial perfusion quantification with CMR arterial spin labeling at 1.5 t and 3.0 t. *Journal of cardiovascular magnetic resonance*, 10, 2008.

[25] Adrienne E. Campbell-Washburn, Anthony N. Price, Jack A. Wells, David L.

Thomas, Roger J. Ordidge, and Mark F. Lythgoe. Cardiac arterial spin labeling using segmented ECG-gated Look-Locker FAIR: variability and repeatability in preclinical studies. *Magnetic resonance in medicine*, 69(1):238–247, January 2013.

[26] Thomas Kampf, Xavier Helluy, Fabian T. Gutjahr, Patrick Winter, Cord B. Meyer, Peter M. Jakob, Wolfgang R. Bauer, and Christian H. Ziener. Myocardial perfusion quantification using the t1 -based FAIR-ASL method: the influence of heart anatomy, cardiopulmonary blood flow and look-locker readout. *Magnetic resonance in medicine*, 71(5):1784–1797, May 2014.

[27] W. R. Bauer, K. H. Hiller, P. Galuppo, S. Neubauer, J. Köpke, A. Haase, C. Waller, and G. Ertl. Fast high-resolution magnetic resonance imaging demonstrates fractality of myocardial perfusion in microscopic dimensions. *Circulation research*, 88(3):340–346, February 2001.

[28] Daniel R. Messroghli, Aleksandra Radjenovic, Sebastian Kozerke, David M. Higgins, Mohan U. Sivananthan, and John P. Ridgway. Modified Look-Locker inversion recovery (MOLLI) for high-resolution t1 mapping of the heart. *Magnetic resonance in medicine*, 52(1):141–146, July 2004.

[29] J. Zhou and P. C. van Zijl. Effect of transit times on quantification of cerebral blood flow by the FAIR t(1)-difference approach. *Magnetic resonance in medicine*, 42(5):890–894, November 1999.

Chapter 5

Development of an ASL sequence for measurement of myocardial perfusion at 3T

In this chapter a method for measuring Myocardial Blood Flow (MBF) in a single breath hold, non-invasively using a Flow-sensitive Alternating Inversion Recovery (FAIR) labelling scheme and combined with a Look-Locker acquisition (here called LL-FAIR-ASL) is presented. The described method allows for the acquisition of both FAIR inversion states (slice-selective and globally-selective) within a single breath hold, providing two T_1 maps as a by-product. The method is assessed by way of simulation, phantom study and in vivo application. The method is further used for quantitative analysis of MBF in healthy volunteers. MBF is measured in three slices in humans with ASL for the first time and is assessed for reproducibility and variability.

5.1 Methods

5.1.1 Sequence Design

The LL-FAIR-ASL sequence was programmed in the Siemens IDEA environment. An existing cardiovascular MR sequence, which provides access to various methods of T_1 measurement (MOLLI, ShMOLLI, SASHA), was used as the starting point, and changes were subsequently made to allow for FAIR acquisition. The inbuilt Navigator band was used for the implementation of the slice-selective inversion pulse. This allowed for the position of the inversion slice to be varied and the width of the inversion profile to be made different from the image slice thickness.

5.1.2 On Scanner Implementation

The LL-FAIR-ASL sequence was implemented on a 3 T whole body scanner (TIM Trio, Siemens, Germany). The final sequence consisted of two identical HS8 adiabatic inversion pulses[1], one slice-selective (SS), one globally-selective (GS) with a duration of 10 ms, time/bandwidth product R = 40 and the scaling factor $\beta = 3.45$. For the SS inversion a slice-selective gradient was applied during the pulse and for the GS inversion the timing of the gradient was shifted such that it was applied after the pulse. This served to ensure that the ASL signal difference was not affected by eddy current driven signals[2]. Each inversion pulse was followed by a block of five cardiac triggered balanced Steady-State Free Precession (bSSFP) imaging readouts[3]. Each readout consisted of LISA excitation pulses, which are Gaussian-like, and included five initial ramp-up pulses and a final half-alpha 'restore pulse'. The two inversion blocks were separated by a gap of three heartbeats to allow for some recovery of the magnetisation, within a manageable breath hold, as shown in Figure 5.1, thus forming a MOLLI 5(3)5 regime. Both SS and GS inversions were collected in a single thirteen heartbeat breath hold. The ordering scheme of the sequence within this

thirteen heartbeat breath hold (SS-GS or GS-SS) was varied. Sequence parameters were based closely on those employed successfully in MOLLI implementations and included a 35° excitation flip angle, image slice thickness of 8 mm, an initial TI of 115 ms (with the following values being 115 ms + RR, 115 ms + 2RR,...), TR/TE of 3 ms/1.5 ms, 320 mm field of view with 75% phase resolution and 6/8 partial Fourier, a 192 x 144 image matrix (interpolated to 384 x 288) and an acceleration factor of GRAPPA 2[4, 5]. All inversion pulses and readouts occurred during the diastolic phase of the cardiac cycle. This timing guaranteed that the signal recovery wasn't corrupted by through-plane bulk cardiac motion, by restricting inversions and readouts to the most stable cardiac phase. Due to the inversion recovery nature of the sequence at least 15 seconds was allowed between scans to allow for full relaxation of the magnetisation.

5.1.3 Simulations

Bloch simulations of the sequence were performed in MATLAB (The Mathworks Inc., Natick, USA) with the acquisition parameters defined above and not accounting for magnetization-transfer effects. The inversion pulses were simulated fully as HS8 pulses with the parameters matching those described above and the power set as per the scanner maximum reference voltage in order to ensure the adiabatic condition is met. Each readout bSSFP readout pulse train was also fully simulated as per the scanner implementation, including the linear ramp-up and final half-alpha pulse. The evolution of the longitudinal magnetisation, M_z, after inversion, and the influence of the readout blocks based on these simulations, is shown in Figure 5.1. Simulations were performed for a range of T_1s (100-2000 ms) and heart rates (40-120 bpm) in order to test the robustness of the sequence against variations in these parameters. In order to determine an appropriate value for the thickness of the slice-selective inversion pulse, a range of thicknesses (8-35 mm) were simulated for the stated range

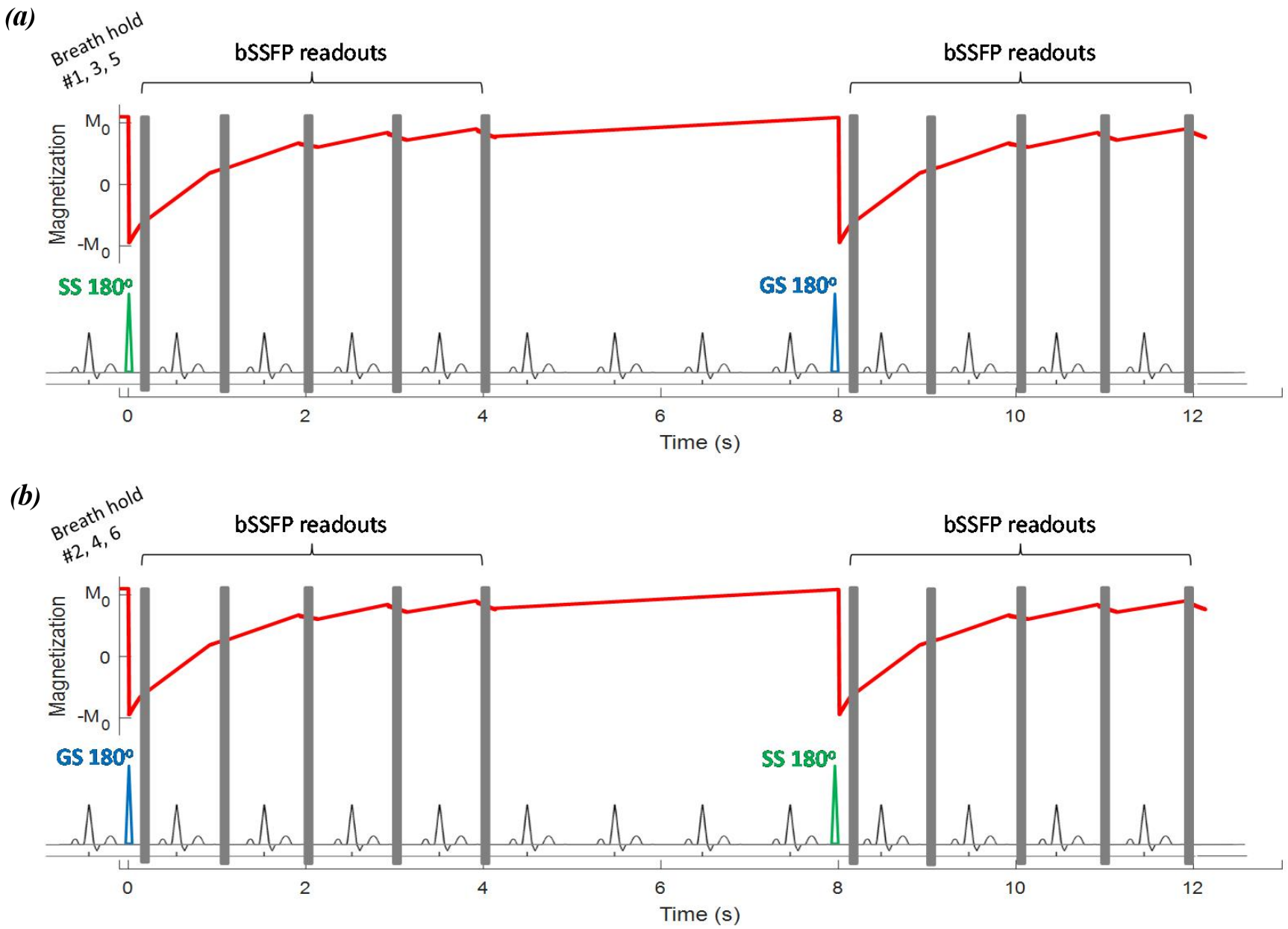


Figure 5.1: Schematic of the LL-FAIR-ASL pulse sequence over 13 heartbeats for (a) breath holds 1,3 and 5 and (b) breath holds 2,4 and 6. 180° pulses (one slice-selective (SS), one globally selective (GS), within a single breath hold, the order of which is varied) are each followed by 5 bSSFP readouts (shown as grey boxes), separated by an R-R interval. The evolution of M_z throughout the sequence is shown in red.

of T_1s, with a fixed image slice profile with thickness of 8 mm FWHM in order to investigate the interaction between the HS8 inversion pulse profile and the image slice profile. The inflow was not simulated, such that the performance of the sequence in measuring only the relaxation under the two different inversion conditions could be investigated to ensure that any difference measured in vivo was due to blood flow and not systematic error.

5.1.4 Phantom Studies

A phantom imaging study was carried out in order to further investigate the performance of the LL-FAIR-ASL sequence in the absence of flow. The data gathered were used to investigate the dependence of T_1 and the apparent T_1 (called T_1*) on heart rate with the LL-FAIR-ASL sequence by plotting these values against a range of simulated heart rates. The length of the gap between the two inversion blocks (measured in heartbeats) was also varied to investigate the effect of imperfect recovery before the second inversion. These experiments were carried out on an integrated calibration phantom distributed by Dr. S. Piechnik, Oxford, for the HCMR study (Clinicaltrials.gov ID: NCT01915615). The phantom was designed to monitor stability of T_1 mapping techniques, and provides a T_1 range of ∼300-3000 ms, and T_2 ∼60-3000 ms. The phantom consists of 9 test objects made of agar and carrageenan water gels doped with nickel chloride. The study was carried out on the 3 T scanner using a 32 channel body receive array. The simulated ECG trigger was varied from 40 bpm to 140 bpm in 20 bpm intervals. The resulting images were loaded into purpose built MATLAB analysis code, where regions of interest (ROIs) were drawn by hand within the confines of each tube and propagated throughout an image series in order to calculate the T_1s of the samples.

5.1.5 In Vivo Studies

ASL image series were acquired on 11 healthy volunteers (31 ± 7 years old, 71 ± 9 kg, two female) at 3 T, in basal, mid-ventricular and apical short-axis slices, as shown in Figure 5.2(b) using the 32 channel body receive array. All volunteers were recruited in accordance with the ethical practices of our institution and their informed consent obtained. Each of the volunteers was scanned twice, on separate days, making 22 scan sessions in total. The data from one subject was discarded due to excessive motion within image series. In 17 of the 20 successful scans, the ASL acquisitions in the mid-ventricular slice were repeated. The basal and apical slices were not repeated within-session due to scan-time restraints. In this study no extra measures were taken to control the condition of the subjects, such as limiting the recent intake if food or caffeine.

After an initial localiser to locate the heart of the subject, planing scans were acquired in the vertical long axis (VLA) and horizontal long axis (HLA) planes. From the resultant images, the appropriate short-axis slice could be acquired. B_0 shimming was performed in a volume over the left ventricle (LV) covering all three slices. A short-axis cine series was then acquired in order to determine the appropriate trigger delay for mid-diastole. All scans were acquired using end-expiration breath holding. In each slice, the sequence as described in Figure 5.1 was run three times with the slice-selective inversion block preceding the globally inverted block (called the SS-GS ordering scheme), then run a further three times with the global inversion block preceding the slice-selective (GS-SS), making for a total of six measurements, from which a single value of the global MBF could be calculated. A slice-selective inversion thickness of 24 mm was used based on the results of the simulation and phantom scans described. This inversion slab and the imaging slice were positioned as described in Figure 5.2(a). In all cases ECG triggering and breath holding were employed and the heart rate of each subject was recorded.

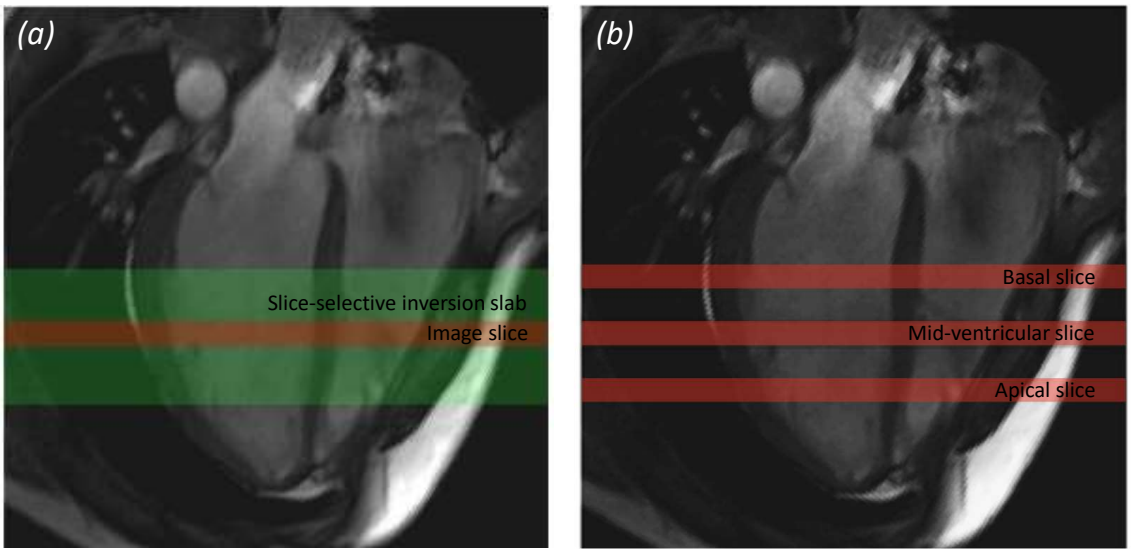


Figure 5.2: A four-chamber view of the heart with (a) the position of the imaging slice in red, and the position of the slice-selective inversion slab in green, and (b) the positions of the basal, mid-ventricular and basal imaging slices.

5.1.6 Image Analysis

An image analysis pipeline was set up and, is shown in Figure 5.3. All image series were loaded into MATLAB and regions of interest (ROIs) were drawn by hand for both the left ventricular myocardium and the blood pool. For the myocardium, the epicardial and endocardial borders were drawn and the myocardium divided into segments as per the 16 segment American Heart Association (AHA) model[6]. All the parameters necessary for the analysis (inversion times, signal intensities, phase data,...) were extracted from the DICOM files and sorted into MATLAB variables. The phase data of the most fully recovered image from each inversion block, in which it is assumed that the signal in all pixels has recovered past the null point, were used as a reference phase map to correct the polarity of the magnitude images on a pixel-by-pixel basis prior to fitting[7]. The phase reference map was subtracted from the phase image for each TI and values in the resultant map which were close to zero were those which had recovered past the null point. Those pixels in the image which

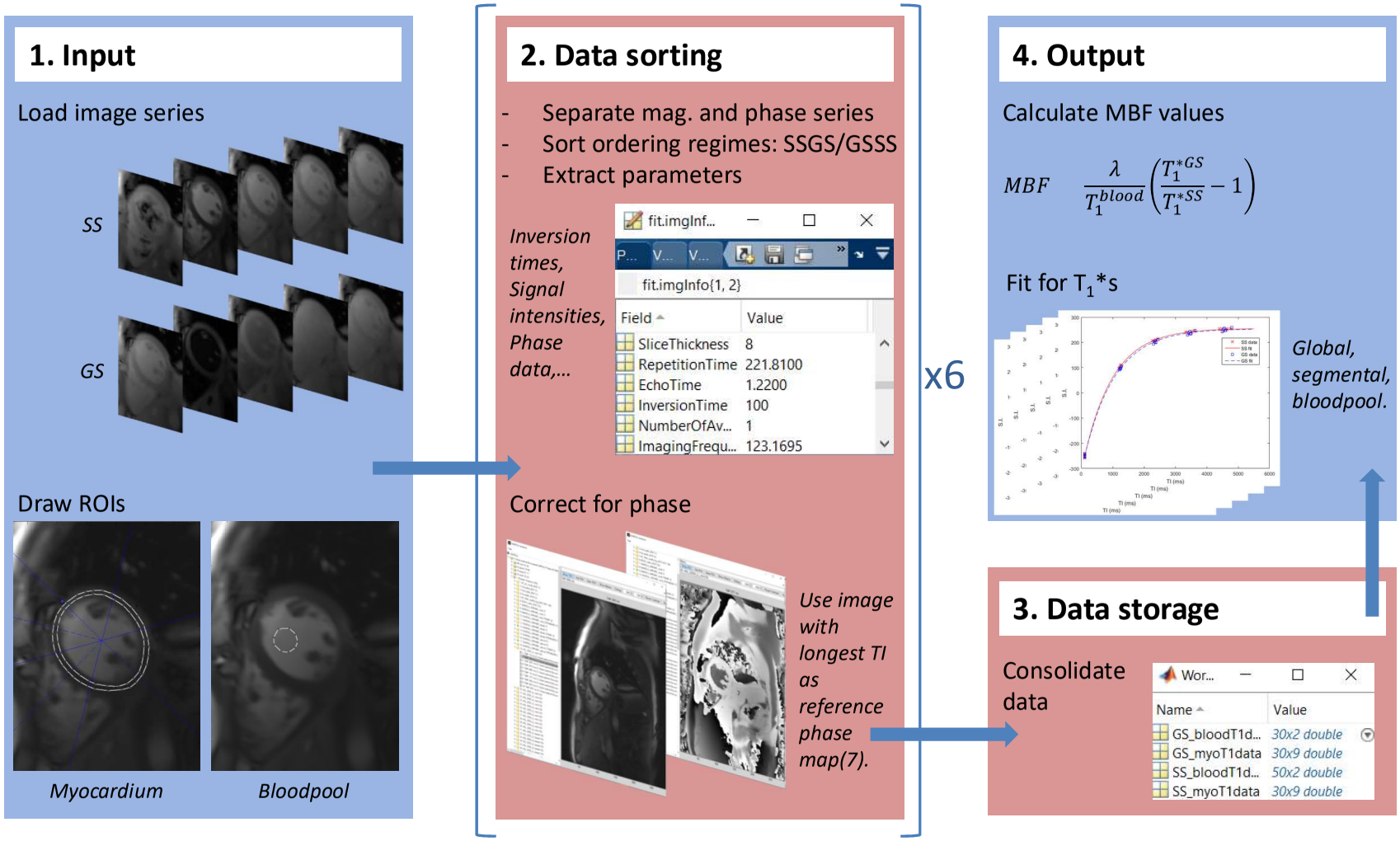


Figure 5.3: The analysis pipeline for quantification of MBF from six breath held acquistions of the LL-FAIR-ASL sequence.

had not recovered past the null point were out of phase with the concomitant pixel in the phase reference map and so had a value which was not close to zero. These pixels could then be multiplied by -1 in the relevant magnitude image in order to restore polarity.

The polarity corrected data for each TI were then consolidated, such that a single pair of inversion recovery curves could be drawn for each set of six averages of the ASL sequence. The apparent T_1 values (T_1*) for the myocardium for both the slice-selective and global inversion blocks were calculated, as was the T_1 of blood from the global data by using a three-parameter least squares fit as described by equation 2.8, from Chapter 2, in the form,

$$S(TI) = A - Bexp\left(\frac{TI}{T_1^*}\right) \tag{5.1}$$

where S was the signal intensity recorded at the inversion time TI and A, B and T_1* were the fitted parameters. Where T_1 values are reported, the correction described by Deichmann and Haase for FLASH images[8] and described in Equation 5.2 was used, though only strictly applicable in the small tip angle regime.

$$T_1 = T_1^*\left(\frac{B}{A} - 1\right) \tag{5.2}$$

The myocardial blood flow (MBF) for each slice was calculated from these data by the Belle quantification model[9], as described in Chapter 4.5.2:

$$MBF = \frac{\lambda}{T_1^{blood}}\left(\frac{T_1^{GS}}{T_1^{SS}} - 1\right) \tag{5.3}$$

where $\lambda = 0.92$ ml/g[10] is the blood-tissue partition coefficient of water, T_1^{blood} is the relaxation time of the blood pool and T_1^{GS} and T_1^{SS} are the values for the longitudinal relaxation time calculated for the myocardium, from the global and slice-selective experiment respectively. For the in vivo study, the T_1^{GS} and T_1^{SS} values used were the

observed T_1*s. As has been discussed previously[11, 12], where the Deichmann-Haase correction is employed the ratio of the relaxation times remains constant T_1^{GS}/T_1^{SS} = T_1^{*GS}/T_1^{*SS} as the fitted values of A and B remain the same for both the global and slice-selective cases. Thus, use of the correction would have no effect on the final value of MBF. The use of T_1* is discussed further later in this work.

5.1.7 Reproducibility and Variability Analysis

The in vivo data were used to perform Bland-Altman analysis[13] in order to assess reproducibility and variation. The mean difference in each case and the value of ± 1.96 times the standard deviations (SD) were calculated, which represent the upper and lower 95% confidence bounds. When normalised to the mean value of MBF, these values give the coefficient of repeatability for both the between-session (CR_{BS}) and within-session cases (CR_{WS}). The variability of the MBF estimates was assessed by the coefficient of variation (CV, equal to the ratio of the standard deviation to the mean) for the whole sample (CV_{all}), and each subject between-session (CV_{BS}) and within-session (CV_{WS}).

5.1.8 Segmental Analysis

Values of MBF were calculated for each of sixteen standard myocardial segments, as defined by the American Heart Association (AHA)[6], in order to assess the viability of the ASL technique at segmental level. For each segment these are reported as the mean and standard deviation across all the volunteers. The coefficient of variation (CV_{seg}) is also reported for all segments.

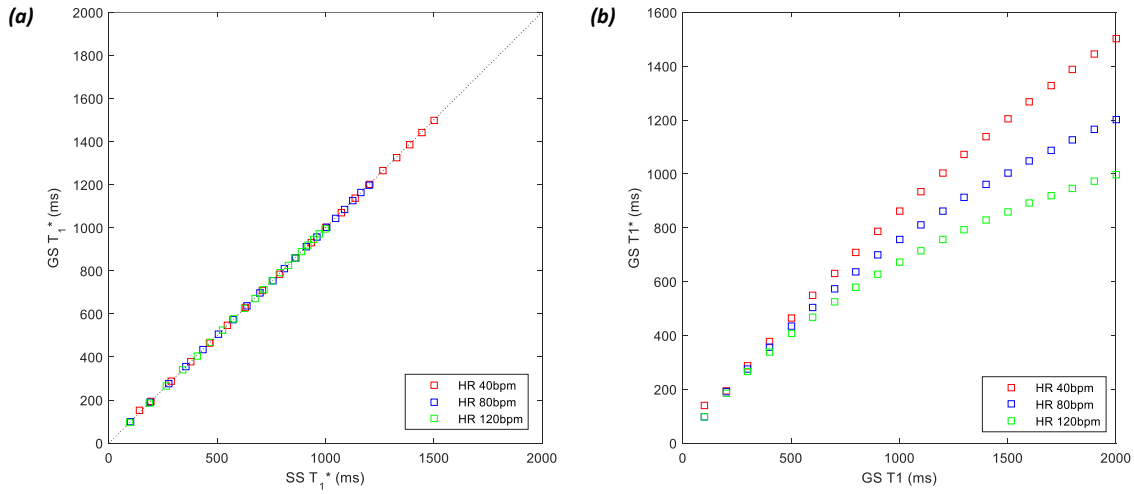


Figure 5.4: (a) Correlation plot of the simulated slice-selective and globally-selective T_1*s, in the absence of flow, for heart rates of 40, 80 and 120 bpm and input T_1 values from 100 to 2000 ms (100 ms steps),and (b) the GS data only, plotted as the true T_1 against the observed T_1*.

5.2 Results

5.2.1 Simulations

T_1* data was plotted for heart rates of 40, 80 and 120 bpm and for the full range of input T_1s. Figure 5.4(a) shows the simulated slice-selective and globally selective T_1*s to agree well in the absence of flow, with an R^2 value of 0.9997 and both the T_1*s shortening with increasing heart rate. The latter effect is better displayed in figure 5.4(b) which shows the GS data only, with the true input T_1 plotted against T_1* for the heart rates of 40, 80 and 120 bpm. It shows that the higher the heart rate the further the calculated T_1* is from the true T_1.

Figure 5.5 shows the results of simulations to determine an appropriate value for the thickness of the slice selective inversion pulse. Results for both T_1 and T_1* are plotted showing the dependence of the calculation on the extT_1.ent of the inversion. The values are stable down to an inversion thickness of 23 mm then decrease with decreasing thickness. The effect is more marked with T_1 than T_1*. For the input T_1

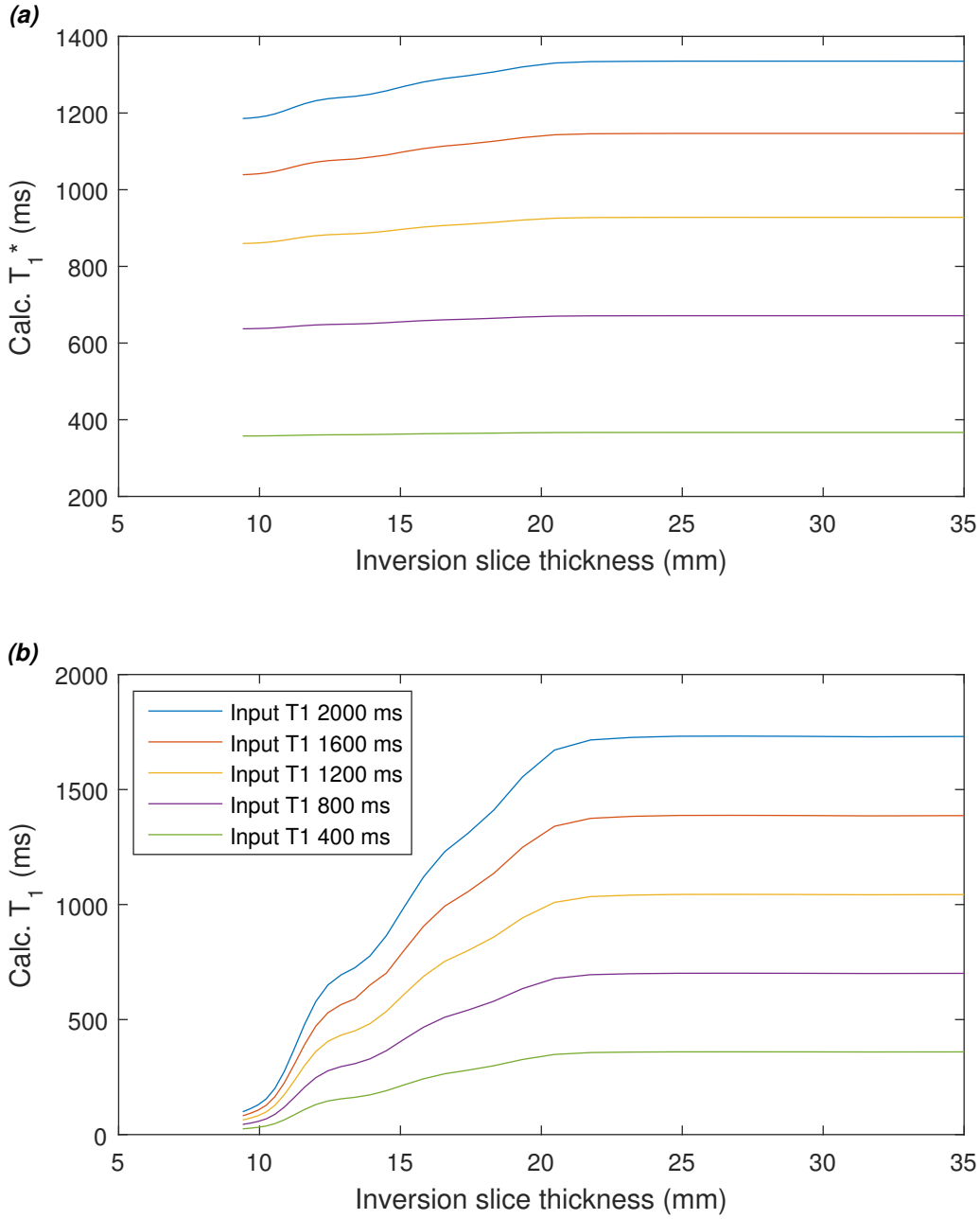


Figure 5.5: For an image slice thickness of 8 mm, the slice-selective HS8 inversion pulse width, varied from 8 to 35 mm, is plotted against the simulated (a) T_1*, and (b) T_1, following the Deichmann-Haase correction, for input T_1 values of 400 to 2000 ms (400 ms steps).

of 1200 ms, approximately in the myocardial range, the T_1* drops from a maximum of 928 ms with the thickest inversion slice to 860 ms with the thinnest, a drop of 7%. The calculated T_1, however, drops from 1043 ms with the thickest slice to just 63 ms with the thinnest, a drop of 94%.

5.2.2 Phantom Studies

An example plot of T_1 and T_1* against simulated heart rate is shown in Figure 5.6 for a gap of 3 heartbeats. The dependence of T_1* on heart rate can be clearly seen for both the SS-GS and GS-SS ordering schemes, decreasing steadily as the heart rate increases. The calculated T_1, however, is stable for the first inversion block in the ordering scheme, whether SS or GS, with a value of 1431 ± 8 ms for the range of heart rates, but decreases rapidly with increasing heart rate, and therefore decreasing recovery time, for the second inversion block. Thus, the calculation of T_1 is dependent on the ordering scheme, whereas the calculation of the T_1*s is not.

5.2.3 In Vivo Studies

Figure 5.7 shows a typical pair of T_1 recovery curves, with inset SS and GS image series. The mean MBF across all the ten volunteers and all twenty scan sessions was 1.04 ± 0.40 ml/g/min in the basal slice, 1.06 ± 0.46 ml/g/min in the mid-ventricle and 1.06 ± 0.38 ml/g/min in the apical slice. The calculated values of MBF for each subject in each session, as well as the mean values, are presented in Figure 5.8(a). The data is presented for all scans in all three slices.

The T_1 of blood, calculated from the GS recovery of the LL-FAIR-ASL sequence and used in the quantification of MBF for each subject was 1842 ± 64 ms across all 20 scans. The mean change in T_1 of blood for a subject between scans was 27.5 ms. The heart rate across all 10 subjects including repeat scans was 57 ± 11 bpm, ranging from 37 to 83 bpm. The mean change in a subject's heart rate between days was just

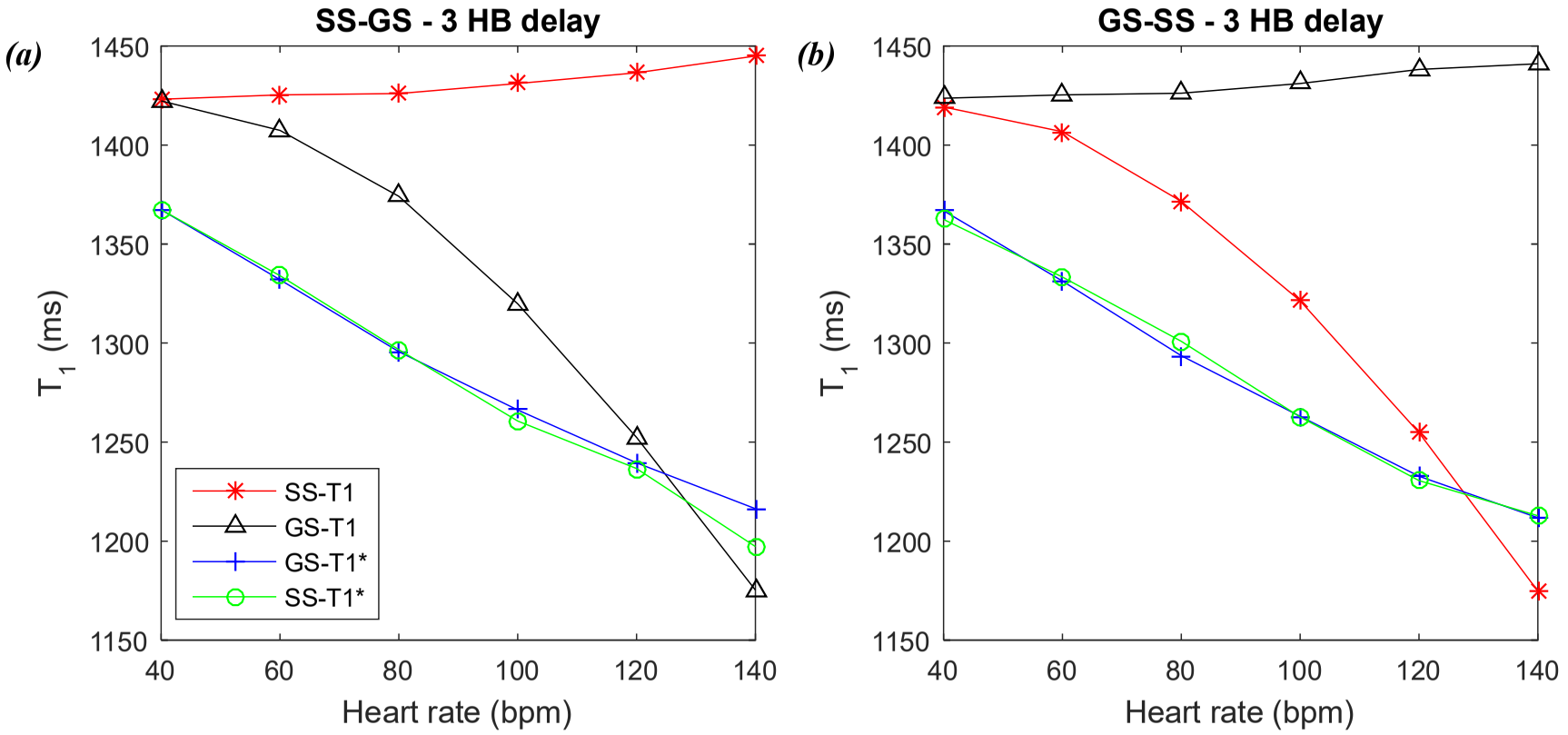


Figure 5.6: Measured T_1* and T_1 of a cardiac phantom, for both the slice-selective and globally-selective inversion blocks plotted against simulated heart rate, from 40-140 bpm. There was a three heartbeat delay between the end of one block and the start of the next. The data are plotted for (a) the slice-selective - globally-selective (SSGS) and (b) the globally-selective - slice-selective (GSSS) ordering scheme.

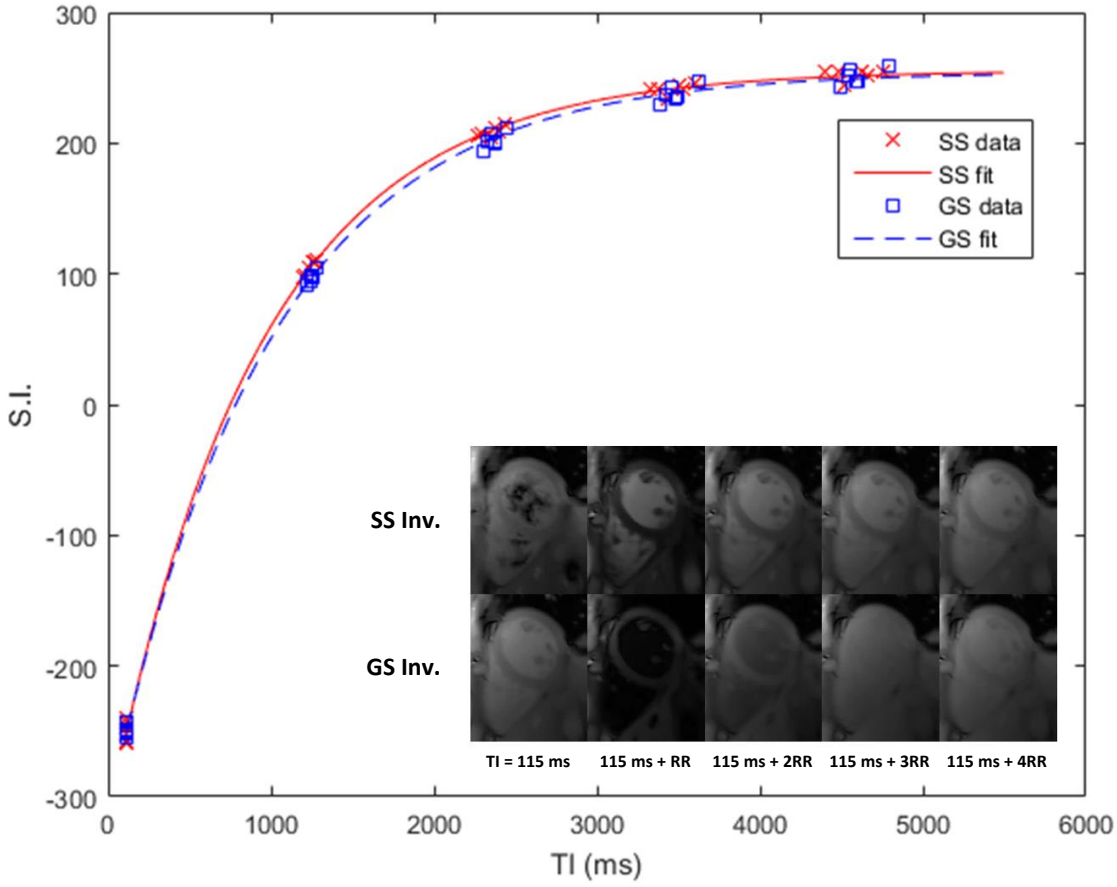


Figure 5.7: A typical slice-selective/globally-selective inversion recovery pair of curves with data points from six breath holds averaged over an ROI encompassing the left ventricular myocardium, and corresponding image series inset from one of the six breath-holds.

MBF Results							
Slice	Mean MBF (mL/g/min)	Std	CV_{all} (%)	CV_{BS} (%)	CV_{WS} (%)	CR_{BS} (%)	CR_{WS} (%)
Basal	1.04	0.40	39	14	-	72	-
Mid	1.06	0.46	43	16	13	61	53
Apical	1.06	0.38	36	17	-	85	-

Table 5.1: MBF results from in vivo scans in three slices, including the mean myocardial blood flow (MBF), the standard deviation and the coefficient of variation (CV) across all scans and the CV and coefficient of reproducibility (CR) for between-session (BS) and within-session (WS) cases.

4.5 bpm. Figure 5.8(b) shows the heart rate of each subject plotted against the MBF calculated for the mid-ventricular slice. A linear fit is also plotted with an R^2 value of 0.78.

5.2.4 Reproducibility and Variability Analysis

Values for the coefficients of variation and reproducibility, for both the between session and within session cases, are presented in Table 5.1. The CV across all scans was calculated as 39, 43 and 36% in the basal, mid-ventricular and apical slices respectively. The CV_{BS} was 14, 16 and 17% in basal, mid and apex, and the CV_{WS} was 13% in the mid-ventricle. The Bland-Altman plots are shown in Figure 5.9. The CR_{WS} was 53% in the mid-ventricle, compared with CR_{BS} values of 72, 61 and 85% in the base, mid and apex.

5.2.5 Segmental Analysis

The mean values and standard deviations of segmental MBF are reported in Table 5.2 along with the coefficient of variation, for all sixteen segments. The range of mean segmental MBF values is 0.87-1.52 mL/g/min. These values are also plotted in Figure 5.10(a), along with previous literature values of MBF in four segments in the mid-ventricle (septum and anterior, lateral and inferior walls) using ^{15}O PET[14]. The

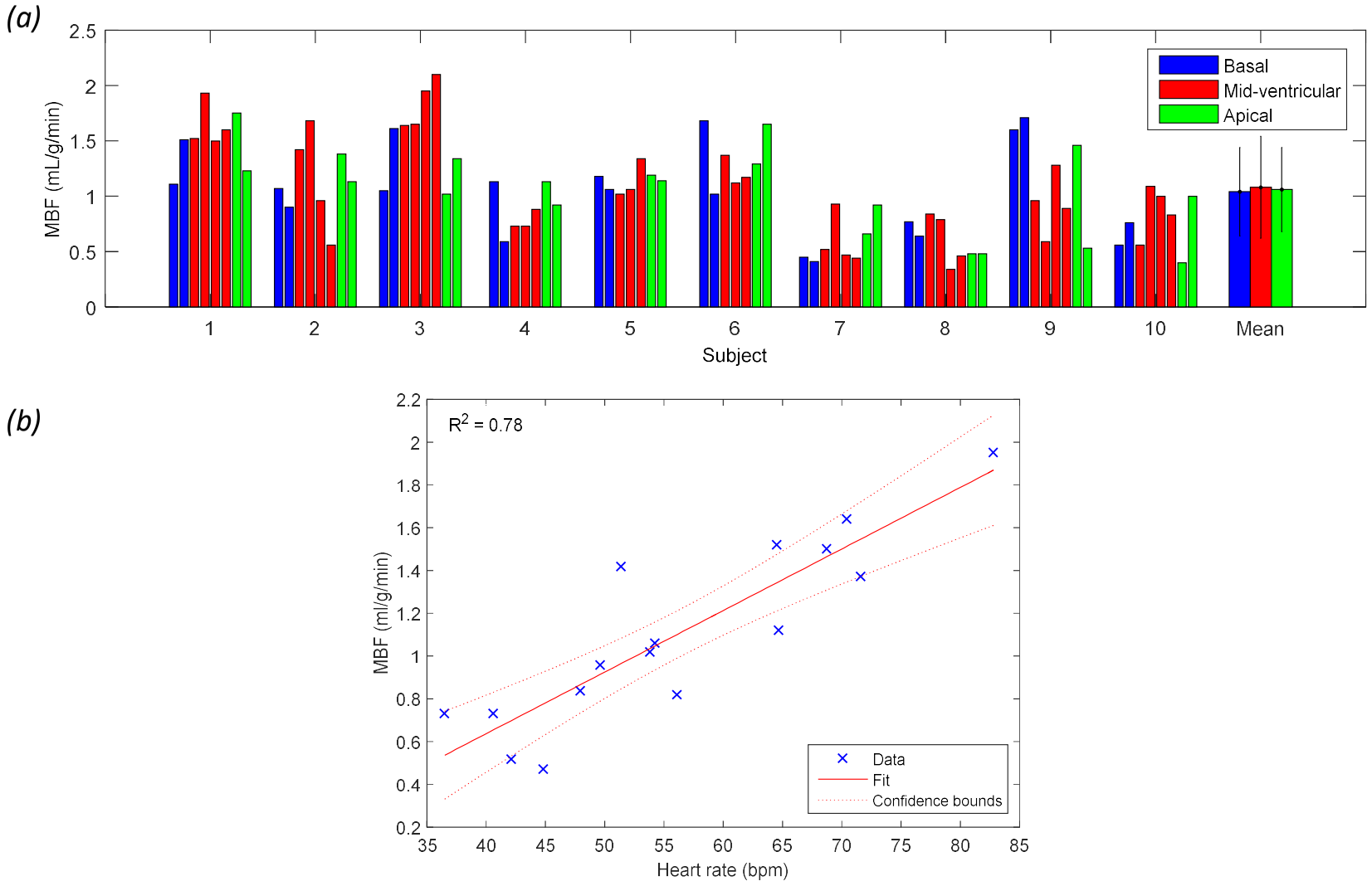


Figure 5.8: (a) Calculated MBF results for both scan sessions for all ten volunteers in basal, mid-ventricular and apical slices represented by blue, red and green bars respectively. Error bars denote the standard deviation, and (b) the mean heart rate for the subject plotted against the MBF calculated in the mid-ventricular slice.

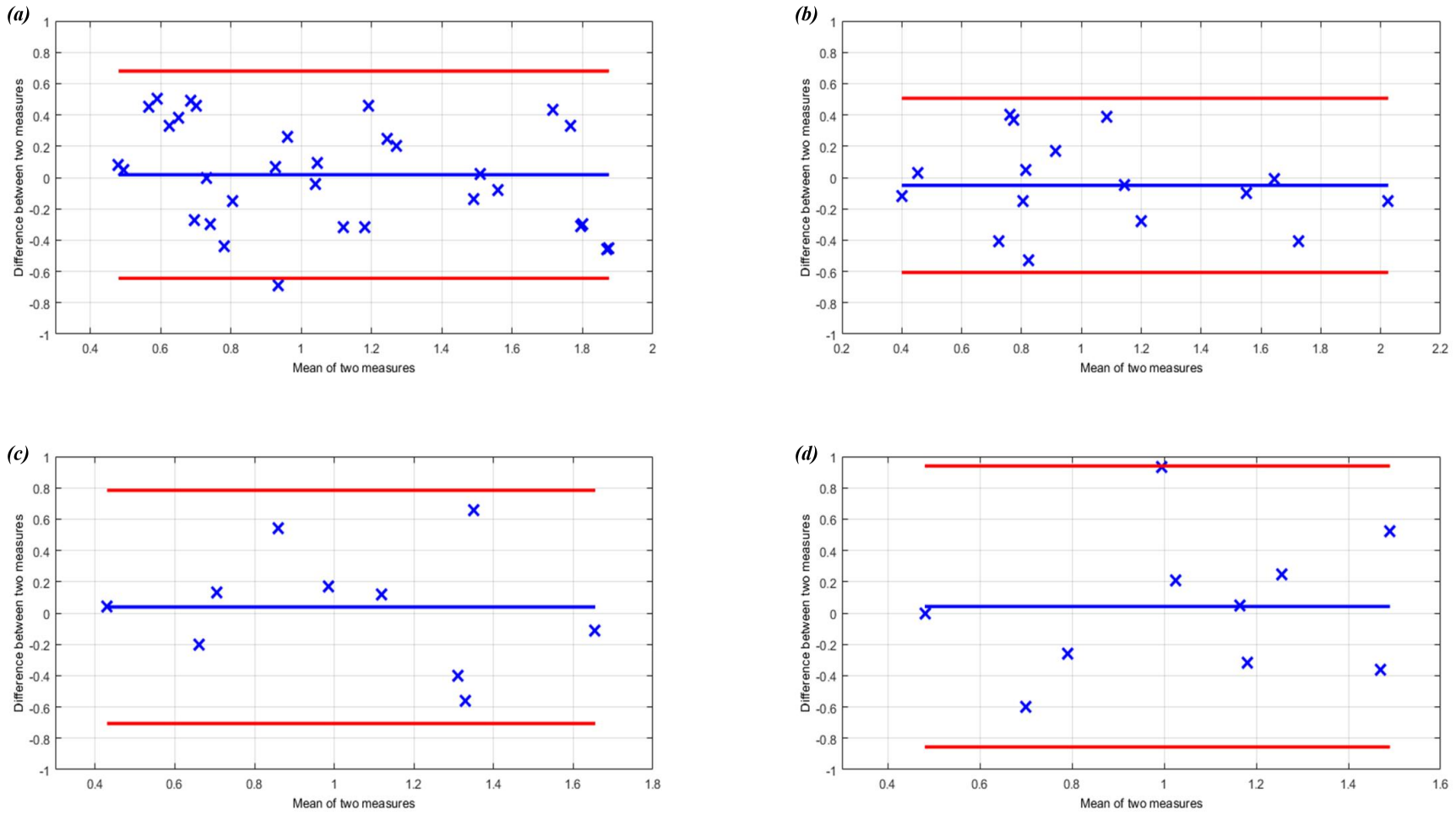


Figure 5.9: Bland-Altman plots for (a) mid-ventricular between-session reproducibility, (b) mid-ventricular within-session reproducibility and the between-session reproducibility for (c) the basal and (d) apical slices. The blue lines represent the mean difference in MBF and the red lines show ± 1.96 times the standard deviation and represent the 95% confidence limits. These are normalised to the mean MBF to calculate the coefficients of reproducibility (CR).

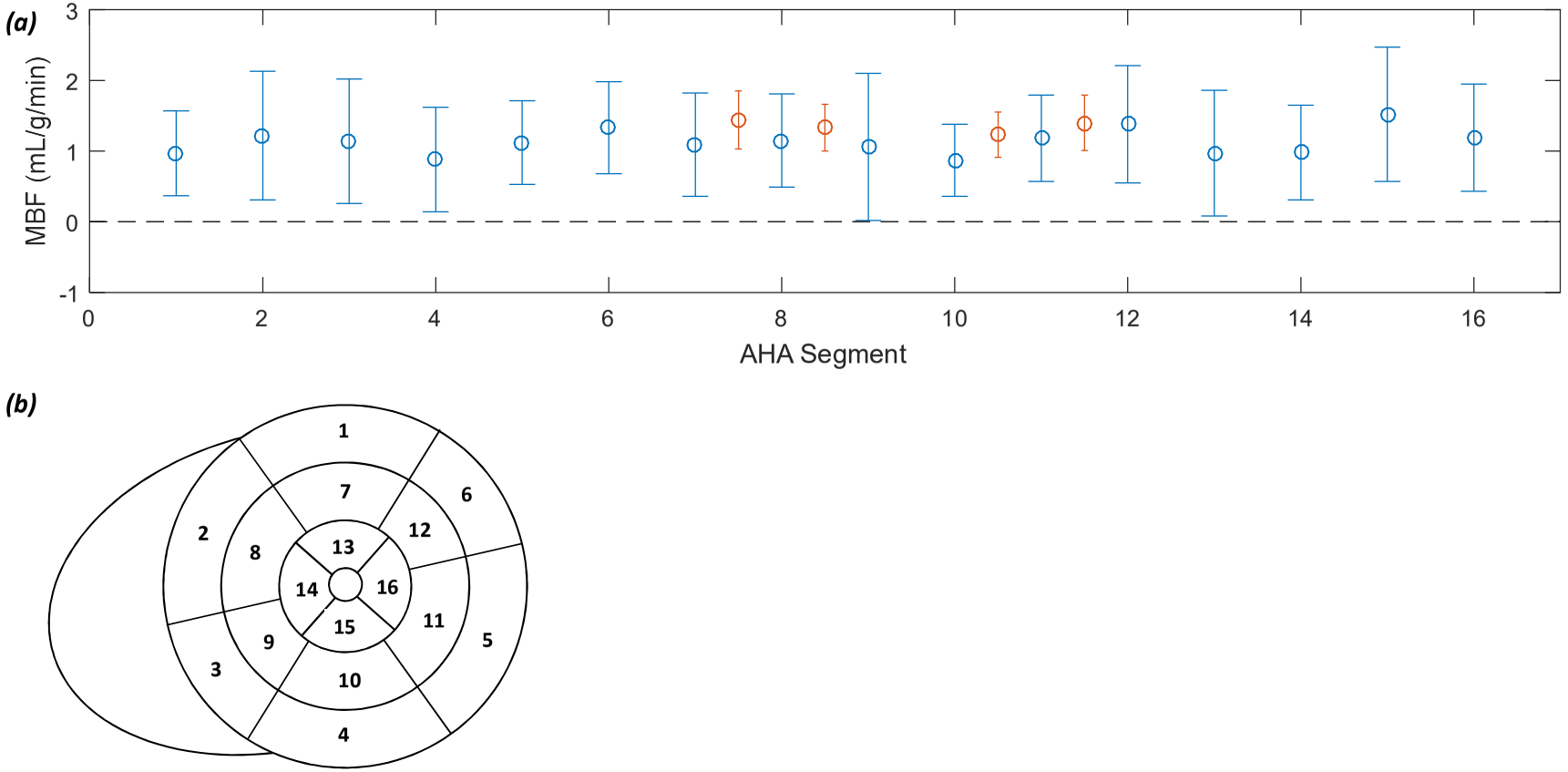


Figure 5.10: The mean ± standard deviation of MBF across all subjects for each myocardial segment as defined by the American Heart Association[6], as described in (b), where segments 1-6 are the basal slice, 7-12 are the mid-ventricular slice and 13-16 are the apical slice. The data points in red are literature values in the septum and anterior, lateral and inferior walls of the mid–ventricle from Chareonthaitawee et al 2001[14].

Segmental MBF Results			
Segment	Mean MBF (mL/g/min)	Std (mL/g/min)	CV_{seg} (%)
1	0.97	0.60	62
2	1.22	0.91	75
3	1.14	0.88	77
4	0.88	0.74	84
5	1.12	0.59	53
6	1.33	0.65	49
7	1.09	0.73	67
8	1.15	0.66	57
9	1.06	1.04	98
10	0.87	0.51	59
11	1.18	0.61	52
12	1.38	0.83	60
13	0.97	0.89	92
14	0.98	0.67	68
15	1.52	0.95	63
16	1.19	0.76	64

Table 5.2: Mean MBF values for each segment, where segments 1-6 are the basal slice, 7-12 are the mid-ventricular slice and 13-16 are the apical slice, as per the American Heart Association (AHA) standard model[6].

numbering of the segments is described in Figure 5.10(b).

5.3 Discussion

In this chapter, a non-invasive method for quantitatively measuring myocardial blood flow using arterial spin labelling was developed and tested via simulation, phantom experiment and in vivo studies. The variation and reproducibility of the method were then investigated in three short axis slices, where previous cardiac ASL studies have been restricted to the mid-ventricle.

The Bloch simulations of the LL-FAIR-ASL sequence show good agreement between the SS and GS T_1*s as presented in Figure 5.4(a). Thus, there is no dependence in the MBF calculation on error in the calculation of the T_1* ratio. This is true of the three simulated heart rates (40, 80 and 120 bpm) despite the expected shortened T_1* with increasing heart rate due to saturation from multiple high flip angle readouts, as seen in the simulated evolution of magnetisation in Figure 5.1.

As observed in Figure 5.5, the calculation of T_1* and T_1 is compromised at lower values of the inversion slice thickness relative to the imaging slice thickness. This occurs due to differences between the inversion profile and the image slice profile. The effect is far more marked in the calculation of T_1 due to the failure of the Deichmann-Haase correction on inversion efficiency. At lower inversion thicknesses the efficiency is low due to the slice containing a mixture of inverted and non-inverted spins. By comparison, T_1* has no dependence on inversion efficiency, providing further motivation for its use over T_1. These data were employed in the choice of inversion thickness for in vivo application of 24 mm.

Varying the simulated heart rate in the phantom scans demonstrates that the values of T_1* are far more stable than those of T_1. Though T_1* is dependent on heart rate, as demonstrated in Figure 5.6, the T_1* values calculated for the SS and GS

Study Comparison					
Source	Method	Age (y)	Gender	Population	MBF_{rest} (mL/g/min)
LL-FAIR-ASL	**ASL**	**31 ± 7**	**8 M/2 F**	**Healthy**	**1.06 ± 0.46**
Zun 2009[15]	ASL	-	8 M/2 F	Healthy	1.36 ± 0.40
Zun 2011[16]	ASL	64 ± 11	10 M/19 F	CAD patients	0.97 ± 0.64
Wang 2010[17]	ASL	39 ± 9	10 M/1 F	Healthy	1.00 ± 0.55
Northrup 2008[18]	ASL	22 ± 2	5 M/3 F	Healthy	1.06 ± 0.19
Jerosch-Herold 2008[19]	CMR - First Pass	63 ± 10	11 M/19 F	Atherosclerosis	1.01 ± 0.22/0.91 ± 0.18*
Hsu 2006[20]	CMR - First Pass	33 ± 4	2 M/8 F	Healthy	1.02 ± 0.22
Manabe 2009[21]	^{82}Rb PET	29 ± 9	8 M/7 F	Healthy	0.99 ± 0.29/1.00 ± 0.25*
Chareonthaitawee 2001[14]	^{15}O PET	46 ± 12	131 M/38 F	Healthy	1.33 ± 0.32

Table 5.3: Comparison of LL-FAIR mid-ventricular resting MBF against literature values for previous cardiac ASL methods, first-pass perfusion CMR and PET. * Results from two separate exams on the same group of patients/volunteers.

cases exhibit the same dependence, meaning heart rate does not bias the calculation of MBF as it is calculated from a ratio of the GS and SS T_1*s. As discussed above, the T_1 correction is highly dependent on the inversion efficiency, and in each ASL ordering scheme the second of the two inversions suffers from apparent poor efficiency due to insufficient time for relaxation between blocks, which is necessary for achievable breath holds. T_1* was used for all MBF calculations as the Deichmann-Haase correction is only strictly applicable in a small angle regime and for inversion pulses applied to spins at equilibrium magnetization[8]. T_1* is independent of inversion efficiency and, as stated earlier the ratio of global to slice selective T_1*s is the same as the ratio of global to slice selective T_1s.

The LL-FAIR-ASL method is attractive as it provides a non-invasive alternative to SPECT, PET and first-pass perfusion CMR. Using this method, MBF can be measured quantitatively in a single slice in six 13 heartbeat breath holds. Each breath hold contains both slice-selective and globally-selective acquisitions, which ensures that the position of the heart and heart rate are the same for each pair. The ability to acquire an SS/GS pair in a single breath hold is an important feature of the LL-FAIR-ASL sequence, as the measured changes in T_1* are small and could easily be lost among systematic errors. The mean MBF, in the mid-ventricular slice, of 1.06 $\pm$ 0.46 ml/g/min compares well with literature values, as presented in Table 5.3[14, 20, 19, 21, 18, 17, 15, 16]. From 5.8(b) it can be seen that there some correlation between the heart rate of the subject and the MBF. Those subjects with a higher heart rate also show a higher value of MBF. As the use of a T_1* ratio in the MBF calculation should be independent of the absolute heart rate of the subject and only be affected by a significant within-scan change in heart rate, it could be that the heart rate itself is a factor in the heterogeneity of resting MBF in normal hearts, along with other factors. However, it could be that a more complex model of MBF quantification could benefit from including a measure of the subject's heart rate.

One potential source of error with the LL-FAIR-ASL technique could be in the choice of TIs. Given the finite arrival time of the ASL bolus, the first readout with the shortest value of TI, may occur before the arrival of the label. in addition, in people with low heart rates in particular, the final TI may occur after the label is decayed. This means that it could be the case that only the middle three of the five readouts are in fact sensitive to perfusion and contribute to the ASL difference signal.

While reproducibility and variability of similar techniques have been investigated in mice[22, 23], to our knowledge this has not been carried out in human myocardium. Resting MBF values for healthy volunteers have previously been shown to be heterogeneous in studies utilising PET[14] and first-pass perfusion CMR[24]. The high observed values for CV_{all} across all subjects, 39, 43 and 36% for basal mid and apical slices respectively, show that our results reflect this heterogeneous nature. This variability, calculated as the coefficient of variation is comparable to similar measures reported for preclinical cardiac ASL[22, 23].

The values of CV_{BS} and CV_{WS} calculated for individual subjects were all below the values reported for CV_{all} except for a single apical slice which gave a CV_{BS} of 43%. However the mean values of CV_{BS} for each slice and CV_{WS} for the mid slice only, are significantly lower than CV_{all}, with a maximum of 17%. This shows that the variation in results exhibited by an individual subject in each case is much less than across the population as a whole. The CV_{BS} shows the variation due to the method, plus re-setup effects such as repositioning, re-localisation, re-shimming etc. The CV_{WS} primarily reflects the methodological effects.

The Bland-Altman analysis shows the mean difference in both the between-session case for all three slices and the within-session case, for the mid slice only, to be close to zero and all bar one of the data points to lie within the $\pm$ 1.96 SD bounds. The values of CR give an indication of the change in MBF required to be detected above systematic errors. The between-session CRs of 72, 61 and 85% for the basal, mid and

apical slices, show the level of repeatability expected across repeat scans. They show the change in MBF required to show a difference over time and is useful to consider if planning a longitudinal study in a patient group. The within-session CR of 53% for the mid-ventricular slice gives a useful indication of the detectable change in MBF. Thus, a change in MBF would be reliably detectable when rising from the mean mid-ventricular MBF, measured with LL-FAIR-ASL, of 1.06 mL/g/min to a value of 1.74 mL/g/min between-session and 1.65 mL/g/min within-session. During vasodilator stress, the change in MBF in non-ischaemic segments of the heart has been shown to be between 300-420%[16, 25, 26], or between 3.24 and 4.54 mL/g/min based on the mean mid-ventricular MBF reported here. Therefore, the expected change in global MBF under stress would be expected to be detectable with the LL-FAIR-ASL method.

Segmental MBF is an important measure in disease, as it allows investigation of MBF changes in the arterial territories of the myocardium. Segmental ischaemic injury can result in myocardial stunning[27], whereby the contractile motion of the heart becomes abnormal. Previous publications using PET[14] and ASL[16] have commented on the spatial heterogeneity of resting MBF within a slice. The relative dispersion, here called the coefficient of variation, was reported as 13% with PET and 68% (range 11% to 152%) with ASL, compared with 67% (with a range of 49% to 98%) with LL-FAIR-ASL. This difference in error between the ASL methods and PET is also reflected in the data plotted in Figure 5.10 and is perhaps expected given the inherently low SNR of the method and the low resolution of the PET method, noted as a limitation by the authors and reported as 8.43 x 8.33 x 6.6 mm^3 full-width half maximum compared with 1.7 x 2.2 x 8 mm^3 with LL-FAIR-ASL. However, given the expected increase in MBF under stress, the difference in perfusion reserve between ischaemic and normal segments, should be detectable.

This study served to validate the LL-FAIR-ASL technique for measurement of

resting MBF in healthy humans. Future studies will be required to validate the method in patient populations under stress and compare the results with standard methods such as first-pass perfusion CMR. In addition, more complex models for quantification of MBF, taking account of such effects as Arterial Transit Time (ATT) and the perturbation of the inversion recovery by the readouts could be implemented. In addition, the partial inversion of the blood pool during slice-selective inversion could be included in the model. Though it is assumed that the inflowing blood in the slice-selective inversion recovery is completely non-inverted, in fact the labelling slab does cover and will therefore invert part of the blood pool in the ventricles. Over the course of the SS epoch, these inverted spins will mix with other, non-inverted spins in the blood pool and arriving from the rest of the body, such that the blood flowing into the image slice will in fact be partially inverted and present with a measurable but very short T_1. It has been shown that the effect of this partial inversion is a systematic underestimation of MBF[11]. However, the expansion of the quantification model to include the above discussed parameters was considered to be beyond the scope of this work.

5.4 Conclusion

The LL-FAIR-ASL sequence for quantitative measurement of MBF was shown to be robust and efficient when performed in vivo. The method is completely non-invasive, not requiring contrast agent, and provides resting MBF values in healthy volunteers which compare well with the literature and display the previously reported heterogeneity within healthy volunteer groups. MBF values are reported globally and segmentally in three slices with a cardiac ASL technique for the first time. The variability of the method was shown to compare favourably with published values in similar techniques employed in preclinical imaging but, to our knowledge, has

not previously been performed in human volunteers. The method was shown to be sensitive enough to detect MBF increase under stress conditions in future studies. The presented results should prove useful in the planning of clinical research studies using this sequence to quantitatively measure MBF at rest and under stress in healthy volunteers or in patient groups.

References

[1] A. Tannús and M. Garwood. Adiabatic pulses. *NMR in biomedicine*, 10(8):423–434, December 1997.

[2] B. P. Poncelet, T. M. Koelling, C. J. Schmidt, K. K. Kwong, T. G. Reese, P. Ledden, H. L. Kantor, T. J. Brady, and R. M. Weisskoff. Measurement of human myocardial perfusion by double-gated flow alternating inversion recovery EPI. *Magnetic resonance in medicine*, 41(3):510–519, March 1999.

[3] Michael Schär, Sebastian Kozerke, Stefan E. Fischer, and Peter Boesiger. Cardiac SSFP imaging at 3 tesla. *Magnetic resonance in medicine*, 51(4):799–806, April 2004.

[4] Mark A. Griswold, Peter M. Jakob, Robin M. Heidemann, Mathias Nittka, Vladimir Jellus, Jianmin Wang, Berthold Kiefer, and Axel Haase. Generalized autocalibrating partially parallel acquisitions (GRAPPA). *Magn. Reson. Med.*, 47(6):1202–1210, June 2002.

[5] Hung Phi P. Do, Terrence R. Jao, and Krishna S. Nayak. Myocardial arterial spin labeling perfusion imaging with improved sensitivity. *Journal of cardiovascular magnetic resonance*, 16, 2014.

[6] Manuel D. Cerqueira, Neil J. Weissman, Vasken Dilsizian, Alice K. Jacobs, Sanjiv Kaul, Waren K. Laskey, Dudley J. Pennell, John A. Rumberger, Thomas Ryan, Mario S. Verani, and American Heart Association Writing Group on Myocardial Segmentation and Registration for Cardiac Imaging. Standardized myocardial segmentation and nomenclature for tomographic imaging of the heart. a statement for healthcare professionals from the cardiac imaging committee of the council on clinical cardiology of the american heart association. *The international journal of cardiovascular imaging*, 18(1):539–542, February 2002.

[7] P. A. Gowland and M. O. Leach. A simple method for the restoration of signal polarity in multi-image inversion recovery sequences for measuring t1. *Magnetic resonance in medicine*, 18(1):224–231, March 1991.

[8] R. Deichmann and A. Haase. Quantification of t1 values by Snapshot-Flash NMR imaging. *J Magn Reson*, 96:608–612, 1992.

[9] V. Belle, E. Kahler, C. Waller, E. Rommel, S. Voll, K. H. Hiller, W. R. Bauer, and A. Haase. In vivo quantitative mapping of cardiac perfusion in rats using a noninvasive MR spin-labeling method. *Journal of magnetic resonance imaging : JMRI*, 8(6):1240–1245, 1998.

[10] S. R. Bergmann, K. A. Fox, A. L. Rand, K. D. McElvany, M. J. Welch, J. Markham, and B. E. Sobel. Quantification of regional myocardial blood flow in vivo with H215O. *Circulation*, 70(4):724–733, October 1984.

[11] Thomas Kampf, Xavier Helluy, Fabian T. Gutjahr, Patrick Winter, Cord B. Meyer, Peter M. Jakob, Wolfgang R. Bauer, and Christian H. Ziener. Myocardial perfusion quantification using the t1 -based FAIR-ASL method: the influence of heart anatomy, cardiopulmonary blood flow and look-locker readout. *Magnetic resonance in medicine*, 71(5):1784–1797, May 2014.

[12] Jörg U. Streif, Karl-Heinz H. Hiller, Christiane Waller, Matthias Nahrendorf, Frank Wiesmann, Wolfgang R. Bauer, Eberhard Rommel, and Axel Haase. In vivo assessment of absolute perfusion in the murine skeletal muscle with spin labeling MRI. magnetic resonance imaging. *Journal of magnetic resonance imaging : JMRI*, 17(1):147–152, January 2003.

[13] J. Martin Bland and DouglasG Altman. Statistical methods for assessing agreement between two methods of clinical measurement. *The Lancet*, 327(8476):307–310, February 1986.

[14] P. Chareonthaitawee, P. A. Kaufmann, O. Rimoldi, and P. G. Camici. Heterogeneity of resting and hyperemic myocardial blood flow in healthy humans. *Cardiovascular research*, 50(1):151–161, April 2001.

[15] Zungho Zun, Eric C. Wong, and Krishna S. Nayak. Assessment of myocardial blood flow (MBF) in humans using arterial spin labeling (ASL): feasibility and noise analysis. *Magnetic resonance in medicine*, 62(4):975–983, October 2009.

[16] Zungho Zun, Padmini Varadarajan, Ramdas G. Pai, Eric C. Wong, and Krishna S. Nayak. Arterial spin labeled CMR detects clinically relevant increase in myocardial blood flow with vasodilation. *JACC. Cardiovascular imaging*, 4(12):1253–1261, December 2011.

[17] Danny J. Wang, Xiaoming Bi, Brian B. Avants, Tongbai Meng, Sven Zuehlsdorff, and John A. Detre. Estimation of perfusion and arterial transit time in myocardium using free-breathing myocardial arterial spin labeling with navigator-echo. *Magnetic resonance in medicine*, 64(5):1289–1295, November 2010.

[18] Benjamin E. Northrup, Kyle S. McCommis, Haosen Zhang, Shuddhadeb Ray, Pamela K. Woodard, Robert J. Gropler, and Jie Zheng. Resting myocardial perfusion quantification with CMR arterial spin labeling at 1.5 t and 3.0 t. *Journal of cardiovascular magnetic resonance*, 10, 2008.

[19] Michael Jerosch-Herold, Gabriela Vazquez, Lu Wang, David R. Jacobs, and Aaron R. Folsom. Variability of myocardial blood flow measurements by magnetic resonance imaging in the multi-ethnic study of atherosclerosis. *Investigative radiology*, 43(3):155–161, March 2008.

[20] Li-Yueh Y. Hsu, Kenneth L. Rhoads, Jessica E. Holly, Peter Kellman, Anthony H. Aletras, and Andrew E. Arai. Quantitative myocardial perfusion anal-

ysis with a dual-bolus contrast-enhanced first-pass MRI technique in humans. *Journal of magnetic resonance imaging : JMRI*, 23(3):315–322, March 2006.

[21] Osamu Manabe, Keiichiro Yoshinaga, Chietsugu Katoh, Masanao Naya, Robert A. deKemp, and Nagara Tamaki. Repeatability of rest and hyperemic myocardial blood flow measurements with 82Rb dynamic PET. *Journal of nuclear medicine : official publication, Society of Nuclear Medicine*, 50(1):68–71, January 2009.

[22] Adrienne E. Campbell-Washburn, Anthony N. Price, Jack A. Wells, David L. Thomas, Roger J. Ordidge, and Mark F. Lythgoe. Cardiac arterial spin labeling using segmented ECG-gated Look-Locker FAIR: variability and repeatability in preclinical studies. *Magnetic resonance in medicine*, 69(1):238–247, January 2013.

[23] Nivedita K. Naresh, Xiao Chen, Eric Moran, Yikui Tian, Brent A. French, and Frederick H. Epstein. Repeatability and variability of myocardial perfusion imaging techniques in mice: Comparison of arterial spin labeling and first-pass contrast-enhanced MRI. *Magnetic resonance in medicine*, 75(6):2394–2405, June 2016.

[24] A. M. Greve, S. Vasu, W. P. Bendettini, and A. E. Arai. Heterogeneity of resting and hyperemic myocardial blood flow in healthy volunteers: a quantitative CMR perfusion pixel-map study. *J Cardiovasc Magn R*, 16(Suppl 1), 2014.

[25] S. S. Abdelmoneim, A. Dhoble, M. Bernier, S. Moir, M. E. Hagen, S. A. Ness, S. S. Abdel-Kader, P. A. Pellikka, and S. L. Mulvagh. Absolute myocardial blood flow determination using real-time myocardial contrast echocardiography during adenosine stress: comparison with single-photon emission computed tomography. *Heart (British Cardiac Society)*, 95(20):1662–1668, October 2009.

[26] Christophe A. Wyss, Pascal Koepfli, Krzysztof Mikolajczyk, Cyrill Burger, Gustav K. von Schulthess, and Philipp A. Kaufmann. Bicycle exercise stress in PET for assessment of coronary flow reserve: repeatability and comparison with adenosine stress. *Journal of nuclear medicine : official publication, Society of Nuclear Medicine*, 44(2):146–154, February 2003.

[27] Charlotte Buchanan, Azharuddin Mohammed, Eleanor Cox, Katrin Köhler, Bernard Canaud, Maarten W. Taal, Nicholas M. Selby, Susan Francis, and Chris W. McIntyre. Intradialytic cardiac magnetic resonance imaging to assess cardiovascular responses in a Short-Term trial of hemodiafiltration and hemodialysis. *Journal of the American Society of Nephrology : JASN*, 28(4):1269–1277, April 2017.

Chapter 6

Optimisation of the LL-FAIR-ASL sequence for improved clinical viability

In this chapter, work undertaken to optimise the utility of the LL-FAIR-ASL sequence for a clinical setting is presented. The aim of this work was to provide a technique which could be employed within a single breath hold, in order to minimise the impact on scan time in a clinical examination. Furthermore, steps were taken to reduce the amount of post hoc analysis required to extract quantitative data from the scans, by implementing online reconstruction of MBF maps.

6.1 Methods

6.1.1 Simulation

Bloch simulations of the LL-FAIR-ASL sequence were run in MATLAB (The Mathworks Inc., Natick, USA) with a flip angle of 45°, TR of 2.3 ms, T_1 of 1200 ms and a heart rate of 60 bpm. All other parameters were as described in Chapter 5.1,

with the HS8 inversion pulses fully simulated with duration of 10 ms, time/bandwidth product R = 40 and the scaling factor $\beta = 3.45$ followed by a block of five cardiac triggered balanced Steady-State Free Precession (bSSFP) readouts. For 15 discrete values of SNR between 25 and 120, 100 repetitions were simulated. The simulations were performed in order to determine whether the dominant source of error in the calculation of MBF was from noise or from artefact, such as due to cardiac motion. The output values for T_1, T_1*, the T_1 and T_1* differences (between the globally-selective and slice-selective inversion blocks, GS - SS) and the bias in the MBF calculation, with no simulated flow, were all investigated.

6.1.2 Optimisation of the sequence In Vivo

As with the development phase described in Chapter 5, all experiments were carried out on a 3 T whole body scanner (TIM Trio, Siemens, Germany). Throughout all scans the same pre-ASL protocol was followed to minimise potential sources of error from outwith the ASL scan protocol. Following initial localisation to a mid-ventricular, short-axis slice, B_0 shimming was performed on a volume tight around the left ventricular myocardium in the imaging slice to minimise frequency variations, in particular the occurrence of bSSFP banding artifacts within the region of interest. A short-axis cine image series was then acquired in order to determine the most appropriate trigger delay (TD) to allow for acquisition in mid-diastole, the most quiescent period of the cardiac cycle. A series of Shortened MOdified Look-Locker Inversion recovery (ShMOLLI)[1] T_1 maps were then acquired for comparison with the T_1 measured in the globally-selective inversion epoch of the LL-FAIR-ASL regime. The ShMOLLI sequence has a 5(1)1(1)1 structure, and employs a conditional analysis algorithm where, for long T_1 values, only the first 5 images are used in the fitting, for the case $0.4T_{RR} < T_1 < T_{RR}$, images 1-6 are fitted and for $T_1 < 0.4T_{RR}$ all 7 images are fitted. The sequence parameters employed, as used routinely in a clinical reasearch

setting, were a flip angle of 35°, image slice thickness of 8 mm, TR = 2.5 ms, TE = 1.05 ms and TI = 110 ms, for a 192 x 192 matrix (interpolated to 384 x 384), 360 mm field of view with 6/8 partial Fourier and rate 2 GRAPPA.

During the ASL scans, instructions were given for end-expiration breath holds and, following the final instruction to hold the breath, a brief pause was introduced in order to eradicate residual gross motion from the end of the breath hold process. After each acquisition, the magnitude image series was checked for motion and, should motion have occurred, the series was reacquired.

For all acquisitions the GS-SS ordering scheme was used, with typical trigger delay (TD) of 500 ms and an inversion time (TI) of 100 ms. The image matrix was reduced to 144 x 108 (interpolated to 288 x 216) with a 360 mm field of view. All other parameters were as described in Chapter 5.1, with image slice thickness of 8 mm, 6/8 partial Fourier and an acceleration factor of GRAPPA 2[2]. In order to determine the ideal values of the remaining parameters for robust measurement of MBF from a single breath hold, a number of parameters were varied, as described below.

Experiment 1: Bandwidth/TR. The receive bandwidth per pixel of the acquisition readout train was adjusted, such that the value of the minimised repetition time (TR) and echo time (TE) could be varied. While utilising a low bandwidth with a longer minimum TR would be expected to provide higher values of SNR, increasing the bandwidth to allow a shorter TR, and thus decreasing the total readout time, would be expected to decrease the influence of physiological noise in the measurement, as well as making the sequence more robust to bSSFP artifacts due to a wider frequency passband with a lower TR.

Five values for the bandwidth of 503, 755, 992, 1240 and 1510 Hz were employed, corresponding to values of TR = 3, 2.5, 2.3, 2.2 and 2.1 ms, TE = 1.22, 1.03, 0.94, 0.93 and 0.92 ms and total readout time = 222, 206, 199, 196 and 195 ms respectively. The SNR was measured by the ratio of the mean signal intensity in the myocardial

ROI ($\overline{SI}$) to the standard deviation of the signal in an ROI drawn in the background of the image, and thus containing only noise (σ_N).

$$SNR = \frac{\overline{SI}}{\sigma_N} \tag{6.1}$$

The signal in the myocardium was taken from the fifth (and final) image in each inversion epoch, when the magnetisation is closest to full recovery. However, it is worth noting that heart rate variations could cause differences in the TI of the fifth image, both within and between subject datasets, and therefore the level of signal recovery. The multiple averages taken in each case should overcome this. It is also worth noting that σ_N is not a strict measure of the noise in the image. Firstly, the rectification of the noise will mean that the noise waveform has been clipped, such that only the positive part remains, and secondly the use of GRAPPA in the image acquisitions means that the background noise is dependent on the location in the image, as it depends on the number, size and location of the surface coil elements in the the RF coil array that are contributing signal to the voxel. However, as the measure of SNR is used only for a like for like comparison and not as an absolute measure, these factors have not been accounted for.

Temporal SNR (tSNR)was calculated as the mean MBF ($\overline{MBF}$) in the myocardial ROI from the six MBF maps acquired for each bandwidth/TR over the standard deviation of MBF from these six repititions (σ_{MBF}).

$$tSNR = \frac{\overline{MBF}}{\sigma_{MBF}} \tag{6.2}$$

The spatial standard deviation (SD) of MBF was also calculated, defined as the standard deviation of pixel values within the myocardial ROI in an MBF map from a single breath hold. This was calculated in order to investigate how the variation of MBF values calculated across the myocardium were affected by the variation of the

sequence parameters.

Experiment 2: Flip angle. The optimal flip angle for a single breath hold LL-FAIR-ASL acquisition was also investigated. The aim was to find an appropriate flip angle to achieve acceptable SNR and minimise error in the calculation of MBF. Flip angles of 15°, 25°, 35°, 45° and 55° were employed for a bandwidth of 992 Hz and TR of 2.3 ms. SNR, tSNR and spatial SD of MBF were calculated as described above.

Experiment 3: T_1 mapping. One of the potential benefits of the LL-FAIR-ASL sequence, is that, along with quantification of MBF, it allows the calculation of a T_1 map. These T_1 maps, calculated from the GS epoch of the acquisition, were validated against the ShMOLLI sequence by Bland-Altman analysis using the parameters defined above..

6.1.3 Online Image Reconstruction and Parametric Mapping

One of the advantages of a robust and reliable ASL method for measuring myocardial perfusion, is the relative simplicity of quantification of perfusion with comparison to other cardiac imaging methods. This occurs due to the ASL signal difference being directly proportional to the blood flow [3]. However, in order to allow a qualitative visualisation of MBF in the myocardium, without further offline analysis, the image reconstruction program in the Siemens ICE environment was programmed to output maps of T_1 (both GS and SS), calculated by an AMOEBA optimisation method[1] and, using these data, calculate and output a map of MBF using equation 5.3. This addition allowed the maps to be available to the user, at the scanner console, in around 10 seconds following acquisition. In order to facilitate the online MBF calculation, using equation 5.3, a constant value for the T_1 of blood was used. A value of 2000 ms was chosen based on the mean of literature values for the T_1 of blood in the left ventricular blood pool at 3 T(2057 $\pm$ 32 ms from[4, 5, 6]) and that reported for the LL-FAIR-ASL sequence in Chapter 5 (1842 $\pm$ 64 ms), giving a value of 2003 ms.

A bespoke colourscale was designed and implemented for the MBF maps, chosen to best represent the range of normal values for blood flow, yet show spatial variation and changes. The scale used for the MBF colourmap was in units of ml/100g/min in order to better show the range of variation. Two versions of the colourmap are calculated for each breathhold. One in which the value of MBF is simply calculated for every pixel in the image, and one in which the MBF map is masked to only display MBF for those pixels for which the GS-T_1 falls within a typical myocardial T_1 range for 3 T. This was chosen to be between 700 and 1500 ms.

6.2 Results

6.2.1 Simulation

Figure 6.1 shows (a) the T_1 and T_1* values, (b) the difference in T_1 and T_1* between the GS and SS cases, and (c) the bias in the MBF calculation, all plotted against a range of SNR values between 25 and 120. None of the values plotted show a dependence on the SNR, though standard deviations are higher for the lowest values of SNR. The mean MBF bias calculated from the values of T_1* across the noise range was 0.03 ± 0.18 ml/g/min and 0.69 ± 0.11 ml/g/min when calculated from the T_1 values.

6.2.2 Optimisation of the Sequence In Vivo

Experiment 1: Bandwidth/TR. The calculated SNR, from equation 6.1, was plotted against both the bandwidth and TR, as shown in figure 6.2, displaying a general trend towards decreasing SNR as the bandwidth increases and TR decreases, with values of SNR ranging from 286.7 ± 39.6 (283.5 ± 39.2) at 755 Hz/2.5 ms to 191.4 ± 38.0 (192.0 ± 39.5) at 1510 Hz/2.1 ms, where SS values of SNR are given in parentheses. The behaviour observed is the same for both the GS and SS inversion

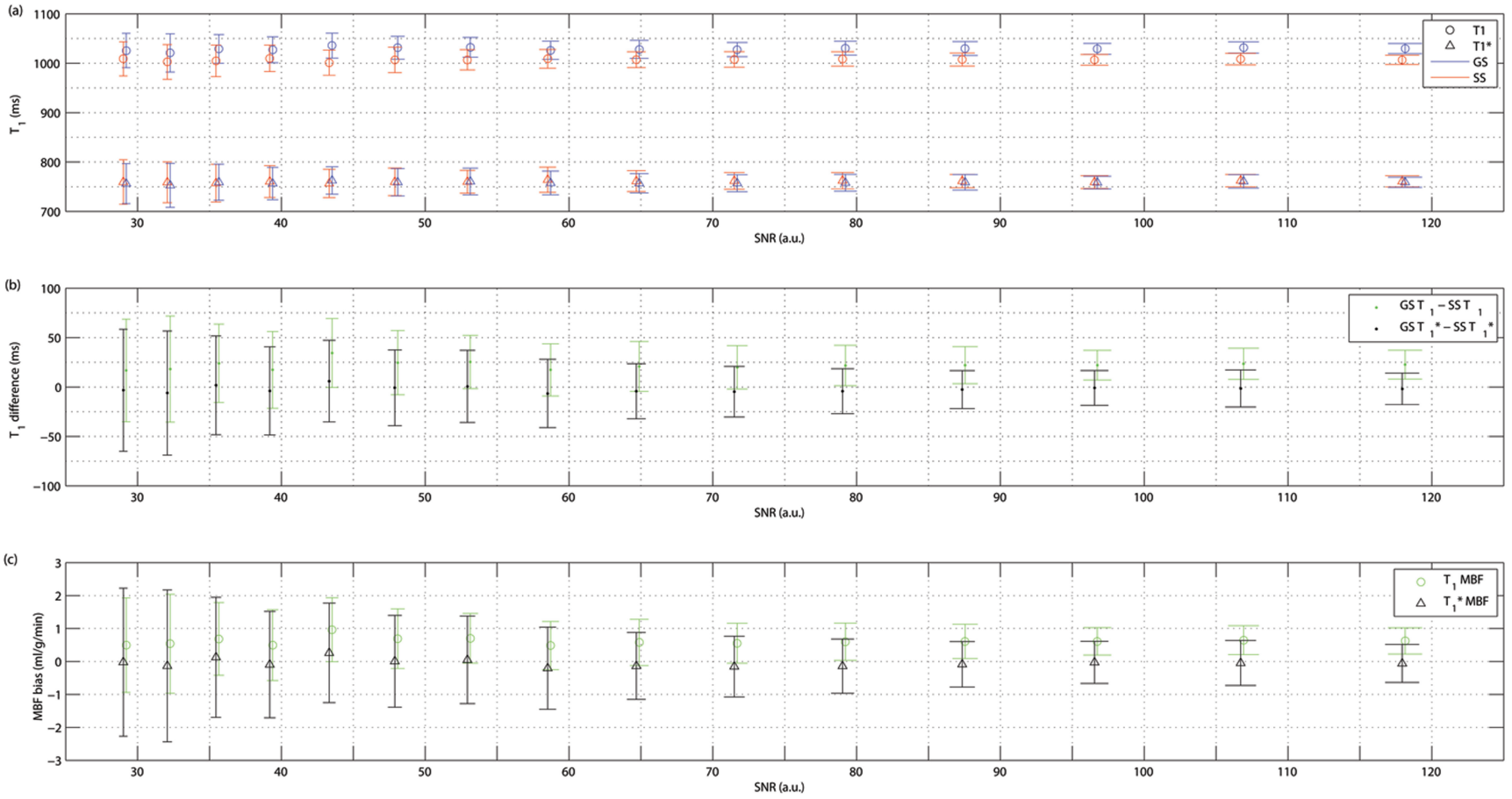


Figure 6.1: The results of Bloch simulations for a range of SNR between 25 and 120, showing (a) the T_1 and T_1* for both GS and SS cases, (b) the T_1 and T_1* difference between the GS and SS inversion blocks, and (c) bias in the MBF calculation. All values are plotted as mean ± standard deviation.

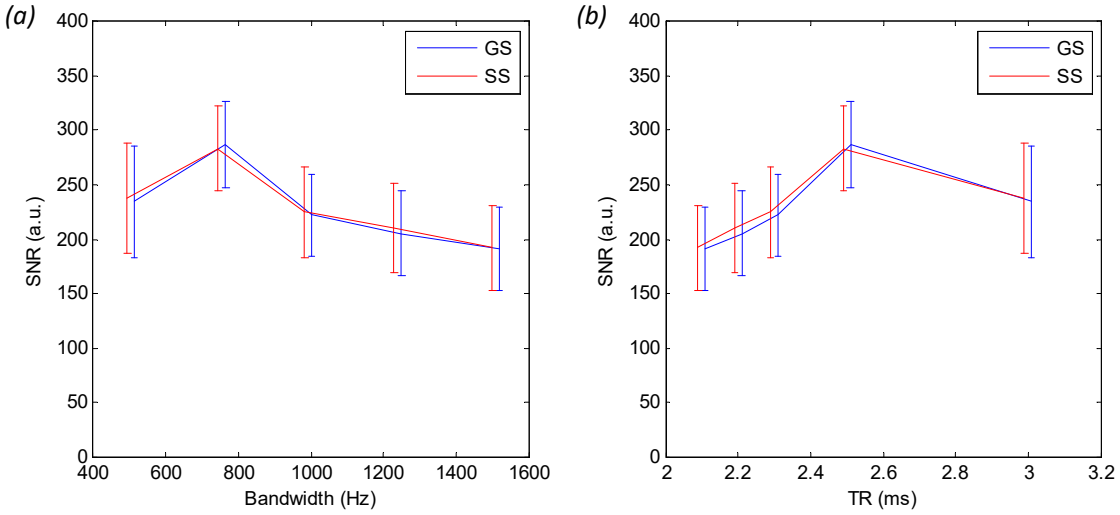


Figure 6.2: SNR as a function of (a) bandwidth in Hz and (b) TR in ms, for both GS (blue) and SS (red) image series. All values are plotted as mean ± standard deviation.

blocks.

The temporal SNR was also plotted against bandwidth, as shown in figure 6.3, along with the standard deviation of MBF. Though the variation in these measurements is high, leading to large error bars, there appears to be a trend toward decreasing standard deviation of MBF with higher bandwidth/lower TR, from 1.80 ± 1.11 ml/g/min at 503 Hz/3.0 ms to 1.33 ± 0.79 ml/g/min at 1240 Hz/2.2 ms. The effect on temporal SNR is less clear.

The effect of varying the bandwidth/TR on the spatial variation of MBF within a region of interest, presented as the standard deviation of pixel values within a prescribed myocardial ROI as drawn on parametric maps of MBF, is shown in figure 6.4. Increasing the bandwidth, and therefore reducing total readout time as well as TR, appears to result in decreasing variation of MBF within the prescribed region with values ranging from 1.29 ± 0.33 ml/g/min at 755 Hz/2.5 ms to 1.11 ± 0.17 ml/g/min at 1240 Hz/2.2 ms. Though this trend is not borne out by the two extreme datapoints.

As a result of these tests a receive bandwidth of 992 Hz and corresponding mini-

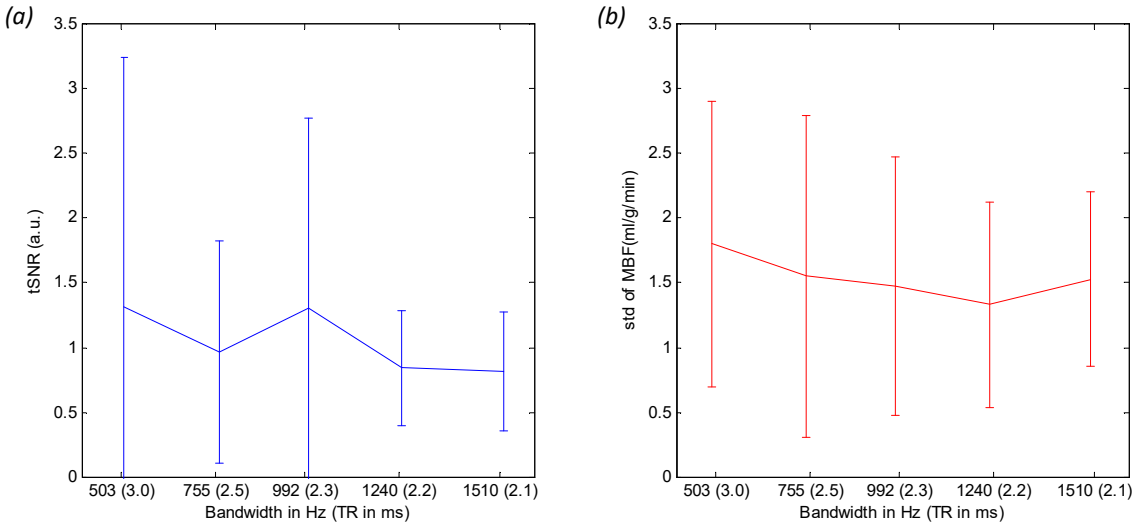


Figure 6.3: The prescribed bandwidth/TR against (a) temporal SNR as defined in equation 6.2, and (b) the standard deviation of MBF. All values are plotted as mean ± standard deviation.

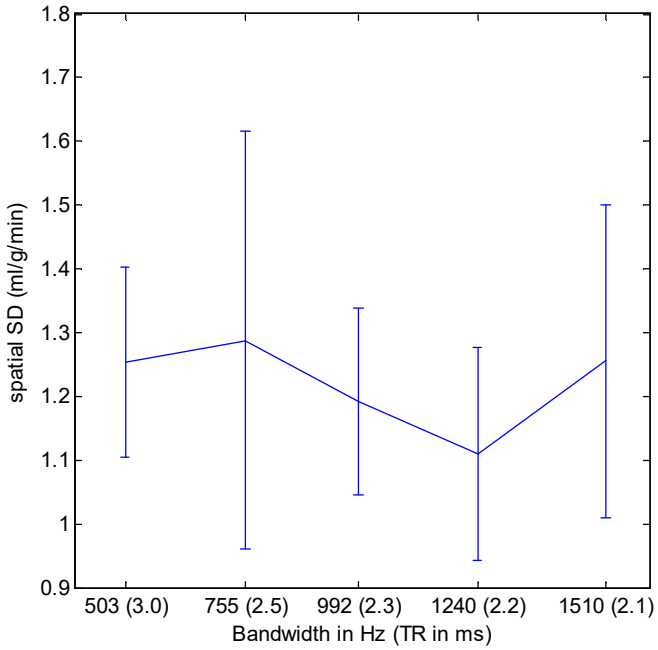


Figure 6.4: The standard deviation of MBF calculated per pixel within the myocardial ROI as a function of bandwidth/TR. All values are plotted as mean ± standard deviation.

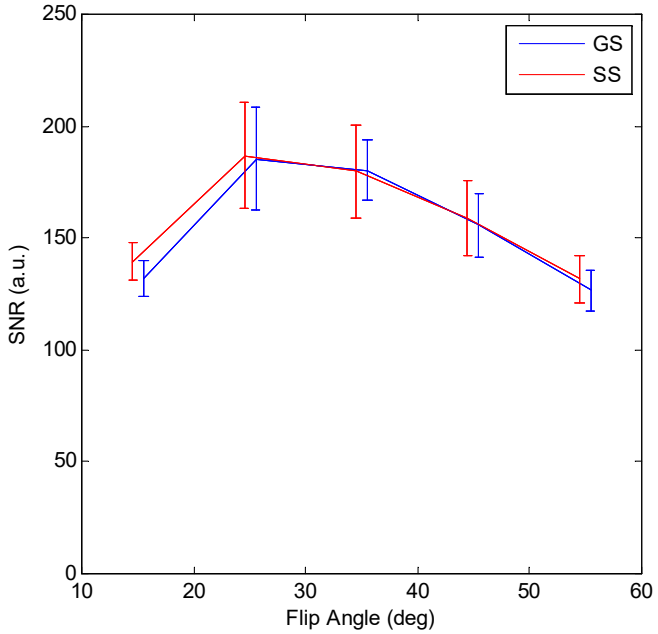


Figure 6.5: SNR as a function of flip angle for both the GS (blue) and SS (red) inversion blocks of the LL-FAIR-ASL sequence. All values are plotted as mean ± standard deviation.

mum TR of 2.3 ms are recommended for use in future studies.

Experiment 2: Flip angle. Figure 6.5 shows the SNR for the range of flip angles 15°, 25°, 35°, 45° and 55° for both the GS and SS inversion blocks. The curves show decreasing SNR as flip angle increases between 25° and 55°, with 15° also giving a low SNR value similar to 55°. The values of SNR decrease from 185.7 ± 23.3 (187.1 ± 23.6) at 25° to 126.6 ± 9.2 (131.6 ± 10.6) at 55°, where the SNR values in parentheses are for the SS inversion block. As with the bandwidth/TR experiment, the curves for the GS and SS cases display the same behaviour.

Again, the temporal SNR and standard deviation of MBF were also plotted for varying flip angle, as shown in figure 6.6. As with the bandwidth/TR experiment there are large error bars in these plots, however there is a clear trend of decreasing standard deviation of MBF with increasing flip angle in figure 6.6(b), decreasing from 1.92 ± 0.77 ml/g/min at 15° to 1.03 ± 0.46 ml/g/min at 45°.

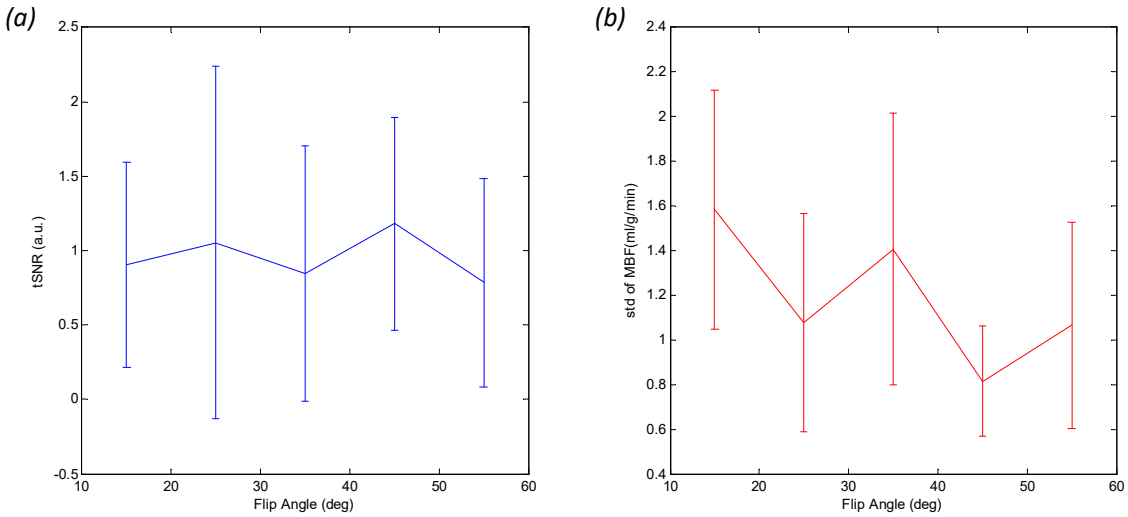


Figure 6.6: The prescribed flip angle against (a) temporal SNR as defined in equation 6.2, and (b) the standard deviation of MBF. All values are plotted as mean ± standard deviation.

Figure 6.7 shows decreasing spatial SD of MBF within the myocardial region as the flip angle is increased. This variation of MBF within the region of interest decreases from 1.66 ± 0.28 ml/g/min at 15° to 1.22 ± 0.14 ml/g/min at 55°.

As a result of these tests a flip angle of 45° is recommended for use in future studies.

Experiment 3: T_1 mapping. Bland-Altman plots comparing the T_1 values displayed in a myocardial ROI in T_1 maps calculated from LL-FAIR-ASL and ShMOLLI acquisitions are shown in figure 6.8 for five values of bandwidth/TR between 503 Hz/3.0 ms and 1510 Hz/2.1 ms in the ASL sequence. The ShMOLLI acquisition used standard parameters as used clinically, which were not varied. The Bland-Altman series shows that there is positive bias toward the ASL T_1 measurement, with the mean difference ranging from 58 to 73 ms. The standard deviation is small, ranging from 8 to 12 ms.

Figure 6.9 shows the Bland-Altman series for varying flip angle in the range 15° to 55° in the ASL sequence. Again, the ShMOLLI acquisition used standard parameters

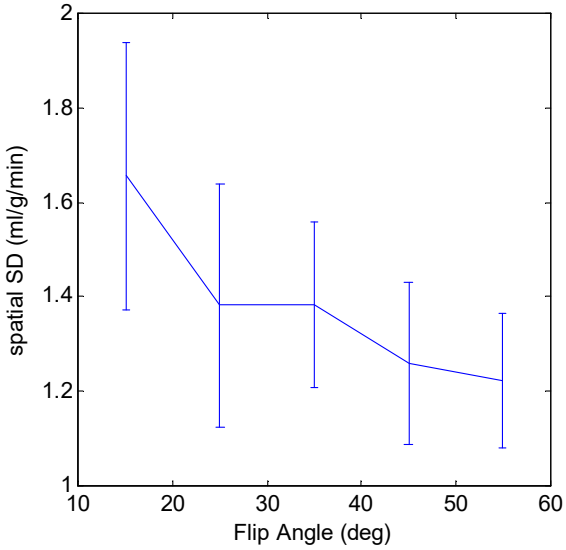


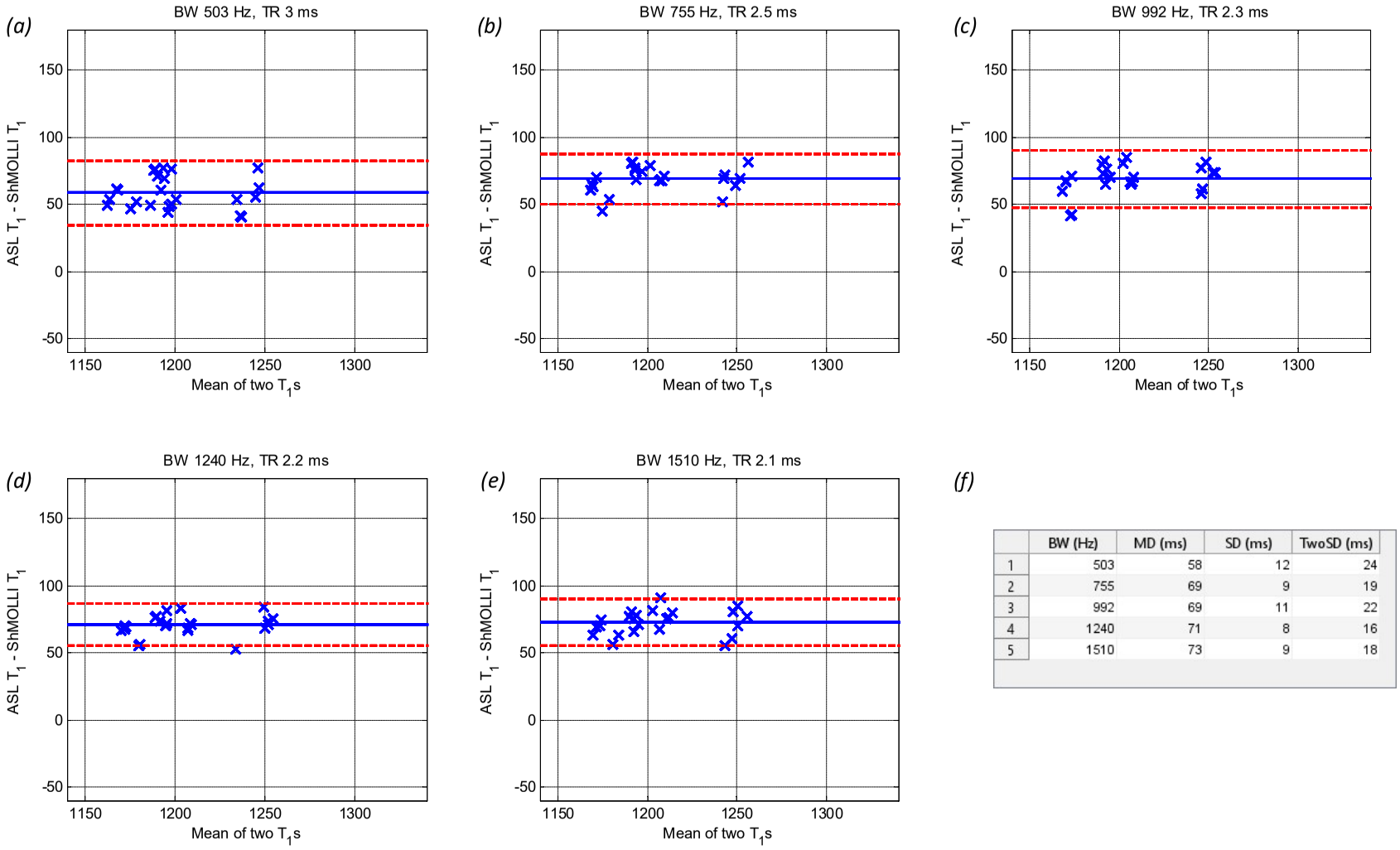
Figure 6.7: The standard deviation of MBF calculated per pixel within the myocardial ROI as a function of flip angle. All values are plotted as mean ± standard deviation.

as used clinically, which were not varied. The higher T_1 values measured by the LL-FAIR-ASL sequence seen in the bandwidth/TR plots of figure 6.8 are replicated in figure 6.9, with lower flip angles showing the largest differences. The mean difference ranges from 116 ms at 15°, to just 14 ms at 55°. There is very little variation in the standard deviation of the measurement across the range of flip angles, ranging from 31 to 35 ms.

At the recommended parameters of 45° flip angle and bandwidth 992 Hz/TR 2.3 ms, the ASL T_1 measurements was 1234 ± 40 ms, compared with 1191 ± 53 ms with ShMOLLI.

6.2.3 Online Image Reconstruction and Parametric Mapping

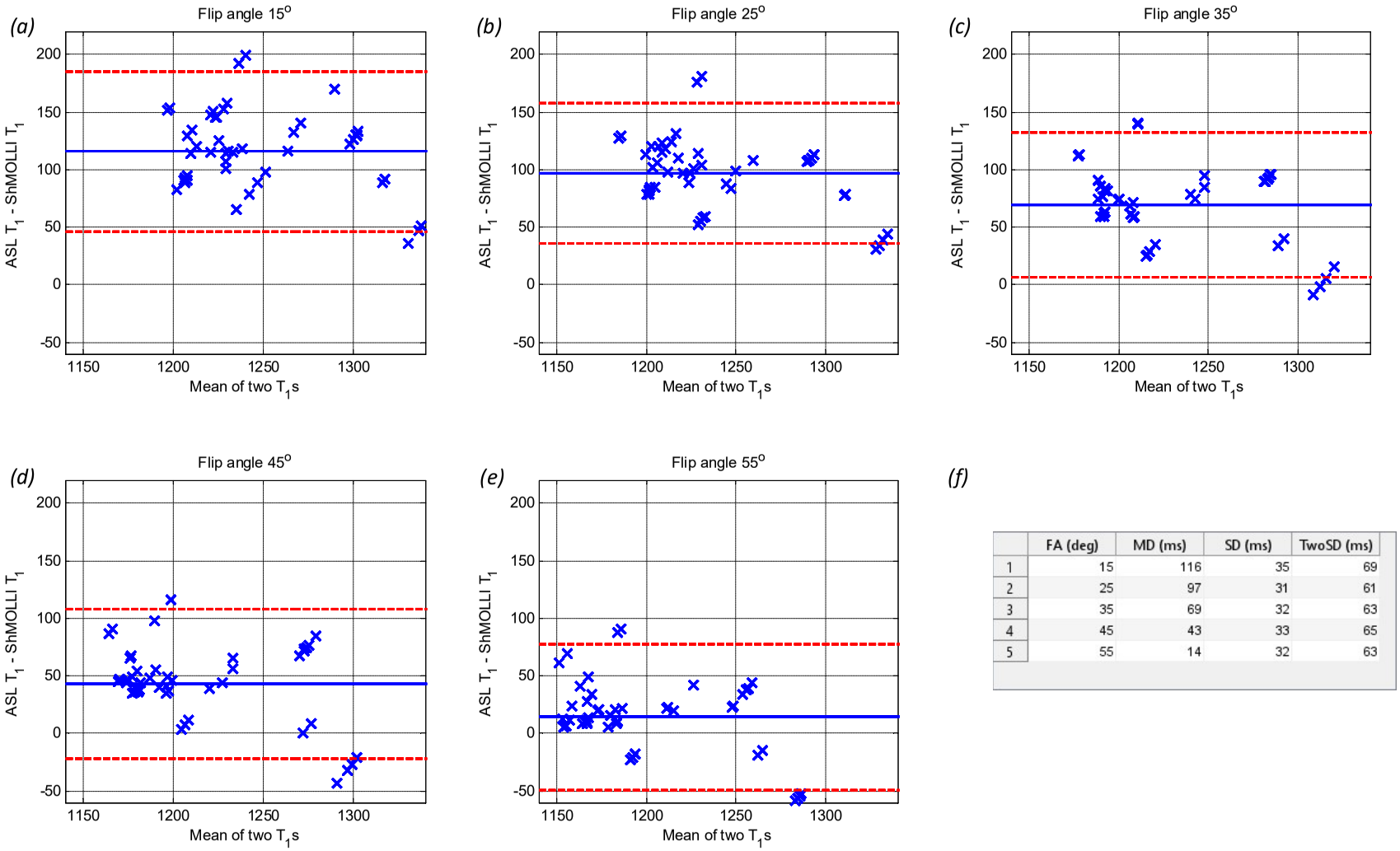
Two image series containing ten magnitude images and ten phase images are output to the scanner console as previously described in Chapter 5. A typical series of magnitude images can be seen in figure 5.7. In addition, a third series of parameter maps is now output. The full output of parameter maps displayed on the scanner console are shown in figure 6.10. The series includes GS and SS maps of T_1, T_1*,



(f)

	BW (Hz)	MD (ms)	SD (ms)	TwoSD (ms)
1	503	58	12	24
2	755	69	9	19
3	992	69	11	22
4	1240	71	8	16
5	1510	73	9	18

Figure 6.8: Bland-Altman plots for the comparison of T_1 values as measured by LL-FAIR-ASL and ShMOLLI for values of bandwidth/TR of (a) 503 Hz/3.0 ms, (b) 755 Hz/2.5 ms, (c) 992 Hz/2.3 ms, (d) 1240 Hz/2.2 ms, and (e) 1510 Hz/2.1 ms in the ASL sequence, with (f) giving the values of mean difference, standard deviation and 1.96 times standard deviation for each.



(f)

	FA (deg)	MD (ms)	SD (ms)	TwoSD (ms)
1	15	116	35	69
2	25	97	31	61
3	35	69	32	63
4	45	43	33	65
5	55	14	32	63

Figure 6.9: Bland-Altman plots for the comparison of T_1 values as measured by LL-FAIR-ASL and ShMOLLI for flip angles of (a) 15°, (b) 25°, (c) 35°, (d) 45°, and (e) 55° in the ASL sequence, with (f) giving the values of mean difference, standard deviation and 1.96 times standard deviation for each.

the R^2 values corresponding to the the T_1 maps, fitting parameters A and B used to calculate the T_1 from the T_1* and inversion efficiency maps, as well as both the unmasked and masked MBF maps. Some of the maps, such as the fitting parameters are output for debugging purposes only, and can be switched off in future.

Figure 6.11 shows an enlarged version of the masked MBF map shown in figure 6.10. Also displayed is a colourbar annotated with values of MBF in ml/g/min. This was produced offline in MATLAB.

6.3 Discussion

In this chapter, the LL-FAIR-ASL sequence introduced and developed in Chapter 5 was further optimised, in order to move toward a single breath hold implementation, using Bloch simulation and in vivo experiments. Though a single breath hold acquisition is desirable, such that the inclusion of ASL in a clinical exam employing a rest/stress test is viable, its implementation is challenging. For instance, the number of perfusion sensitive measurements during the recovery is limited, with the first and last TIs often not sensitive to perfusion, as discussed in section 5.3. Without the averaging previously employed, in many cases (e.g. with low heart rate) there will only be 3 perfusion sensitive readouts for each recovery (SS and GS). The bandwidth/TR and flip angle were varied in order to find optimal values which balance the need for good SNR with temporal SNR. In addition, online reconstruction was also implemented, to allow the display of parametric MBF maps, as well as T_1 maps.

The results of the Bloch simulations presented in figure 6.1 show that mean bias in the MBF calculation due to T_1 variation does not vary with SNR, though it should be noted that the variation in the MBF bias is larger at low values of SNR. When the MBF bias is calculated from T_1* the mean is very close to zero, but when calculated from T_1 there is a considerable positive bias present across the whole range of SNR

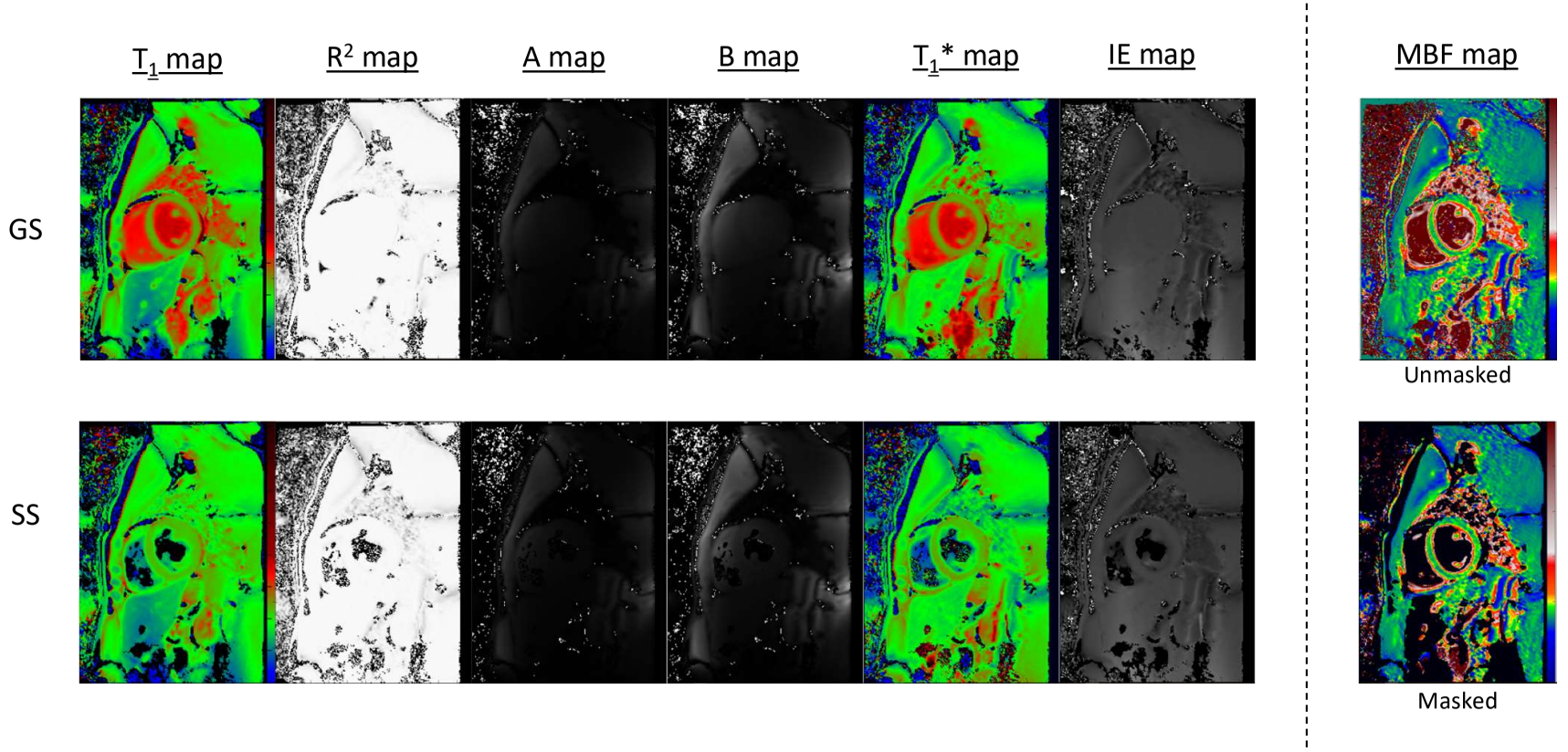


Figure 6.10: The output of parameter maps to the scanner console, including T_1 maps, T_1* maps, R^2 maps, A and B fitting parameter maps and inversion efficiency (IE) maps for both the GS and SS inversion blocks, and two MBF maps, one masked for normal values of myocardial T_1. The range of T_1 values used for masking was between 700 and 1500 ms.

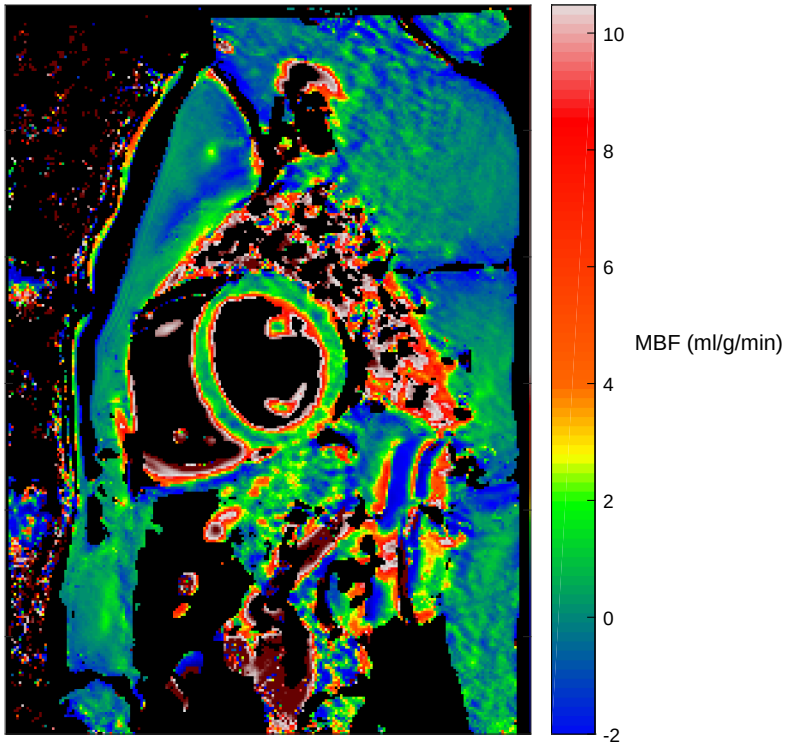


Figure 6.11: An enlarged MBF colourmap masked for myocardial T_1 as produced by the online scanner image reconstruction, with the additional of a quantified colourbar.

values, as detailed in section 6.2.1. This bias is caused by the incomplete recovery of the magnetisation between the two inversion epochs of the LL-FAIR-ASL sequence and would be expected to vary with heart rate. This shows further justification for the use of T_1* as the basis for MBF calculation, as discussed in Chapter 5. These results show that the main source of variation in MBF measurement in vivo is not due to the limited SNR of the method, but from artefact, for instance due to physiological motion.

The simulation results regarding noise suggest that optimising the sequence to reduce its sensitivity to motion is preferred to optimising for maximum available SNR. By increasing the receive bandwidth of the sequence, and thereby allowing for a shorter minimum TR, we reduce the total time required for the readout such that there is a shorter period during which motion can affect the measurement. In addition, the spatial variation of the method, as characterised by the standard deviation of MBF within a myocardial ROI, also decreases as the length of the readout is decreased. This approach, points to the recommendation of decreasing the readout time by decreasing the TR from that which was previously used (TR of 3.0 ms).

The original implementation of the LL-FAIR-ASL sequence, presented in Chapter 5, employed a flip angle of 35°. This was chosen as it was the standard flip angle used for the Look-Locker T_1 mapping techniques on which the sequence was based, such as MOLLI and ShMOLLI[7, 8, 1]. One of the reasons stated in the T_1 mapping works for choosing 35°, instead of the 50° employed in the original MOLLI implementation, had been to reduce the sensitivity of the techniques to heart rate, caused in part by the disturbance of the recovery of the magnetisation by the high readout flip angle while not sacrificing too much SNR. As previously stated in Chapter 5, the use of T_1* in place of T_1 for the calculation relieves this dependence, allowing different values of flip angle to be explored.

As a result of increasing the flip angle both the temporal variation (figure 6.6(b))

and spatial variation (figure 6.7) of MBF show a considerable decrease. Thus, it is recommended that the flip angle be increased in order to benefit from these changes. A flip angle of 45° is recommended, as any benefit of increasing further would seem to be marginal, while leading to greater perturbation of the recovery of the magnetisation before the start of the second inversion epoch.

The results from the Bland-Altman analysis presented in figures 6.8 and 6.9 show that there is a positive bias in the measurement of T_1 with LL-FAIR-ASL when compared with ShMOLLI. It is suspected that this is due to the T_1 measurement being made with the application of a single inversion epoch, rather than the 5(1)1(1)1 regime of ShMOLLI. The further two single readout inversion epochs in the ShMOLLI sequence would only be employed for the measurement of shorter T_1 than that expected from myocardium. However, as the calculation of T_1 occurs on a per pixel basis, and there is some variation within the myocardial region, as well as heart rates, upon which the conditional algorithm of ShMOLLI depends, in some myocardial pixels the later epochs will be employed. It is worth noting that Look-Locker methods tend to underestimate T_1, although this is not to suggest that the ASL method is in any way more accurate.

The variability of the T_1 calculated from the ASL sequence compares well with the ShMOLLI results and could in some clinical circumstances be used in place of T_1 mapping in order to provide a measure of both T_1 and MBF. This may be of interest, for instance, in cases of diffuse myocardial fibrosis (DMF), where fibrous connective tissue forms in the myocardium, interfering with the function of the heart[9]. The most common cause of DMF is coronary artery disease. As well as measuring perfusion with ASL, the myocardial T_1 values would give an indication of the composition of the tissue, where a correlation has been shown between the T_1 and a histological measure of fibrosis[10].

It should be noted that the behaviour of ASL T_1 mapping has not been char-

acterised in disease, so for instance if used in pathology which lead to a shortening of T_1, such as iron overload or Anderson-Fabry disease, it seems unlikely that LL-FAIR-ASL will measure the change in T_1 with the same precision and accuracy as a dedicated T_1 method which has been optimised for shorter T_1 species. Likewise, if the organ of interest is not the heart, but one with a shorter native T_1, such as the liver, LL-FAIR-ASL could not be recommended as a substitute for a T_1 mapping sequence.

The parametric maps output by the sequence, as presented in figures 6.10 and 6.11 give a useful qualitative indication of MBF direct to the user. In, addition it allows an experienced operator to assess the data quality and decide whether to reacquire the data. However, perhaps the most useful outcome of the reconstruction of MBF maps, is in the quantitative analysis. This analysis is significantly streamlined in comparison to the pipeline detailed in Chapter 5. Regions of interest can simply be drawn directly onto the MBF map and the values extracted. Furthermore, if data quality has been compromised, perhaps by patient motion, then this can be spotted immediately and the data reacquired.

This chapter represents a further step towards a clinically viable method for non-invasive, quantitative measurement of MBF using ASL. A single breath hold technique is desirable due to the limited time for data acquisition in a clinical setting, particularly under stress conditions. Despite the improvements detailed above, the inherent variations in the measurement of MBF remain high. While this represents a step in the right direction it would seem that myocardial ASL in a single breath hold is not quite robust enough yet for clinical use.

6.4 Conclusion

By employing the recommended parameters for LL-FAIR-ASL, the results of MBF measurement can be improved in terms of reducing the temporal variation and spatial variation of MBF values, as well a providing an adequate T_1 map, at least in healthy volunteers. The utility of the method is further improved by the inclusion of online reconstruction of T_1 maps and MBF maps, giving the user direct access to qualitative results and simplifying offline quantitative analysis considerably. However, the variations in the measurement of MBF remain too high to allow routine clinical use of the sequence in single breath hold form.

References

[1] Stefan K. Piechnik, Vanessa M. Ferreira, Erica Dall'Armellina, Lowri E. Cochlin, Andreas Greiser, Stefan Neubauer, and Matthew D. Robson. Shortened modified Look-Locker inversion recovery (ShMOLLI) for clinical myocardial t1-mapping at 1.5 and 3 t within a 9 heartbeat breathhold. *Journal of cardiovascular magnetic resonance*, 12, November 2010.

[2] Mark A. Griswold, Peter M. Jakob, Robin M. Heidemann, Mathias Nittka, Vladimir Jellus, Jianmin Wang, Berthold Kiefer, and Axel Haase. Generalized autocalibrating partially parallel acquisitions (GRAPPA). *Magn. Reson. Med.*, 47(6):1202–1210, June 2002.

[3] Frank Kober, Terrence Jao, Thomas Troalen, and Krishna S. Nayak. Myocardial arterial spin labeling. *Journal of cardiovascular magnetic resonance*, 18, April 2016.

[4] Christopher T. Sibley, Justin Huang, Martin Ugander, Abiola Oki, Jing Han, Marcelo S. Nacif, Andreas Greiser, Daniel R. Messroghli, Peter Kellman, Andrew E. Arai, David A. Bluemke, and Songtao Liu. Myocardial and blood t1 quantification in normal volunteers at 3T. *Journal of Cardiovascular Magnetic Resonance*, 13(Suppl 1):P51+, 2011.

[5] Jason J. Lee, Songtao Liu, Marcelo S. Nacif, Martin Ugander, Jing Han, Nadine Kawel, Christopher T. Sibley, Peter Kellman, Andrew E. Arai, and David A. Bluemke. Myocardial t1 and extracellular volume fraction mapping at 3 tesla. *Journal of Cardiovascular Magnetic Resonance*, 13(1):75+, 2011.

[6] Nadine Kawel, Evrim B. Turkbey, Jeffrey J. Carr, John Eng, Antoinette S. Gomes, W. Gregory Hundley, Craig Johnson, Sofia C. Masri, Martin R. Prince, Rob J. van der Geest, João A. C. Lima, and David A. Bluemke. Normal left

ventricular myocardial thickness for Middle-Aged and older subjects with Steady-State free precession cardiac magnetic ResonanceClinical perspective. *Circulation: Cardiovascular Imaging*, 5(4):500–508, July 2012.

[7] Daniel R. Messroghli, Aleksandra Radjenovic, Sebastian Kozerke, David M. Higgins, Mohan U. Sivananthan, and John P. Ridgway. Modified Look-Locker inversion recovery (MOLLI) for high-resolution t1 mapping of the heart. *Magnetic resonance in medicine*, 52(1):141–146, July 2004.

[8] Daniel R. Messroghli, Andreas Greiser, Mirko Fröhlich, Rainer Dietz, and Jeanette Schulz-Menger. Optimization and validation of a fully-integrated pulse sequence for modified look-locker inversion-recovery (MOLLI) t1 mapping of the heart. *Journal of magnetic resonance imaging : JMRI*, 26(4):1081–1086, October 2007.

[9] C. S. BURWELL and E. D. ROBIN. Diagnosis of diffuse myocardial fibrosis. *Circulation*, 20:606–614, October 1959.

[10] Sacha Bull, Steven K. White, Stefan K. Piechnik, Andrew S. Flett, Vanessa M. Ferreira, Margaret Loudon, Jane M. Francis, Theodoros D. Karamitsos, Bernard D. Prendergast, Matthew D. Robson, Stefan Neubauer, James C. Moon, and Saul G. Myerson. Human non-contrast t1 values and correlation with histology in diffuse fibrosis. *Heart (British Cardiac Society)*, 99(13):932–937, July 2013.

Chapter 7

Conclusions

The aim of this thesis was to develop a non-invasive, quantitative and fully repeatable method of measuring Myocardial Blood Flow (MBF) by applying the techniques of Arterial Spin Labelling (ASL). In this chapter, the contribution of this work is summarised and some possible future directions for this research are suggested.

In Chapter 5, the LL-FAIR-ASL sequence for the non-invasive, quantitative measurement of myocardial perfusion is presented. Bloch equation simulations of the new sequence were carried out, as were a series of phantom experiments, in order to characterise the sequence. The sequence was then applied in vivo on 10 healthy volunteers, each of whom were scanned on two separate days. The mean values of MBF across all scans were 1.04 ± 0.40 mL/g/min in the basal slice, 1.06 ± 0.46 mL/g/min in the mid-ventricle and 1.06 ± 0.38 mL/g/min in the apical slice, where all values are averaged spatially over the whole slice and temporally over six measurements. This is believed to be the first time in which values of MBF measured with cardiac ASL have been reported in three slices. The value of MBF for the mid-ventricular slice compared well with literature values as measured with CMR first-pass perfusion, Positron Emission Tomography (PET) using both ^{82}Rb and ^{15}O isotopes and with previously published myocardial ASL techniques. The MBF data was also analysed

segmentally according to the standardised AHA model[1], with all the mean values of MBF falling in the range of 0.87–1.52 mL/g/min. In addition to this, the MBF data was used for a reproducibility study, the first such study using a cardiac ASL method in humans, which confirmed the known heterogeneous nature of resting MBF in healthy people[2, 3]. This study also reported the detectable change in MBF both within-session and longitudinally. These results should prove useful in the planning of a clinical study with the LL-FAIR-ASL sequence. The work presented in this chapter formed the basis of a publication in the scientific journal Magnetic Resonance in Medicine (MRM)[4].

In Chapter 6, the LL-FAIR-ASL sequence was optimised with the goal of removing the need entirely for spatial and temporal averaging and providing a measure of MBF within a single breath hold. It was found that sequence parameters of 45° flip angle and a receive bandwidth of 992 Hz with corresponding minimum repetition time (TR) of 2.3 ms were found to balance the need for adequate signal-to-noise ratio and reduced temporal and spatial variation. However, although improvements in these metrics were shown following optimisation, the variation in MBF values remains too high to allow for routine clinical measurements in a single breath hold. The parametric maps of myocardial T_1 compare well with widely implemented T_1 mapping techniques, such as ShMOLLI[5], however the ASL T_1 maps have not been characterised in disease as yet. In conjunction with this optimisation work, online reconstruction of parametric maps of MBF was implemented such that the maps were available to the operator, on the scanner console, in around 10 seconds following the end of the acquisition. This online reconstruction served to significantly simplify the quantification process compared with the analysis pipeline described in Chapter 5 and we believe this to be the first instance of online reconstruction of MBF maps with a clinical cardiac ASL sequence.

7.1 Future Directions

The ultimate goal in the implementation of a cardiac ASL technique remains to allow routine clinical use of the sequence. The reproducibility study detailed in Chapter 5 showed that the sequence, in its spatial and temporal averaging form is sensitive enough to detect change in MBF due to pharmacological stress. The optimisation of the sequence detailed in Chapter 6 attempted to establish a protocol with greater viability for introduction to clinical use given the time limits, with partial success. The next logical step of the work presented in this thesis would be the inclusion of the sequence in clinical studies. In particular, use of the ASL technique in a study where first-pass perfusion was performed, in both healthy volunteers and a patient group, allowing for comparison of results, would provide a further validation of the sequence. The LL-FAIR-ASL sequence with online reconstruction of parametric maps is available for use in our laboratory by clinical researchers.

One of the aims of this project initially, had been the implementation of the myocardial ASL protocol at 7 tesla. Increased static magnetic field strength is attractive in ASL for a number of reasons. These include the expected higher signal-to-noise ratio at higher values of $\mathbf{B}_0$, the longer T_1 of blood at higher field strengths, which serves to increase the length of time for which the label is present in the target tissue before decaying and finally, an increase in the ASL signal difference[6]. However, the implementation of cardiac MR pulse sequences at 7 T remains problematic, with decreased T_2* times leading to quicker signal decay, electrocardiogram (ECG) mistriggering being more common due to the increased magnetohydrodynamic effect[7], greater B_1 power deposition meaning Specific Absorption Ratio (SAR) limits are reached sooner[8] and the shorter wavelength of the radiofrequency pulses at the 7 T Larmor frequency ($\approx$ 300 MHz) leading to constructive and destructive interference giving a very non-uniform B_1^+ field[9]. The effects of these latter two difficulties can be mitigated by the use of B_1 shimming schemes with a parallel transmit system[10].

As yet, the LL-FAIR-ASL sequence has not been implemented at 7 T. The main hurdle to overcome for this to be achievable is the implementation of effective inversion pulses both globally and within a specified selective inversion slab. Under the inhomogeneous B_1^+ conditions described above and with limited power available, achieving a uniform and complete inversion deep in the chest has been shown to be difficult[11] even using adiabatic pulses. Upgraded hardware, such as RF amplifiers and cardiac transmit/receive arrays has made the project more viable, as could more advanced pulse design, such as multi-spoke parallel transmit (pTx) pulses which have been shown to provide greater homogeneity and lower power deposition than B_1 shimming techniques[12]. However, as this has not yet been demonstrated for inversion pulses in the heart, it has proved to be beyond the scope of this thesis.

In this work, a simple dual T_1 quantification, based on the Belle model[13] was employed. However, some limitation with this model exist. Firstly, there are several assumptions inherent in the model. The longitudinal relaxation of the magnetisation exhibits biexponential behaviour, which is approximated as a monoexponential recovery[13, 14]. The model also assumes a uniform constant value for the blood-tissue partition coefficient, λ[15]. The Belle model also describes the myocardial tissue as a two-compartment model, where the intracapillary and extravascular spaces are assumed to be in fast exchange. Secondly, there are a number of effects of which the model does not take account. For instance, in employing a Look-Locker readout scheme, the recovery of the magnetisation is disturbed by the multiple readouts, affecting the calculation of perfusion. Work investigating this has been carried out in both the brain[16] and in the hearts of mice[14]. In the former study, an expanded three-compartment signal difference model was developed for an LL-FAIR-EPI sequence in which the transit time of arteriolar blood was included, as during this time the blood is under the influence of the LL-readout pulses before entering the capillary space. In the latter study, the Belle model was expanded for an LL-FAIR-FLASH

preclinical sequence to account for both the effect of the LL-readout train and of the partial inversion of the bloodpool. This occurs due to the choice of a selective inversion slab, which takes in the ventricular bloodpools, meaning that inflowing blood in the imaging slice following the slab-selective inversion, assumed to be non-inverted, is in fact a mixture of inverted and non-inverted blood. In order to improve the quantification of MBF with the sequence presented in this thesis, a more advanced quantification model, which takes into account the factors listed above, as well as arterial transit time (ATT)[17], would require validation in the human heart.

Further to this work, it would also be of interest to characterise the performance of the LL-FAIR-ASL sequence in other organs. Some initial exploratory work has been carried out in the liver, both in vivo and in a perfused ex vivo system. Initial results have been promising. The application of ASL to the liver brings slightly different benefits and challenges to employing it in the heart. For instance, the physiological noise due to motion, such a problem in the heart, would be expected to be far less in the liver, however this is counterbalanced by the significantly shorter value of T_1 (717 $\pm$ 48 ms from a ShMOLLI acquisition corrected for the presence of iron[18]). One possible future study in liver perfusion would be to perform ASL fasted and after a meal, as there would be expected to be a detectable change in the value of blood flow.

7.2 Summary

This aim of this thesis was to develop a non-invasive, quantitative, repeatable technique for the measurement of MBF in the human heart by applying the principles of ASL. The method was developed and characterised and this work has been published in MRM[4]. The method was further optimised in a step towards single breath hold acquisition and online reconstruction of parametric maps of MBF was implemented. The LL-FAIR-ASL protocol is available within our institution for use

by interested clinical research partners.

References

[1] Manuel D. Cerqueira, Neil J. Weissman, Vasken Dilsizian, Alice K. Jacobs, Sanjiv Kaul, Waren K. Laskey, Dudley J. Pennell, John A. Rumberger, Thomas Ryan, Mario S. Verani, and American Heart Association Writing Group on Myocardial Segmentation and Registration for Cardiac Imaging. Standardized myocardial segmentation and nomenclature for tomographic imaging of the heart. a statement for healthcare professionals from the cardiac imaging committee of the council on clinical cardiology of the american heart association. *The international journal of cardiovascular imaging*, 18(1):539–542, February 2002.

[2] P. Chareonthaitawee, P. A. Kaufmann, O. Rimoldi, and P. G. Camici. Heterogeneity of resting and hyperemic myocardial blood flow in healthy humans. *Cardiovascular research*, 50(1):151–161, April 2001.

[3] A. M. Greve, S. Vasu, W. P. Bendettini, and A. E. Arai. Heterogeneity of resting and hyperemic myocardial blood flow in healthy volunteers: a quantitative CMR perfusion pixel-map study. *J Cardiovasc Magn R*, 16(Suppl 1), 2014.

[4] Graeme A. Keith, Christopher T. Rodgers, Michael A. Chappell, and Matthew D. Robson. A look-locker acquisition scheme for quantitative myocardial perfusion imaging with FAIR arterial spin labeling in humans at 3 tesla. *Magnetic Resonance in Medicine*, September 2016.

[5] Stefan K. Piechnik, Vanessa M. Ferreira, Erica Dall'Armellina, Lowri E. Cochlin, Andreas Greiser, Stefan Neubauer, and Matthew D. Robson. Shortened modified Look-Locker inversion recovery (ShMOLLI) for clinical myocardial t1-mapping at 1.5 and 3 t within a 9 heartbeat breathhold. *Journal of cardiovascular magnetic resonance*, 12, November 2010.

[6] Jiongjiong Wang, David C. Alsop, Lin Li, John Listerud, Julio B. Gonzalez-At,

Mitchell D. Schnall, and John A. Detre. Comparison of quantitative perfusion imaging using arterial spin labeling at 1.5 and 4.0 tesla. *Magnetic resonance in medicine*, 48(2):242–254, August 2002.

[7] J. J. Suttie, L. Delabarre, A. Pitcher, P. F. van de Moortele, S. Dass, C. J. Snyder, J. M. Francis, G. J. Metzger, P. Weale, K. Ugurbil, S. Neubauer, M. Robson, and T. Vaughan. 7 tesla (t) human cardiovascular magnetic resonance imaging using FLASH and SSFP to assess cardiac function: validation against 1.5 t and 3 t. *NMR in biomedicine*, 25(1):27–34, January 2012.

[8] C. J. Snyder, L. DelaBarre, G. J. Metzger, P-F F. van de Moortele, C. Akgun, K. Ugurbil, and J. T. Vaughan. Initial results of cardiac imaging at 7 tesla. *Magnetic resonance in medicine*, 61(3):517–524, March 2009.

[9] J. Thomas Vaughan, Carl J. Snyder, Lance J. DelaBarre, Patrick J. Bolan, Jinfeng Tian, Lizann Bolinger, Gregor Adriany, Peter Andersen, John Strupp, and Kamil Ugurbil. Whole-body imaging at 7T: preliminary results. *Magnetic resonance in medicine*, 61(1):244–248, January 2009.

[10] Gregory J. Metzger, Carl Snyder, Can Akgun, Tommy Vaughan, Kamil Ugurbil, and Pierre-Francois F. Van de Moortele. Local b1+ shimming for prostate imaging with transceiver arrays at 7T based on subject-dependent transmit phase measurements. *Magnetic resonance in medicine*, 59(2):396–409, February 2008.

[11] Christopher T. Rodgers, Stefan K. Piechnik, Lance J. Delabarre, Pierre-François F. Van de Moortele, Carl J. Snyder, Stefan Neubauer, Matthew D. Robson, and J. Thomas Vaughan. Inversion recovery at 7 t in the human myocardium: measurement of t(1), inversion efficiency and b(1) (+). *Magnetic resonance in medicine*, 70(4):1038–1046, October 2013.

[12] Sebastian Schmitter, Lance DelaBarre, Xiaoping Wu, Andreas Greiser, Dingxin

Wang, Edward J. Auerbach, J. Thomas Vaughan, Kâmil Uğurbil, and Pierre-François F. Van de Moortele. Cardiac imaging at 7 tesla: Single- and two-spoke radiofrequency pulse design with 16-channel parallel excitation. *Magnetic resonance in medicine*, 70(5):1210–1219, November 2013.

[13] V. Belle, E. Kahler, C. Waller, E. Rommel, S. Voll, K. H. Hiller, W. R. Bauer, and A. Haase. In vivo quantitative mapping of cardiac perfusion in rats using a noninvasive MR spin-labeling method. *Journal of magnetic resonance imaging : JMRI*, 8(6):1240–1245, 1998.

[14] Thomas Kampf, Xavier Helluy, Fabian T. Gutjahr, Patrick Winter, Cord B. Meyer, Peter M. Jakob, Wolfgang R. Bauer, and Christian H. Ziener. Myocardial perfusion quantification using the t1 -based FAIR-ASL method: the influence of heart anatomy, cardiopulmonary blood flow and look-locker readout. *Magnetic resonance in medicine*, 71(5):1784–1797, May 2014.

[15] S. R. Bergmann, K. A. Fox, A. L. Rand, K. D. McElvany, M. J. Welch, J. Markham, and B. E. Sobel. Quantification of regional myocardial blood flow in vivo with H215O. *Circulation*, 70(4):724–733, October 1984.

[16] S. T. Francis, R. Bowtell, and P. A. Gowland. Modeling and optimization of Look-Locker spin labeling for measuring perfusion and transit time changes in activation studies taking into account arterial blood volume. *Magnetic resonance in medicine*, 59(2):316–325, February 2008.

[17] Danny J. Wang, Xiaoming Bi, Brian B. Avants, Tongbai Meng, Sven Zuehlsdorff, and John A. Detre. Estimation of perfusion and arterial transit time in myocardium using free-breathing myocardial arterial spin labeling with navigator-echo. *Magnetic resonance in medicine*, 64(5):1289–1295, November 2010.

[18] Rajarshi Banerjee, Michael Pavlides, Elizabeth M. Tunnicliffe, Stefan K. Piech-

nik, Nikita Sarania, Rachel Philips, Jane D. Collier, Jonathan C. Booth, Jurgen E. Schneider, Lai Mun M. Wang, David W. Delaney, Ken A. Fleming, Matthew D. Robson, Eleanor Barnes, and Stefan Neubauer. Multiparametric magnetic resonance for the non-invasive diagnosis of liver disease. *Journal of hepatology*, 60(1):69–77, January 2014.

Appendix

MRM paper 2016

ISMRM abstract 2015

ISMRM abstract 2016

ISMRM poster prize 2016

FULL PAPER

Magnetic Resonance in Medicine 00:00–00 (2016)

A Look-Locker Acquisition Scheme for Quantitative Myocardial Perfusion Imaging with FAIR Arterial Spin Labeling in Humans at 3 Tesla

Graeme A. Keith,[1]* Christopher T. Rodgers,[1] Michael A. Chappell,[2] and Matthew D. Robson [1]

Purpose: A novel method for quantitative measurement of myocardial blood flow (MBF) using arterial spin labeling (ASL) in a single breath-hold is presented, evaluated by simulations, phantom studies and in vivo studies and tested for reproducibility and variability.

Methods: A flow-sensitive alternating inversion recovery (FAIR) ASL method with Look-Locker readout (LL-FAIR-ASL) was implemented at 3 tesla. Scans were performed on 10 healthy volunteers and MBF measured in three slices. The method was investigated for reproducibility by Bland-Altman analysis and statistical measures, the coefficients of reproducibility (CR) and variation (CV) are reported.

Results: The MBF values for the basal, mid, and apical slices were 1.04 ± 0.40, 1.06 ± 0.46, and 1.06 ± 0.38 ml/g/min, respectively (mean $\pm$ SD), which compare well with literature values. The CV across all scans, 43%, was greater than the between-session and within-session values, at 16 and 13%, respectively, for the mid-ventricular slice. The change in MBF required for detection, from the CR, was 61% between-session and 53% within-session for the mid-ventricle.

Conclusion: This study shows the feasibility of the LL-FAIR-ASL method for the quantification of MBF. The statistical measures reported will allow the planning of future clinical research studies involving rest and stress measurements. **Magn Reson Med 000:000–000, 2016.** **© 2016 The Authors Magnetic Resonance in Medicine published by Wiley Periodicals, Inc. on behalf of International Society for Magnetic Resonance in Medicine. This is an open access article under the terms of the Creative Commons Attribution License, which permits use, distribution and reproduction in any medium, provided the original work is properly cited.**

Key words: ASL; MBF; FAIR; heart; human

INTRODUCTION

Cardiovascular magnetic resonance (CMR) imaging is a powerful tool for the investigation of common pathologies of the heart such as congenital heart disease, coronary artery disease, and cardiomyopathies (1). One of the most useful processes that CMR allows us to investigate is the perfusion of blood in the myocardial tissue. In clinical practice, this is achieved with the use of an intravenous extracellular contrast agent, such as Gadolinium-DPTA (2), where the transit of the agent through the capillary bed of the myocardium can be observed. These first-pass techniques provide clinically applicable methods of imaging perfusion, but suffer from several drawbacks, such as significant problems with image artifacts (3), cost, the risk of the contrast agent itself to patients with renal conditions (4), and the difficulty of performing multiple serial evaluations owing to the lingering presence of the contrast agent.

An attractive alternative to first-pass perfusion CMR techniques and other, nuclear based modalities, such as single-photon emission computed tomography (SPECT) (5,6) or positron emission tomography (PET) (7,8), would be to use arterial spin labeling (ASL). ASL is a noninvasive technique which uses magnetic labeling strategies to allow the proton spins present in the blood water to act as an endogenous contrast agent (9,10). In one of the simplest ASL experiments, known as flow-sensitive alternating inversion recovery (FAIR) (11,12), two images or sets of images are collected, one in which a globally selective (GS) inversion pulse is applied before the readout (the control image) such that the spins of the myocardial tissue of interest and those of the inflowing blood are both inverted. The second image set is preceded by a slice-selective (SS) inversion through a slice of the myocardium (the tag or label image) such that the myocardial tissue in the imaging slice is again inverted but the blood water spins flowing into the image slice remain in thermomagnetic equilibrium. The effect of the presence of these inflowing spins in the SS experiment is to cause an apparent shortening of the longitudinal relaxation time (T_1) of the tissue. It is the size of the difference in the observed T_1 values between the two measurements that allows us to quantitatively evaluate the blood flow to the myocardium.

The measurement of T_1 values in the myocardium, often in the form of T_1 mapping techniques, has emerged as a useful tool in CMR (13). One established, robust method often used for T_1 mapping is the modified Look-Locker inversion recovery (MOLLI) (14–16) sequence and it's variants, which allow for the measurement and parametric mapping of the myocardial T_1 in vivo, in a single breath-hold. In this approach, an inversion pulse is applied and the relaxation of the longitudinal magnetization is sampled following an inversion time, TI, then

[1]Oxford Centre for Clinical Magnetic Resonance Research, University of Oxford, John Radcliffe Hospital, Oxford, United Kingdom.

[2]Institute of Biomedical Engineering, University of Oxford, Old Road Campus, Oxford, United Kingdom.

Grant sponsor: MRC; Grant number: G0900883; Grant sponsor: the Wellcome Trust; Grant sponsor: the Royal Society; Grant number: 098436/Z/12/Z.

*Correspondence to: Graeme A. Keith, Oxford Centre for Clinical Magnetic Resonance Research, University of Oxford, John Radcliffe Hospital, Oxford, UK OX3 9DU. E-mail: graeme.keith@cardiov.ox.ac.uk

Received 4 May 2016; revised 28 July 2016; accepted 28 July 2016

DOI 10.1002/mrm.26388

Published online 00 Month 2016 in Wiley Online Library (wileyonlinelibrary.com).

© 2016 The Authors Magnetic Resonance in Medicine published by Wiley Periodicals, Inc. on behalf of International Society for Magnetic Resonance in Medicine.

again following the equivalent of one R–R interval, measured by electrocardiograph (ECG) -gating, and so on to build up a relaxation curve allowing the quantification of T_1. Different variants of the technique use different inversion-readout schemes (3(3)3(3)5 for MOLLI, 5(1)1(1)1 for ShMOLLI and so on, indicating the number of look-locker images acquired and the duration of the gaps between acquisitions, all in units of heart beats).

In this work, a method for measuring myocardial blood flow (MBF) noninvasively using a FAIR labeling scheme combined with a Look-Locker acquisition (LL-FAIR-ASL) (17) is presented. The described method allows for the acquisition of both FAIR inversion states (SS and GS) within a single breath-hold. The method is assessed by way of simulation, phantom study, and in vivo application. The method is further used for quantitative analysis of MBF in healthy volunteers. MBF is measured in three slices in humans with ASL for the first time and is assessed for reproducibility and variability.

METHODS

Sequence Design

The LL-FAIR-ASL sequence was implemented on a 3 tesla (3 T) whole-body scanner (TIM Trio, Siemens, Germany). The sequence consisted of two HS8 adiabatic inversion pulses (18), one SS, one GS with a duration of 10 ms, time/bandwidth product $R = 40$ and $\beta = 3.45$. Each inversion pulse was followed by a block of five cardiac triggered balanced steady-state free precession (bSSFP) readouts (19). The readout consisted of LISA excitation pulses, which are Gaussian-like, and included five initial ramp-up pulses and a final half-alpha "restore pulse." The two inversion blocks were separated by a gap of three heartbeats to allow for some recovery of the magnetization, within a manageable breath-hold, as shown in Figure 1, thus forming a MOLLI 5(3)5 regime. Both SS and GS inversions were collected in a single thirteen heartbeat breath-hold. The ordering scheme of the sequence within this thirteen heart beat breath-hold (SS-GS or GS-SS) was varied. Sequence parameters were based closely on those used successfully in MOLLI implementations and included a 35° excitation flip angle, image slice thickness of 8 mm, an initial TI of 115 ms (with the following values being 115 ms + RR, 115 ms + 2RR,...), TR/TE of 3 ms/1.5 ms, 320 mm field of view with 75% phase resolution and 6/8 partial Fourier, a 192×144 image matrix (interpolated to 384×288) and an acceleration factor of GRAPPA 2 (20). All inversion pulses and readouts occurred during the diastolic phase of the cardiac cycle. This timing guaranteed that the signal recovery was not corrupted by through-plane bulk cardiac motion, by restricting inversions and readouts to the most stable cardiac phase. Due to the inversion recovery nature of the sequence at least 15 s was allowed between scans to allow for full relaxation of the magnetization.

Simulation

Bloch simulations of the sequence were performed in MATLAB (The Mathworks Inc., Natick, MA) with the acquisition parameters defined above and not accounting for magnetization-transfer effects. The inversion pulses were simulated fully as HS8 pulses with the parameters matching those described above and the power set as per the scanner maximum output voltage to simulate the actual B_1 power used on the scanner to ensure the adiabatic condition is met. The evolution of the longitudinal magnetization, M_z, after inversion, and the influence of the readout blocks, based on these simulations, is shown in Figure 1. Simulations were performed for a range of T_1s (100–2000 ms) and heart rates (40–140 bpm) to test the robustness of the sequence against variations in these parameters. To determine an appropriate value for the thickness of the SS inversion pulse, a range of thicknesses (8–35 mm) were simulated for the stated range of T_1s, with a fixed image slice profile with thickness of 8 mm full width half maximum to investigate the interaction between the HS8 inversion pulse profile and the image slice profile. The inflow was not simulated, such that the performance of the sequence in measuring only the relaxation under the two different inversion conditions could be investigated to ensure that any difference measured in vivo was due to blood flow and not systematic error.

Phantom Studies

A phantom imaging study was carried out to further investigate the performance of the LL-Fair-ASL sequence in the absence of flow. The data gathered were used to investigate the dependence of T_1 and T_1^* on heart rate with the LL-FAIR-ASL sequence by plotting these values against a range of simulated heart rates. The length of the gap between the two inversion blocks (measured in heartbeats) was also varied to investigate the effect of imperfect recovery before the second inversion. These experiments were carried out on an integrated calibration phantom distributed by Dr. S. Piechnik, Oxford, for the HCMR study (Clinicaltrials.gov ID: NCT01915615). The phantom was designed to monitor stability of T_1 mapping techniques, and provides a T_1 range of ~300–3000 ms, and T_2 ~60–3000 ms. The phantom consists of nine test objects made of agar, carrageenan water gels doped with nickel chloride. The study was carried out on the 3 T scanner using a 32-channel body receive array. The simulated ECG trigger was varied from 40 bpm to 140 bpm in 20-bpm intervals. The resulting images were loaded into MATLAB for analysis, where regions of interest (ROIs) were drawn by hand within the confines of each tube and propagated throughout an image series to calculate the T_1s of the samples.

In Vivo Studies

ASL image series were acquired on 11 healthy volunteers (31 ± 7 years old; 71 ± 9 kg; two female) at 3T, in basal, mid-ventricular, and apical short axis slices using the 32-channel body receive array. All volunteers were recruited in accordance with the ethical practices of our institution and their informed consent obtained. Each of the volunteers was scanned twice, on separate days, making 22 scan sessions in total. The data from one subject was discarded due to excessive motion within the image series. In 17 of the 20 successful scans, the ASL acquisitions in the mid-ventricular slice were repeated. B_0 shimming was performed in a volume over the left

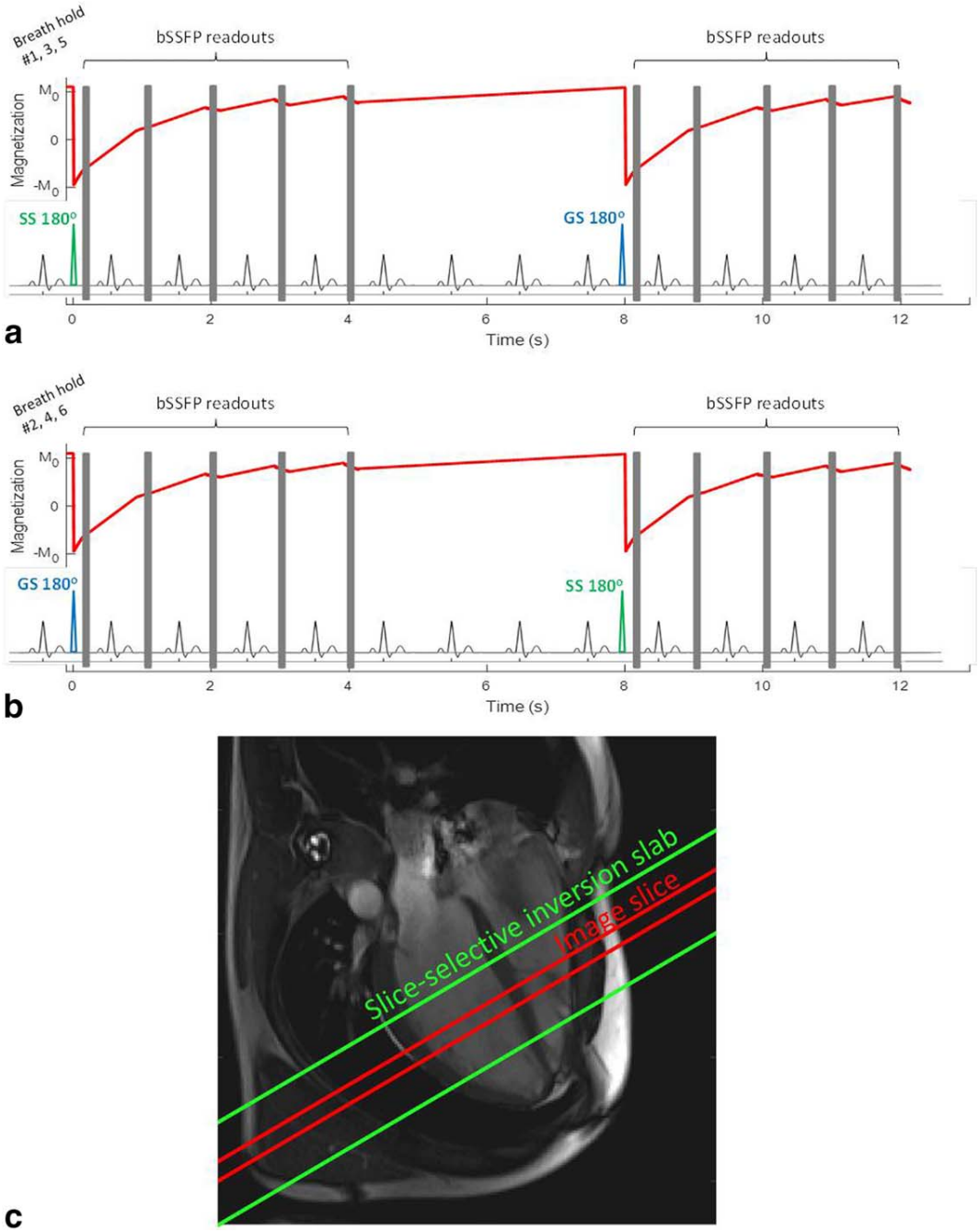


FIG. 1. A schematic of the LL-FAIR-ASL pulse sequence over 13 heartbeats for breath-holds 1, 3, and 5 (**a**) and breath-holds 2, 4, and 6 (**b**). 180° pulses (one SS, one GS, within a single breath-hold, the order of which is varied) are each followed by 5 bSSFP readouts (shown as gray boxes), separated by an R–R interval. The evolution of M_z throughout the sequence is shown in red. (**c**) A four-chamber view of the heart with the position of the imaging slice in red, and the position of the SS inversion slab in green.

ventricle (LV) covering all three slices. In each slice, the sequence as described in Figure 1 was run three times with the SS inversion block preceding the GS inversion block (called the SS-GS ordering scheme), then run a further three times with the GS inversion block preceding the SS (GS-SS), making for a total of six measurements, from which a single value of MBF could be calculated. An SS inversion thickness of 24 mm was used based on the results of the simulation and phantom scans described. This inversion slab and the imaging slice were positioned as described in Figure 1c. In all cases, ECG triggering and breath-holding were used. No motion correction or image registration was used.

Image Analysis

All image series were loaded into MATLAB and regions of interest (ROIs) were drawn by hand for both the left

ventricular myocardium and the blood pool. For the myocardium, the epicardial and endocardial borders were drawn and the myocardium divided into segments as per the American Heart Association (AHA) model (21). The apparent T_1 values (T_1^*) for the myocardium for both the SS and global inversion blocks were calculated, as was the T_1 of blood from the global data by using a three-parameter least squares fit as described by:

$$S(TI) = A - Be^{\left(-TI/T_1^*\right)} \quad [1]$$

where S was the signal intensity recorded at time TI and A, B, and T_1^* were the fitted parameters. Where T_1 values are reported, the correction described by Deichmann and Haase for FLASH images (22) and described in Eq. [2] was used, although only strictly applicable in the small tip angle regime.

$$T_1 = T_1^*\left(\frac{B}{A} - 1\right) \quad [2]$$

The phase data of the most fully recovered image from each inversion block were used to correct the polarity of the magnitude images on a pixel-by-pixel basis before fitting (23). The myocardial blood flow (MBF) for each slice was calculated from these data by the Belle quantification model (24):

$$MBF = \frac{\lambda}{T_1^{blood}}\left(\frac{T_1^{GS}}{T_1^{SS}} - 1\right) \quad [3]$$

where $\lambda = 0.92$ mL/g (25) is the blood-tissue partition coefficient of water, T_1^{blood} is the relaxation time of the blood pool and T_1^{GS} and T_1^{SS} are the values for the longitudinal relaxation time calculated for the myocardium, from the GS and SS experiment, respectively. For the in vivo study, the T_1^{GS} and T_1^{SS} values used were the observed T_1^*s. As has been discussed previously (26,27), where the Deichmann-Haase correction is used the ratio of the relaxation times remains constant ${T_1}^{\text{GS}}/{T_1}^{\text{SS}} = {T_1^*}^{\text{GS}}/{T_1^*}^{\text{SS}}$ as the fitted values of A and B should remain the same for both the GS and SS cases. Thus, use of the correction would have no effect on the final value of MBF. The use of T_1^* is discussed further later in this work

Reproducibility and Variability Analysis

The in vivo data were used to perform Bland-Altman analysis (28) to assess reproducibility and variation. The mean difference in each case and the value of ± 1.96 times the standard deviations (SD) were calculated, which represent the upper and lower 95% confidence bounds. When normalized to the mean value of MBF, these values give the coefficient of repeatability for both the between-session (CR_{BS}) and within-session cases (CR_{WS}). The variability of the MBF estimates was assessed by the coefficient of variation (CV, equal to the ratio of the standard deviation to the mean) for the whole sample (CV_{all}), and each subject between-session (CV_{BS}) and within-session (CV_{WS}).

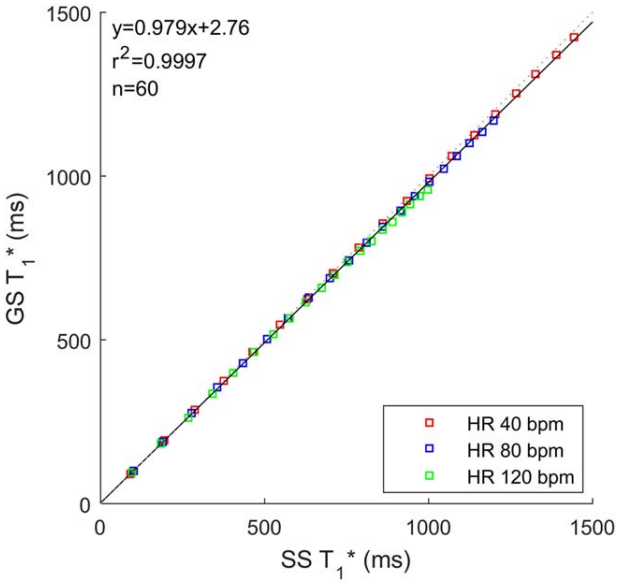


FIG. 2. Correlation plot of the simulated SS and GS T_1^* s, in the absence of flow, for heart rates of 40, 80, and 120 bpm and input T_1 values from 100 to 2000 ms (100 ms steps).

Segmental Analysis

Values of MBF were calculated for each of the 16 standard myocardial segments as defined but the AHA (21) to assess the viability of the ASL technique at segmental level. For each segment, these are reported as the mean and standard deviation across all the volunteers. The coefficient of variation (CV_{seg}) is also reported for all segments.

RESULTS

Simulation

T_1^* data were plotted for heart rates of 40, 80, and 120 bpm and for the full range of input T_1s. Figure 2 shows the simulated SS and GS T_1^*s to agree well in the absence of flow, with an R^2 value of 0.9996 and both the T_1^*s shortening with increasing heart rate.

Figure 3 shows the results of simulations to determine an appropriate value for the thickness of the SS inversion pulse. Results for both T_1 and T_1^* are plotted showing the dependence of the calculation on the extent of the inversion. The values are stable down to an inversion thickness of 23 mm then decrease with decreasing thickness. The effect is more marked with T_1 than T_1^*. For the input T_1 of 1200 ms, approximately in the myocardial range, the T_1^* drops from a maximum of 928 ms with the thickest inversion slice to 860 ms with the thinnest, a drop of 7%. The calculated T_1, however, drops from 1043 ms with the thickest slice to just 63 ms with the thinnest, a drop of 94%.

Phantom Studies

An example plot of T_1 and T_1^* against simulated heart rate is shown in Figure 4 for a gap of three heart beats. The dependence of T_1^* on heart rate can be clearly seen

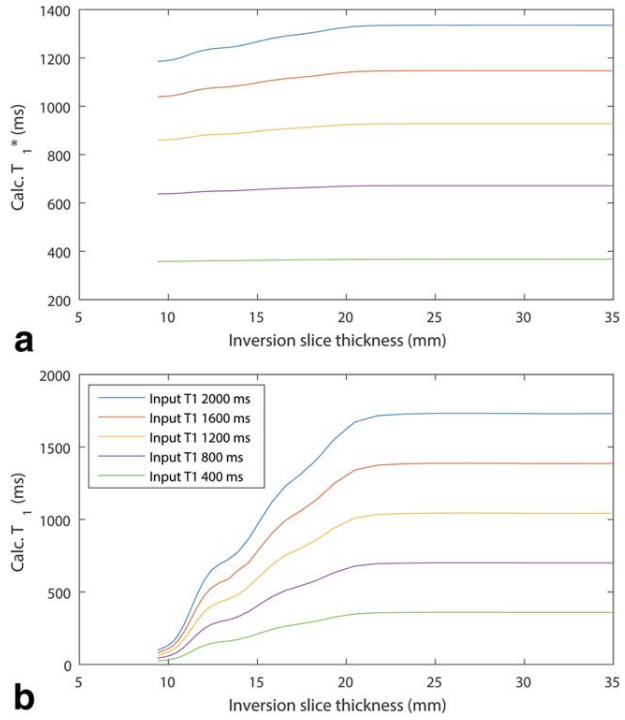


FIG. 3. For an image slice thickness of 8 mm, the SS HS8 inversion pulse width, varied from 8 to 35 mm, is plotted against the simulated observed T_1^* (**a**), and T_1 (**b**) (following the Deichmann-Haase correction) for input T_1 values of 400 to 2000 ms (400 ms steps).

for both the SS-GS and GS-SS ordering schemes, decreasing steadily as the heart rate increases. The calculated T_1, however, is stable for the first inversion block in the ordering scheme, whether SS or GS, with a value of 1431 ± 8 ms for the range of heart rates, but decreases rapidly with increasing heart rate, and, therefore, decreasing recovery time, for the second inversion block. Thus, the calculation of T_1 is dependent on the ordering scheme, whereas the calculation of the T_1^* s is not.

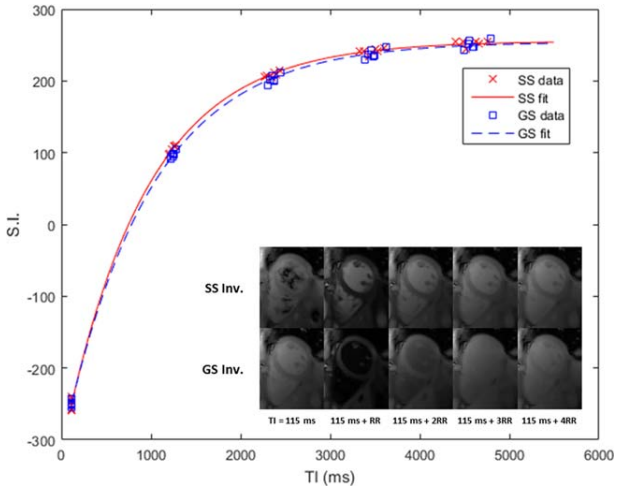


FIG. 5. A typical pair of SS and GS inversion recovery curves with data points from six breath-holds averaged over an ROI encompassing the left ventricular myocardium, and corresponding image series inset from one of the six breath-holds.

In Vivo Studies

Figure 5 shows a typical pair of T_1 recovery curves, with inset SS and GS image series. The mean MBF across all the 10 volunteers and all 2 scan sessions was 1.04 ± 0.40 mL/g/min in the basal slice, 1.06 ± 0.46 mL/g/min in the mid-ventricle and 1.06 ± 0.38 mL/g/min in the apical slice. The calculated values of MBF for each subject in each session, as well as the mean values, are presented in Figure 6. The data are presented for all scans in all three slices.

Reproducibility and Variability Analysis

Values for the coefficients of variation and reproducibility, for both the between session and within session cases, are presented in Table 1. The CV across all scans was calculated as 39, 43, and 36% in the basal, mid-

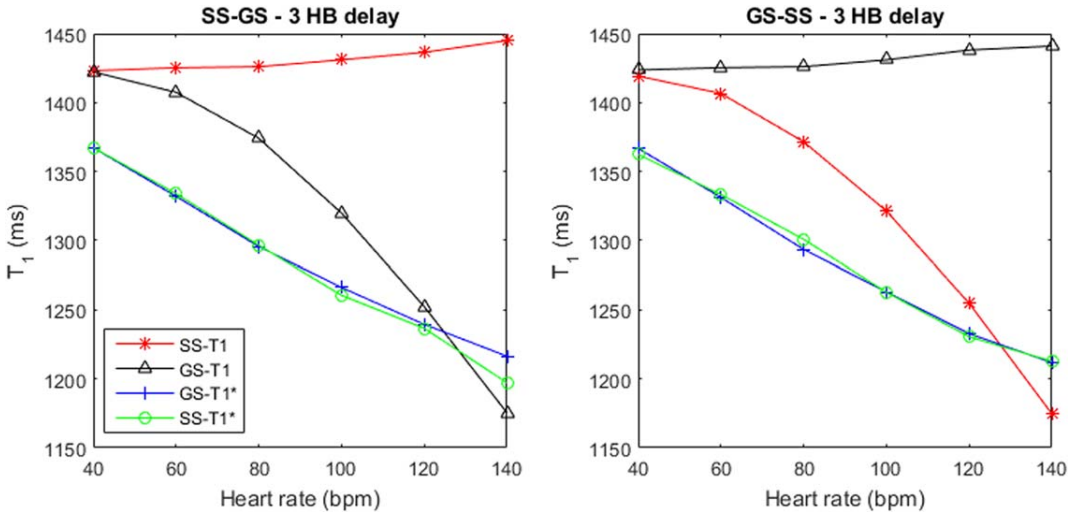


FIG. 4. Measured T_1^* and T_1 of a cardiac phantom, for both the SS and GS inversion blocks plotted against simulated heart rate, from 40–140 bpm. There was a three heartbeat delay between the end of one block and the start of the next. The data are plotted for the SS-GS (**a**) and the GS-SS (**b**) ordering scheme.

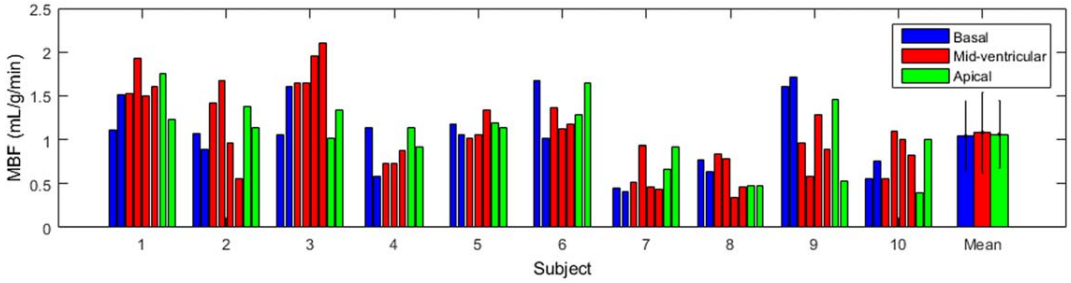


FIG. 6. Calculated MBF results for both scan sessions for all 10 volunteers in basal, mid-ventricular, and apical slices represented by blue, red, and green bars, respectively. Error bars denote the standard deviation.

ventricular, and apical slices, respectively. The CV_{BS} was 14, 16, and 17% in basal, mid, and apex; and the CV_{WS} was 13% in the mid-ventricle. The CR_{WS} was 53% in the mid-ventricle, compared with CR_{BS} values of 72, 61, and 85% in the base, mid, and apex.

Segmental Analysis

The mean values and standard deviations of segmental MBF are reported in Table 2 along with the coefficient of variation, for all 16 segments. The range of mean segmental MBF values is 0.87–1.52 mL/g/min. These values are also plotted in Figure 7a, along with previous literature values of MBF in four segments in the mid-ventricle (septum and anterior, lateral, and inferior walls) using ^{15}O PET (29). The numbering of the segments is described in Figure 7b.

DISCUSSION

In this study, a noninvasive method for quantitatively measuring myocardial blood flow using arterial spin labelling was developed and tested by means of simulation, phantom experiment and in vivo studies. The variation and reproducibility of the method were then investigated in three short axis slices, where previous cardiac ASL studies have been restricted to the mid-ventricle.

The Bloch simulations of the LL-FAIR-ASL sequence show good agreement between the SS and GS T_1^*s as presented in Figure 2. Thus, there is no dependence in the MBF calculation on error in the calculation of the T_1^* ratio. This is true of the three simulated heart rates (40, 80, and 120 bpm), despite the expected shortened T_1^* with increasing heart rate due to saturation from multiple high flip angle readouts, as seen in the simulated evolution of magnetization in Figure 1.

As observed in Figure 3, the calculation of T_1^* and T_1 is compromised at lower values of the inversion slice thickness relative to the imaging slice thickness. This occurs due to differences between the inversion profile and the image slice profile. The effect is far more marked in the calculation of T_1 due to the reliance of the Deichmann-Haase correction on inversion efficiency. At lower inversion thicknesses the efficiency is low due to the slice containing a mixture of inverted and noninverted spins. By comparison, T_1^* has little dependence on inversion efficiency, providing further motivation for its use over T_1. These data were used in the choice of inversion thickness for in vivo application of 24 mm.

Varying the simulated heart rate in the phantom scans demonstrates that the values of T_1^* are far more stable than those of T_1. Although T_1^* is dependent on heart rate, as demonstrated in Figure 4, the T_1^* values calculated for the SS and GS cases exhibit the same dependence, meaning heart rate does not bias the calculation of MBF as it is calculated from a ratio of the GS and SS T_1^*s. As discussed above, the T_1 correction is highly dependent on the inversion efficiency, and in each ASL ordering scheme the second of the two inversions suffers from apparent poor efficiency due to insufficient time for relaxation between blocks, which is necessary for achievable breath-holds. T_1^* was used for all MBF calculations as the Deichmann-Haase correction is only strictly applicable in a small angle regime and for inversion pulses applied to spins at equilibrium magnetization (22). T_1^* is independent of inversion efficiency and, as stated earlier the ratio of GS to SS T_1^*s is the same as the ratio of GS to SS T_1s.

The LL-FAIR-ASL method is attractive as it provides a noninvasive alternative to SPECT, PET, and first-pass perfusion CMR. Using this method, MBF can be measured quantitatively in a single slice in six 13-heartbeat breath-holds. Each breath-hold contains both SS and GS acquisitions, which ensures that the position of the heart and heart rate are the same for each pair. The ability to acquire an SS/GS pair in a single breath-hold is an important feature of the LL-FAIR-ASL sequence, as the measured changes in T_1^* are small and could easily be

Table 1
MBF Results from In Vivo Scans in Three Slices, Including the mean myocardial blood flow (MBF), the standard deviation and the CV across all scans and the CV and CR for between session (BS) and within session (WS) Cases

Slice	Mean MBF (mL/g/min)	SD (mL/g/min)	CV_{all} (%)	CV_{BS} (%)	CV_{WS} (%)	CR_{BS} (%)	CR_{WS} (%)
Basal	1.04	0.40	39	14		72	
Mid	1.06	0.46	43	16	13	61	53
Apical	1.06	0.38	36	17		85	

Table 2
Mean MBF Values for Each Segment, Where Segments 1-6 Are the Basal Slice, 7-12 Are the Mid-ventricular Slice, and 13-16 Are the Apical Slice

Segment	Mean MBF (mL/g/min)	SD (mL/g/min)	CV_{seg} (%)
1	0.97	0.6	62
2	1.22	0.91	75
3	1.14	0.88	77
4	0.88	0.74	84
5	1.12	0.59	53
6	1.33	0.65	49
7	1.09	0.73	67
8	1.15	0.66	57
9	1.06	1.04	98
10	0.87	0.51	59
11	1.18	0.61	52
12	1.38	0.83	60
13	0.97	0.89	92
14	0.98	0.67	68
15	1.52	0.95	63
16	1.19	0.76	64

lost among systematic errors. The mean MBF, in the mid-ventricular slice, of 1.06 ± 0.46 mL/g/min compares well with literature values, as presented in Table 3 (29–36).

While reproducibility and variability of similar techniques have been investigated in mice (37,38), to our knowledge this has not been carried out in human myocardium. Resting MBF values for healthy volunteers have previously been shown to be heterogeneous in studies using PET (29) and first-pass perfusion CMR (39). The high observed values for CV_{all} across all subjects, 39, 43, and 36% for basal, mid, and apical slices, respectively, show that our results reflect this heterogeneous nature. This variability, calculated as the coefficient of variation is comparable to similar measures reported for preclinical cardiac ASL (37,38).

The values of CV_{BS} and CV_{WS} calculated for individual subjects were all below the values reported for CV_{all} except for a single apical slice which gave a CV_{BS} of 43%. However, the mean values of CV_{BS} for each slice and CV_{WS} for the mid slice only, are significantly lower than CV_{all}, with a maximum of 17%. This shows that the variation in results exhibited by an individual subject in each case is much less than across the population as a whole. The CV_{BS} shows the variation due to the method, plus re-setup effects such as repositioning, re-localization, re-shimming etc. The CV_{WS} primarily reflects the methodological effects.

The Bland-Altman analysis showed the mean difference in both the between-session case for all three slices and the within-session case, for the mid slice only, to be close to zero and all bar one of the data points to lie within the ± 1.96 SD bounds. The values of CR give an indication of the change in MBF required to be detected above systematic errors. The between-session CRs of 72, 61, and 85% for the basal, mid, and apical slices, show the level of repeatability expected across repeat scans. They show the change in MBF required to show a difference over time and is useful to consider if planning a longitudinal study in a patient group. The within-session CR of 53% for the mid-ventricular slice gives a useful indication of the detectable change in MBF. Thus, a change in MBF would be reliably detectable when rising from the mean mid-ventricular MBF, measured with LL-FAIR-ASL, of 1.08 mL/g/min to a value of 1.74 mL/g/min between-session and 1.65 mL/g/min within-session. During vasodilator stress, the change in MBF in non-ischemic segments of the heart has been shown to be between 300 and 420% (35,40,41), or between 3.24 and 4.54 mL/g/min based on the mean mid-ventricular MBF reported here. Therefore, the expected change in global MBF under stress should be detectable with the LL-FAIR-ASL method.

Segmental MBF is an important measure in disease, as it allows investigation of MBF changes in the arterial territories of the myocardium. Previous publications using PET (29) and ASL (35) have commented on the spatial heterogeneity of resting MBF within a slice. The relative dispersion, here called the coefficient of variation, was

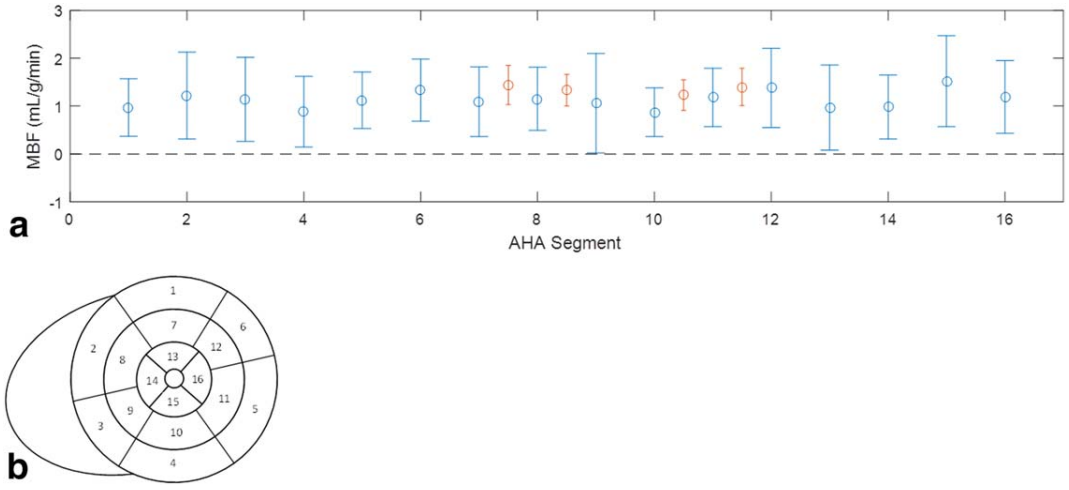


FIG. 7. The mean ± standard deviation of MBF across all subjects for each myocardial segment as defined by the AHA (**a**), as described in (**b**), where segments 1–6 are the basal slice, 7–12 are the mid-ventricular slice, and 13–16 are the apical slice. The data points in red are literature values in the septum and anterior, lateral and inferior walls of the mid–ventricle from Chareonthaitawee et al 2001 (29).

Table 3
Comparison of LL-FAIR Mid-ventricular Resting MBF against Literature Values for Previous Cardiac ASL Methods, First-Pass Perfusion CMR, and PET

Source	Method	Age (y)	Gender	Population	MBF_{rest} (mL/g/min)
LL-FAIR-ASL	ASL	31 ± 7	8 M/2 F	Healthy	1.06 ± 0.46
Zun 2009(36)	ASL		8 M/2 F	Healthy	1.36 ± 0.40
Zun 2011(35)	ASL	64 ± 11	10 M/19 F	CAD patients	0.97 ± 0.64
Wang 2010(34)	ASL	39 ± 9	10 M/1 F	Healthy	1.00 ± 0.55
Northrup 2008(33)	ASL	22 ± 2	5 M/3 F	Healthy	1.06 ± 0.19
Jerosch-Herold 2008(31)	CMR - First Pass	63 ± 10	11 M/19 F	Atherosclerosis	1.01 ± 0.22/ 0.91 ± 0.18[a]
Hsu 2006(30)	CMR - First Pass	33 ± 4	2 M/8 F	Healthy	1.02 ± 0.22
Manabe 2009(32)	^{82}Rb PET	29 ± 9	8 M/7 F	Healthy	0.99 ± 0.29/ 1.00 ± 0.25*
Chareonthaitawee 2001(29)	^{15}O PET	46 ± 12	131 M/38 F	Healthy	1.33 ± 0.32

[a]Results from two separate exams on the same group of patients/volunteers.

reported as 13% with PET and 68% (range, 11% to 152%) with ASL, compared with 67% (with a range of 49% to 98%) with LL-FAIR-ASL. This difference in error between the ASL methods and PET is also reflected in the data plotted in Figure 7 and is perhaps expected given the inherently low signal-to-noise ratio of the method and the low resolution of the PET method, noted as a limitation by the authors and reported as $8.43 \times 8.33 \times 6.6\,mm^3$ full-width half maximum compared with $1.7 \times 2.2 \times 8\,mm^3$ with LL-FAIR-ASL. However, given the expected increase in MBF under stress, the difference in perfusion reserve between ischemic and normal segments, should be detectable.

This study served to validate the LL-FAIR-ASL technique for measurement of resting MBF in healthy humans. Future studies will be required to validate the method in patient populations under stress and compare the results with standard methods such as first-pass perfusion CMR. Image registration methods may be used to compensate for residual motion within breath-holds, particularly in studies involving patients. In addition, more complex models for quantification of MBF, taking account of such effects as arterial transit time, the partial inversion of the blood pool during SS inversion and the perturbation of the inversion recovery by the readouts could be implemented. However, these studies are beyond the scope of this work.

CONCLUSIONS

The LL-FAIR-ASL sequence for quantitative measurement of MBF was shown to be robust and efficient when performed in vivo. The method is completely noninvasive, not requiring contrast agent, and provides resting MBF values in healthy volunteers which compare well with the literature and display the previously reported heterogeneity within healthy volunteer groups. MBF values are reported globally in three slices with a cardiac ASL technique for the first time. The variability of the method was shown to compare favorably with published values in similar techniques used in preclinical imaging but, to our knowledge, has not previously been performed in human volunteers. The method was shown to be sensitive enough to detect MBF increase under stress conditions in future studies. The presented results should prove useful in the planning of clinical research studies using this sequence to quantitatively measure MBF at rest and under stress in healthy volunteers or in patient groups.

ACKNOWLEDGMENT

C.T.R. is funded by the Wellcome Trust and the Royal Society.

REFERENCES

1. Pennell DJ, Sechtem UP, Higgins CB, Manning WJ, Pohost GM, Rademakers FE, van Rossum AC, Shaw LJ, Yucel EK. Clinical indications for cardiovascular magnetic resonance (CMR): Consensus Panel report. Eur Heart J 2004;25:1940–1965.
2. Gerber BL, Raman SV, Nayak K, Epstein FH, Ferreira P, Axel L, Kraitchman DL. Myocardial first-pass perfusion cardiovascular magnetic resonance: history, theory, and current state of the art. J Cardiovasc Magn Reson 2008;10:18.
3. Di Bella EV, Parker DL, Sinusas AJ. On the dark rim artifact in dynamic contrast-enhanced MRI myocardial perfusion studies. Magn Reson Med 2005;54:1295–1299.
4. Sieber MA, Lengsfeld P, Walter J, Schirmer H, Frenzel T, Siegmund F, Weinmann HJ, Pietsch H. Gadolinium-based contrast agents and their potential role in the pathogenesis of nephrogenic systemic fibrosis: the role of excess ligand. J Magn Reson Imaging 2008;27:955–962.
5. Ben-Haim S, Murthy VL, Breault C, et al. Quantification of myocardial perfusion reserve using dynamic SPECT imaging in humans: a feasibility study. J Nucl Med 2013;54:873–879.
6. Garcia EV. Are SPECT measurements of myocardial blood flow and flow reserve ready for clinical use? Eur J Nucl Med Mol Imaging 2014;41:2291–2293.
7. Bergmann SR, Herrero P, Markham J, Weinheimer CJ, Walsh MN. Noninvasive quantitation of myocardial blood-flow in human-subjects with oxygen-15-labeled water and positron emission tomography. J Am Coll Cardiol 1989;14:639–652.
8. Lortie M, Beanlands RSB, Yoshinaga K, Klein R, DaSilva JN, Dekemp RA. Quantification of myocardial blood flow with Rb-82 dynamic PET imaging. Eur J Nucl Med Mol Imaging 2007;34:1765–1774.
9. Detre JA, Leigh JS, Williams DS, Koretsky AP. Perfusion imaging. Magn Reson Med 1992;23:37–45.
10. Detre JA, Zhang W, Roberts DA, Silva AC, Williams DS, Grandis DJ, Koretsky AP, Leigh JS. Tissue specific perfusion imaging using arterial spin labeling. NMR in biomedicine 1994;7:75–82.
11. Kim SG. Quantification of relative cerebral blood flow change by flow-sensitive alternating inversion recovery (FAIR) technique: application to functional mapping. Magn Reson Med 1995;34:293–301.
12. Kim SG, Tsekos NV. Perfusion imaging by a flow-sensitive alternating inversion recovery (FAIR) technique: application to functional brain imaging. Magn Reson Med 1997;37:425–435.
13. Moon JC, Messroghli DR, Kellman P, et al. Myocardial T1 mapping and extracellular volume quantification: a Society for Cardiovascular

Magnetic Resonance (SCMR) and CMR Working Group of the European Society of Cardiology consensus statement. J Cardiovasc Magn Reson 2013;15:92.
14. Piechnik SK, Ferreira VM, Dall'Armellina E, Cochlin LE, Greiser A, Neubauer S, Robson MD. Shortened Modified Look-Locker Inversion recovery (ShMOLLI) for clinical myocardial T1-mapping at 1.5 and 3 T within a 9 heartbeat breathhold. J Cardiovasc Magn Reson 2010; 12:69.
15. Messroghli DR, Radjenovic A, Kozerke S, Higgins DM, Sivananthan MU, Ridgway JP. Modified Look-Locker inversion recovery (MOLLI) for high-resolution T1 mapping of the heart. Magn Reson Med 2004; 52:141–146.
16. Look DC, Locker DR. Time saving in measurement of NMR and EPR relaxation times. Rev Sci Instrum 1970;41:250.
17. Keith GA RC, Chappell, MA, Robson MD. A Look-Locker acquisition scheme for quantitative myocardial perfusion imaging by arterial spin labelling in humans at 3 T. In Proceedings of the 23rd Annual Meeting of ISMRM, Toronto, 2015. Abstract 2690.
18. Tannus A, Garwood M. Adiabatic pulses. NMR in biomedicine 1997; 10:423–434.
19. Schar M, Kozerke S, Fischer SE, Boesiger P. Cardiac SSFP imaging at 3 Tesla. Magn Reson Med 2004;51:799–806.
20. Do HP, Jao TR, Nayak KS. Myocardial arterial spin labeling perfusion imaging with improved sensitivity. J Cardiovasc Magn Reson 2014; 16:15.
21. Cerqueira MD, Weissman NJ, Dilsizian V, et al. Standardized myocardial segmentation and nomenclature for tomographic imaging of the heart - a statement for healthcare professionals from the Cardiac Imaging Committee of the Council on Clinical Cardiology of the American Heart Association. Circulation 2002;105:539–542.
22. Deichmann R, Haase A. Quantification of T1 values by SnapshotFlash NMR Imaging. J Magn Reson 1992;96:608–612.
23. Gowland PA, Leach MO. A simple method for the restoration of signal polarity in multi-image inversion recovery sequences for measuring T1. Magn Reson Med 1991;18:224–231.
24. Belle V, Kahler E, Waller C, Rommel E, Voll S, Hiller KH, Bauer WR, Haase A. In vivo quantitative mapping of cardiac perfusion in rats using a noninvasive MR spin-labeling method. J Magn Reson Imaging 1998;8:1240–1245.
25. Bergmann SR, Fox KA, Rand AL, McElvany KD, Welch MJ, Markham J, Sobel BE. Quantification of regional myocardial blood flow in vivo with H215O. Circulation 1984;70:724–733.
26. Kampf T, Helluy X, Gutjahr FT, Winter P, Meyer CB, Jakob PM, Bauer WR, Ziener CH. Myocardial perfusion quantification using the T1-based FAIR-ASL method: the influence of heart anatomy, cardiopulmonary blood flow and look-locker readout. Magn Reson Med 2014;71:1784–1797.
27. Streif JUG, Hiller KH, Waller C, Nahrendorf M, Wiesmann F, Bauer WR, Rommel E, Haase A. In vivo assessment of absolute perfusion in the murine skeletal muscle with spin labeling MRI. J Magn Reson Imaging 2003;17:147–152.
28. Bland JM, Altman DG. Statistical methods for assessing agreement between two methods of clinical measurement. Lancet 1986;1:307–310.
29. Chareonthaitawee P, Kaufmann PA, Rimoldi O, Camici PG. Heterogeneity of resting and hyperemic myocardial blood flow in healthy humans. Cardiovasc Res 2001;50:151–161.
30. Hsu LY, Rhoads KL, Holly JE, Kellman P, Aletras AH, Arai AE. Quantitative myocardial perfusion analysis with a dual-bolus contrast-enhanced first-pass MRI technique in humans. J Magn Reson Imaging 2006;23:315–322.
31. Jerosch-Herold M, Vazquez G, Wang L, Jacobs DR Jr, Folsom AR. Variability of myocardial blood flow measurements by magnetic resonance imaging in the multi-ethnic study of atherosclerosis. Invest Radiol 2008;43:155–161.
32. Manabe O, Yoshinaga K, Katoh C, Naya M, deKemp RA, Tamaki N. Repeatability of rest and hyperemic myocardial blood flow measurements with 82Rb dynamic PET. J Nucl Med 2009;50:68–71.
33. Northrup BE, McCommis KS, Zhang H, Ray S, Woodard PK, Gropler RJ, Zheng J. Resting myocardial perfusion quantification with CMR arterial spin labeling at 1.5 T and 3.0 T. J Cardiovasc Magn Reson 2008;10:53.
34. Wang DJ, Bi X, Avants BB, Meng T, Zuehlsdorff S, Detre JA. Estimation of perfusion and arterial transit time in myocardium using free-breathing myocardial arterial spin labeling with navigator-echo. Magn Reson Med 2010;64:1289–1295.
35. Zun Z, Varadarajan P, Pai RG, Wong EC, Nayak KS. Arterial spin labeled CMR detects clinically relevant increase in myocardial blood flow with vasodilation. JACC Cardiovasc Imaging 2011;4:1253–1261.
36. Zun Z, Wong EC, Nayak KS. Assessment of myocardial blood flow (MBF) in humans using arterial spin labeling (ASL): feasibility and noise analysis. Magn Reson Med 2009;62:975–983.
37. Campbell-Washburn AE, Price AN, Wells JA, Thomas DL, Ordidge RJ, Lythgoe MF. Cardiac arterial spin labeling using segmented ECG-gated Look-Locker FAIR: variability and repeatability in preclinical studies. Magn Reson Med 2013;69:238–247.
38. Naresh NK, Chen X, Moran E, Tian Y, French BA, Epstein FH. Repeatability and variability of myocardial perfusion imaging techniques in mice: comparison of arterial spin labeling and first-pass contrast-enhanced MRI. Magn Reson Med 2016;75:2394–2405.
39. Greve AM HL, Vasu S, Bendettini, WP, Arai AE. Heterogeneity of resting and hyperemic myocardial blood flow in healthy volunteers: a quantitative CMR perfusion pixel-map study. J Cardiovasc Magn Reson 2014;16(Suppl 1):21.
40. Abdelmoneim SS, Dhoble A, Bernier M, Moir S, Hagen ME, Ness SAC, Abdel-Kader SS, Pellikka PA, Mulvagh SL. Absolute myocardial blood flow determination using real-time myocardial contrast echocardiography during adenosine stress: comparison with single-photon emission computed tomography. Heart 2009;95:1662–1668.
41. Wyss CA, Koepfli P, Mikolajczyk K, Burger C, von Schulthess GK, Kaufmann PA. Bicycle exercise stress in PET for assessment of coronary flow reserve: repeatability and comparison with adenosine stress. J Nucl Med 2003;44:146–154.

A Look-Locker Acquisition Scheme for Quantitative Myocardial Perfusion Imaging by Arterial Spin Labelling in Humans at 3 T

GraemeAKeith1,ChristopherTRodgers1,MichaelAChappell2,andMatthewDRobson1

1OxfordCentreforClinicalMagneticResonanceResearch,UniversityofOxford,Oxford,Oxfordshire,UnitedKingdom, 2InstituteofBiomedicalEngineering,UniversityofOxford,Oxford,Oxfordshire,UnitedKingdom

Target Audience: ASL, myocardial perfusion

Purpose: Arterial Spin Labelling (ASL) provides a non-invasive alternative to contrast-enhanced Cardiovascular Magnetic Resonance (CMR imaging, for the investigation of myocardial perfusion. In the standard Flow-Sensitive Alternating Inversion Recovery (FAIR) ASL experiment, two images are collected, one following a slice-selective inversion (SS), the other following a global inversion (GS). In the slice-selective case, the non-inverted inflowing spins entering the image slice cause the value of the myocardial T_1 to be short compared to that acquired for the globally inverted acquisition, where the inflowing spins are fully inverted. This difference in T_1 values is inherently related[1] to the perfusion of the myocardial tissue. Previous studies using ASL to measure perfusion in the human myocardium have employed a single inversion time, which can then be varied between scans[1-3]. However, in small animal imaging, a Look-Locke (LL) style acquisition has been demonstrated[4,5]. In this work we present an efficient Look-Locker based acquisition scheme for FAIR-ASL for us in human subjects, with timing optimised to reduce sensitivity to cardiac motion.

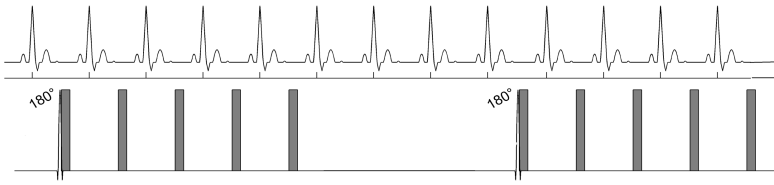


Figure 1: Schematic of the LL-FAIR-ASL pulse sequence over 13 heartbeats. 180° pulses (alternating between SS and GS) are each followed by 5 bSSFP readouts, separated by an R-R interval.

Methods: Data was collected in 4 healthy male volunteers (30 ± 9y) on a clinical Siemens 3 T scanner (Trio, Siemens Healthcare, Germany). Ethics approval was granted for all scans. The LL-FAIR-ASL sequence employed a slice selective inversion, followed by five bSSFP image acquisitions, each synchronised to the R-wave. After a gap of three heart beats, to allow for some recovery of the longitudinal magnetisation, the experiment was repeated with a global inversion within the same 13 R-R interval breath-hold, as shown in Figure 1. This timing guarantees that the signal recovery isn't corrupted by through-plane cardiac motion, by restricting inversions and readouts to the most stable cardiac phase, mid-diastole. The order of the two inversions was then switched, such that the global inversion preceded the slice-selective inversion, and the effect on the mean apparent T_1s investigated. Sequence parameters of the bSSFP readout were flip angle of 35°, an initial value of TI of 130 ms (with the following values being 130 ms + RR, 130 ms + 2RR,…), GRAPPA 2, Partial Fourier 6/8. The imaging slice thickness was 8 mm and the selective and global inversions used an HS8 pulse thickness of 20 mm and ∞ respectively. In each subject the scan was run 5 times for each ordering scheme (SS-GS and GS-SS), such that a total of 10 averages was taken. These ten breath hold scans could be run in less than 15 minutes. The data was fitted for the apparent values of T_1^{SS} and T_1^{GS} using a three-parameter fit. These values from the two ordering schemes were pooled and then used to calculate an estimate of the Myocardial Blood Flow (MBF) using the equation[6]: $MBF = \frac{\lambda}{T_1^{blood}}\left(\frac{T_1^{GS}}{T_1^{SS}} - 1\right)$, where λ = 0.92 mL/g is the blood-tissue partition coefficient.

	SS 1st		GS 1st	
Volunteer	**SS-T_1* (ms)**	**GS-T_1* (ms)**	**SS-T_1* (ms)**	**GS-T_1* (ms**
1	813 ± 42	882 ± 23	843 ± 19	843 ± 1
2	887 ± 22	947 ± 51	892 ± 16	960 ± 2
3	743 ± 35	958 ± 88	848 ± 47	840 ± 2
4	939 ± 14	982 ± 10	957 ± 17	980 ± 1

Table 1: Mean apparent T_1 values for each volunteer, with standard deviations for both SS GS and GS-SS ordering schemes

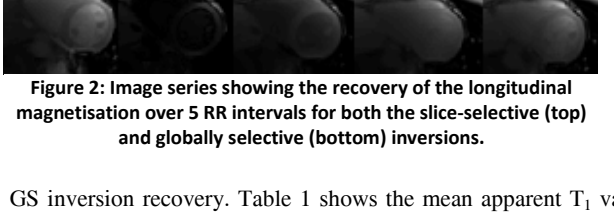


Figure 2: Image series showing the recovery of the longitudinal magnetisation over 5 RR intervals for both the slice-selective (top) and globally selective (bottom) inversions.

Volunteer	MBF (mL/g/min)
1	1.58 ± 0.7
2	2.16 ± 1.3
3	3.94 ± 0.5
4	1.09 ± 0.1

Table 2: Mean MBF values in with standard deviations

Results & Discussion: Figure 2 shows an image series typical of those collected, showing the differing effects of the SS and GS inversion recovery. Table 1 shows the mean apparent T_1 values for each of the four volunteers. It can be seen that, although in both ordering schemes the magnetisation recovers quicker in the slice-selective case, the difference between the apparent T_1s (SS and GS) when the global inversion is applied first is significantly reduced. This occurs due to incomplete recovery of the magnetisation between inversions, which in the GS SS case also affects inflowing spins. As the calculation of myocardial perfusion relies on the ratio between these two values of the apparent T_1, it is important to employ both ordering schemes in order to eliminate any bias which may occur due to the incomplete recovery. Although the calculated values for apparent T_1 are not stable between volunteers, the results for each proved to be reproducible, with low values for the standard deviation. Values for MBF for the four volunteers, in mL/g/min, are presented in Table 2. Previously reported values for MBF using single TI myocardial ASL techniques have been presented, in the range 0.74-2.40 ± 1.2 mL/g/min, in normal volunteers at rest.

Conclusion: The use of a Look-Locker acquisition for a FAIR-ASL experiment allows for the collection of an entire time series for both SS and GS inversion in a minimum of two breath holds, with reordering of inversion pulses, while restricting both the inversion pulses and readouts to the most stable cardiac phase, mid-diastole. It allows for the calculation of reproducible values of the apparent T_1, which can be used to calculate and estimate of the MBF. This can be achieved in 13 heartbeats, without the use of intravenous contrast agents, which makes this an attractive and viable technique for the investigation of myocardial perfusion and changes in perfusion in patients.

References: (1) Zun et al, MRM 2009; 62:975-983. (2) Wacker et al, JMRI 2003; 18:555-560. (3) Wang et al, MRM 2010; 64:1289-1295. (4) Campbell-Washburn et al, MRM 2013; 69: 238-247. (5) Kober et al, MRM 2004; 51:62-67. (6) Belle et al, JMRI 1998; 8:1240-1245.

Acknowledgments: This work was supported by MRC grants. CTR is funded by the Wellcome Trust and the Royal Society [098436/Z/12/Z].

Reproducibility and Variability of a Look-Locker FAIR ASL Sequence for Quantitative Measurement of Myocardial Blood Flow in Healthy Human Volunteers at 3T

G.A. Keith[1], C.T. Rodgers[1], M.A. Chappell[2], M.D. Robson[1]

[1]Oxford Centre for Clinical Magnetic Resonance Research, University of Oxford, John Radcliffe Hospital, Oxford, United Kingdom. [2]Institute of Biomedical Engineering, University of Oxford, Oxford, Oxfordshire, United Kingdom.

Purpose: A previously reported method[(1)] for non-invasive quantitation of myocardial blood flow (MBF), employing FAIR labelling and a Look-Locker readout, was assessed for reproducibility and variability. These measures are important to consider when planning a clinical study as they indicate the change required for measurement above systematic error, and describe the variation due to factors introduced between and within sessions. It is important in measurements of MBF to observe changes in pathology and under stress.

Methods: The LL-FAIR-ASL sequence (Figure 1) employed slice-selective (SS) and globally-selective (GS) HS8 inversion pulses, each followed by 5 bSSFP readouts in mid-diastole on successive heartbeats. There was a gap of 3 heartbeats between the two blocks to allow some relaxation and the order of the inversion pulses was varied. Six mid-ventricular scans were acquired (3 SS-GS, 3 GS-SS). Sequence parameters are shown in Table 1. Fifteen seconds was allowed between scans to allow for full relaxation. T_1 values were calculated for both the SS and GS-IR experiments by a three-parameter fit (Figure 2). The ratio of these T_1s was related to MBF by the Belle model[(2)].

Data was collected in 8 healthy volunteers (7 male, 31±7y) on a 3T scanner (Trio, Siemens) with ethics approval. Volunteers were scanned twice, on separate days, to assess between-session reproducibility, and during 11 scans the protocol was repeated to assess within-session reproducibility. These data were used to produce Bland-Altman plots[(3)] to describe the two measures. The myocardium of the entire left ventricle was treated as a single ROI. The variability of the MBF estimates was assessed by the coefficient of variation (SD/mean) for the whole sample (CV_{all}), and each subject between-session (CV_{BS}) and within-session (CV_{WS}).

Results: The MBF was 1.15±0.47 ml/g/min which compares well with literature values, where resting MBF has been reported as 0.97±0.64 ml/g/min with single-TI ASL[(4)], 1.33±0.32 ml/g/min with PET[(5)] and 1.02 ± 0.22 ml/g/min using first-pass CMR[(6)]. The values of MBF for each subject are presented in Figure 3. CV_{all} was 40%. The between-session and within-session Bland-Altman plots are shown in Figure 4(a) and (b) respectively and show the mean-difference in each case and the value of ±1.96 times SD which represent the upper and lower 95% confidence bounds. When normalised to the mean MBF, these equate to a coefficient of repeatability (CR) of 38% between-session and 39% within-session. The mean CV_{BS} and CV_{WS} were calculated as 10% and 9% respectively.

Discussion: The LL-FAIR-ASL method is attractive as a non-invasive alternative to SPECT, PET and first-pass CMR. While reproducibility and variability of similar techniques have been investigated in mice[(7,8)], to our knowledge this has not been carried out in human myocardium. Resting MBF values for healthy volunteers have previously been shown to be heterogeneous in studies utilising PET[(5)] and first-pass CMR[(9)]. The high observed CV_{all}, 40%, shows that our results reflect this heterogeneous nature. The Bland-Altman plots show the mean difference in both the between-session and within-session cases to be close to zero and all bar one of the data points to lie within the ±1.96 SD bounds. The CR_{BS} of 38% shows the level of reproducibility expected across repeat scans. It indicates the change in MBF required to show a difference over time and is useful to consider if planning longitudinal studies in patient groups. The CR_{WS} of 39% gives a useful indication of the detectable change in MBF, which is significantly less than the 3-4-fold increase expected under vasodilator stress[(4,6)].

The variability compares favourably to similar measures reported for preclinical cardiac ASL[(7)] and brain ASL in humans[(10)]. The mean values of CV_{BS} and CV_{WS} were 10% and 9%, below the 40% observed for all subjects. This shows that the variation in results exhibited by an individual is much less than across the population as a whole. The CV_{BS} shows the variation due to the method, plus effects such as repositioning, re-localisation, scanner adjustments etc. The CV_{WS} primarily reflects the methodological effects.

The use of a single ROI to represent the whole myocardium is a limitation of this study. MBF is known to exhibit spatial heterogeneity[5,11]. Further investigation of the sensitivity of the method to this is required.

Conclusion: The results presented suggest that a future clinical study applying the LL-FAIR-ASL method at rest and stress will have the sensitivity required to detect the expected change in MBF. The variability of the method was shown to compare favourably with published values in similar techniques. These results should prove useful in the planning of future clinical studies using this method.

Acknowledgments: This work was supported by MRC grants. CTR is funded by the Wellcome Trust and the Royal Society [098436/Z/12/Z].

Figures/Tables:

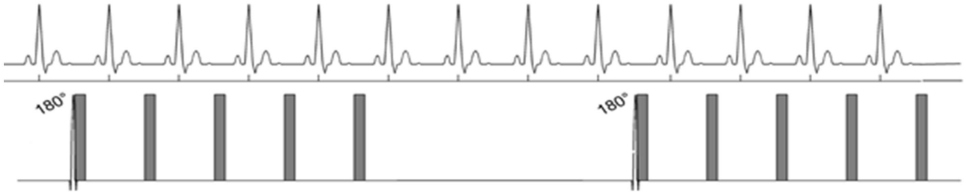


Figure 1: Schematic of the LL-FAIR-ASL pulse sequence over 13 heartbeats. 180° pulses (alternating between SS and GS) are each followed by 5 bSSFP readouts (shown as grey columns), separated by an R-R interval. All inversion pulses and readouts are ECG-triggered to mid-diastole. The order of IR pulses is varied.

Sequence parameters	
Exc. flip angle (°)	35
Image slice thickness (mm)	8
Inv. Slice thickness (mm)	24
Inversion time (ms)	115 (then 115 + RR, …)
Repitition time (ms)	3
Echo time (ms)	1.5
Field of view (mm)	320
Phase resolution (%)	75
Matrix size	192x144
Partial Fourier	6/8
GRAPPA factor	2

Table 1: LL-FAIR-ASL sequence parameters

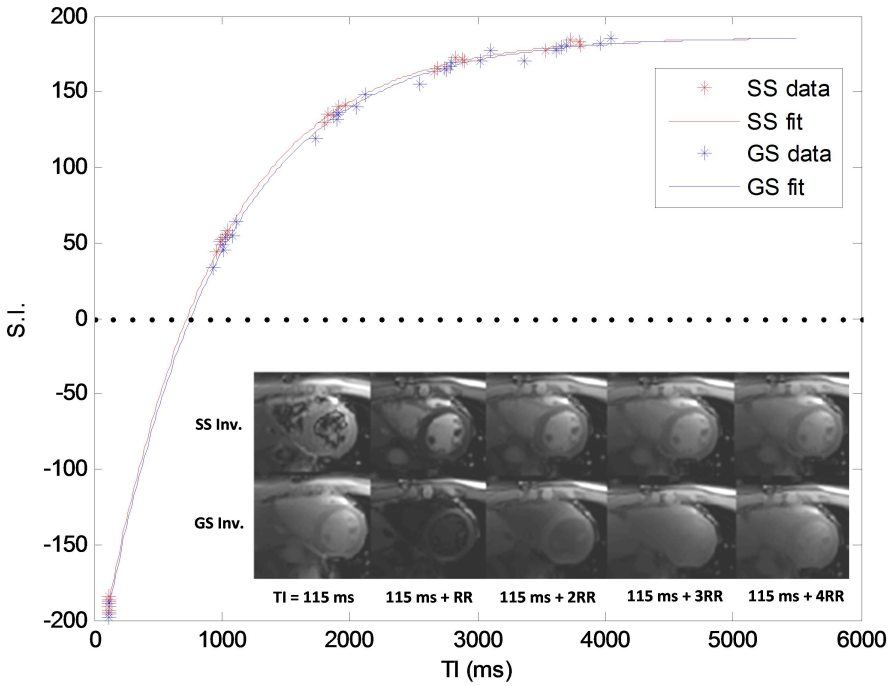


Figure 2: Calculated T_1 curves for SS and GS cases. Inset images are collected in a single breath hold.

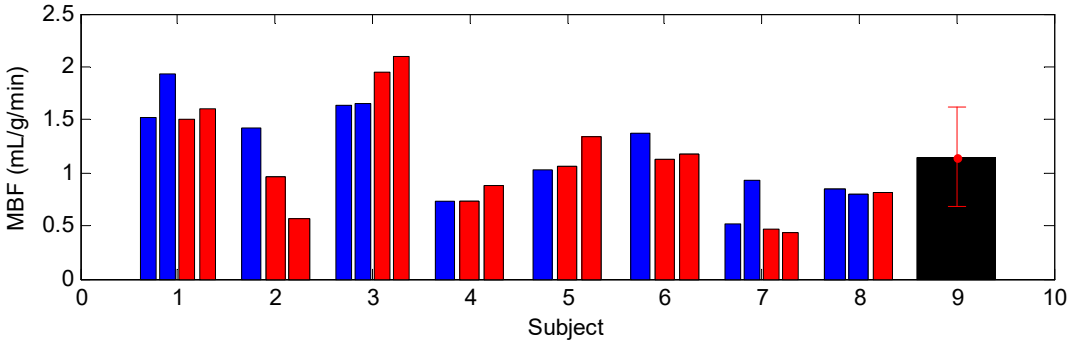


Figure 3: MBF measurements per subject in the mid-ventricular slice. Results in blue are from session 1 and those in red from session 2 for each subject. The black bar is the mean across the sample with the standard deviation.

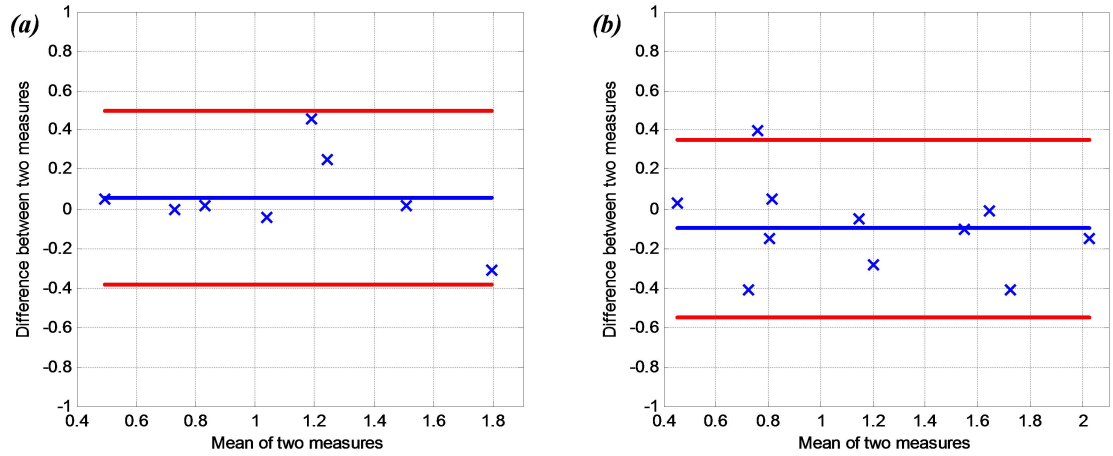


Figure 4: Bland-Altman plots for (a) between-session and (b) within-session reproducibility. The blue lines represent the mean difference in MBF and the red lines show ± 1.96 times the standard deviation and represent the 95% confidence limits. These are normalised to the mean MBF to calculate the coefficients of reproducibility.

Synopsis: A previously presented arterial spin labelling (ASL) method was tested for reproducibility and variability. These measures are important to consider when planning a clinical study. The results presented show that the method has the sensitivity required to detect changes in MBF in pathology and under stress. The variation in individuals is shown to be less than across the sample as a whole. This knowledge will be useful in the planning of future clinical research studies.

References:

1. Keith GA RC, Chappell, MA, Robson MD. A Look-Locker Acquisition Scheme for Quantitative Myocardial Perfusion Imaging by Arterial Spin Labelling in Humans at 3 T. 2015; Toronto. p p 2690.
2. Belle V, Kahler E, Waller C, Rommel E, Voll S, Hiller KH, Bauer WR, Haase A. In vivo quantitative mapping of cardiac perfusion in rats using a noninvasive MR spin-labeling method. J Magn Reson Imaging 1998;8(6):1240-1245.
3. Bland JM, Altman DG. Statistical methods for assessing agreement between two methods of clinical measurement. Lancet 1986;1(8476):307-310.
4. Zun Z, Varadarajan P, Pai RG, Wong EC, Nayak KS. Arterial spin labeled CMR detects clinically relevant increase in myocardial blood flow with vasodilation. JACC Cardiovasc Imaging 2011;4(12):1253-1261.
5. Chareonthaitawee P, Kaufmann PA, Rimoldi O, Camici PG. Heterogeneity of resting and hyperemic myocardial blood flow in healthy humans. Cardiovasc Res 2001;50(1):151-161.
6. Hsu LY, Rhoads KL, Holly JE, Kellman P, Aletras AH, Arai AE. Quantitative myocardial perfusion analysis with a dual-bolus contrast-enhanced first-pass MRI technique in humans. J Magn Reson Imaging 2006;23(3):315-322.
7. Campbell-Washburn AE, Price AN, Wells JA, Thomas DL, Ordidge RJ, Lythgoe MF. Cardiac arterial spin labeling using segmented ECG-gated Look-Locker FAIR: variability and repeatability in preclinical studies. Magnetic resonance in medicine : official journal of the Society of Magnetic Resonance in Medicine / Society of Magnetic Resonance in Medicine 2013;69(1):238-247.
8. Naresh NK, Chen X, Moran E, Tian Y, French BA, Epstein FH. Repeatability and variability of myocardial perfusion imaging techniques in mice: Comparison of arterial spin labeling and first-pass contrast-enhanced MRI. Magnet Reson Med 2015.
9. Greve AM HL, Vasu S, Bendettini, WP, Arai AE. Heterogeneity of resting and hyperemic myocardial blood flow in healthy volunteers: a quantitative CMR perfusion pixel-map study. J Cardiovasc Magn R 2014;16(Suppl 1):21.
10. Gevers S, van Osch MJ, Bokkers RP, Kies DA, Teeuwisse WM, Majoie CB, Hendrikse J, Nederveen AJ. Intra- and multicenter reproducibility of pulsed, continuous and pseudo-continuous arterial spin labeling methods for measuring cerebral perfusion. J Cereb Blood Flow Metab 2011;31(8):1706-1715.
11. Zun Z, Wong EC, Nayak KS. Assessment of myocardial blood flow (MBF) in humans using arterial spin labeling (ASL): feasibility and noise analysis. Magnetic resonance in medicine : official journal of the Society of Magnetic Resonance in Medicine / Society of Magnetic Resonance in Medicine 2009;62(4):975-983.





Perfusion Study Group

GRAEME KEITH

is bestowed

3rd Place

for Best ASL Poster Winner entitled:

REPRODUCIBILITY & VARIABILITY OF A LOOK-LOCKER FAIR ASL seq.

24th Annual Meeting & Exhibition
07-13 May 2016
Singapore

on behalf of the **Perfusion Study Group Committee**

Fernando Calamante, Ph.D., Chair

Valerij G. Kiselev, Ph.D., Vice Chair
Thomas Christen, Ph.D. , Trainee Representative
Linda Knutsson, Ph.D., Secretary
David C. Alsop, Ph.D., Past Chair